



UNIVERSITY OF  
BIRMINGHAM

VISCOELASTIC PROPERTIES OF THE BLADDER AND DESIGN OF A  
SURGICAL INSTRUMENT FOR THE REMOVAL OF BLADDER TUMOURS

by

**SPENCER CHARLES BARNES**

A thesis submitted to the

University of Birmingham for the degree of

DOCTOR OF PHILOSOPHY

School of Mechanical Engineering

University of Birmingham

January 2016

UNIVERSITY OF  
BIRMINGHAM

**University of Birmingham Research Archive**

**e-theses repository**

This unpublished thesis/dissertation is copyright of the author and/or third parties. The intellectual property rights of the author or third parties in respect of this work are as defined by The Copyright Designs and Patents Act 1988 or as modified by any successor legislation.

Any use made of information contained in this thesis/dissertation must be in accordance with that legislation and must be properly acknowledged. Further distribution or reproduction in any format is prohibited without the permission of the copyright holder.

## Abstract

There are various problems with the treatments for bladder cancer. The studies in this thesis aimed to decrease these problems or conduct research that would aid future work and development in the area.

The mechanical properties of normal and malignant bladder tissue were quantified using dynamic mechanical analysis (DMA). A uniaxial testing machine applied sinusoidally varying strains to specimens and the response stresses were measured; from this the elastic and viscous components of the soft tissues were calculated. *Porcine* bladder tissue was used as a model for normal bladder and exhibited a higher modulus than tumourous bladder tissue. Potentially these viscoelastic properties have many utilities, which include but are not limited to: diagnosis of bladder tumours, computational modelling of the bladder, comparison to current replacement materials, manufacture of more appropriate bladder replacement materials and manufacture of synthetic tumours for surgical trainers.

One problem with the procedure for removing non-muscle invasive bladder cancer (NMIBC) is tumour re-implantation. An add-on instrument was designed, manufactured and tested to attempt to stop the travel of tumourous cells which could then re-implant. A prototype of the device was manufactured using the shape memory metal nickel titanium in conjunction with latex. The device would open into a cone shape once inside the bladder to physically prevent the movement of tumour cells away from the tumour site. The prototype was successfully tested in replica surgical conditions with blue dyes. With development, it is hoped that this design can assist in reducing the high recurrence rate of NMIBC.

*aan mijn familie*

## Acknowledgements

To my supervisors Professor Duncan Shepherd and Dr Daniel Espino for their patience, help and advice. Without their continued guidance and expertise the work detailed in this thesis would not have been possible.

To Dr Rik Bryan (Institute of Cancer and Genomic Sciences, University of Birmingham) for his assistance in all things medicine, the bladder and cancer.

To Mr Richard Viney, Mr Prashant Patel, Dr Gareth Bicknell (all Institute of Cancer and Genomic Sciences, University of Birmingham), Beverley Davies (Health and Safety Unit, University of Birmingham) and Mr Mark Stott (Royal Devon & Exeter NHS Foundation Trust) for a range of assistance, including, but not limited to: device design, allowing me to view bladder cancer procedures and help with acquiring tissue specimens.

To the mechanical engineering technical staff (University of Birmingham): Mr Carl Hingley, Mr Peter Thornton, Mr Simon Rowan, Mr Lee Gauntlett and Mr Jack Garrod for all of their technical support.

To the EPSRC for funding this PhD, GKN for the scholarship and the IMechE for the travel grant to the World Congress on Medical Physics and Biomedical Engineering, Toronto.

To the Biomedical Engineering Research Group (the lab), especially David Eckold who, I am sure, would have submitted his own PhD thesis at least six months earlier had I not been there!

To my friends and family.

## **Table of Contents**

<b>Abstract .....</b>	<b>i</b>
<b>Table of Contents .....</b>	<b>iv</b>
<b>List of Figures .....</b>	<b>viii</b>
<b>List of Tables.....</b>	<b>xiii</b>
<b>Acronyms.....</b>	<b>xiv</b>
<b>Chapter 1 - Introduction .....</b>	<b>1</b>
<b>Chapter 2 - Background .....</b>	<b>4</b>
2.1 Chapter Overview .....	4
2.2 Urinary Bladder.....	4
2.2.1 Human Urinary System .....	4
2.2.2 Anatomy of the Urinary Bladder .....	5
2.2.3 Structure of the Bladder Wall .....	7
2.2.4 Micturition.....	8
2.3 Bladder Cancer .....	10
2.3.1 Bladder Cancer Overview .....	10
2.3.2 Bladder Cancer Grade and Architecture .....	11
2.3.3 Non-Muscle and Muscle Invasive Bladder Cancer .....	12
2.3.4 Muscle Invasive Bladder Treatment.....	13
2.3.5 Non-Muscle Invasive Bladder Treatment.....	14
2.3.6 Non-Muscle Invasive Bladder Treatment Problems .....	17
2.3.7 Bladder Cancer Summary.....	19

2.4 Mechanical Properties of Materials .....	19
2.4.1 Introduction .....	19
2.4.2 Stiffness .....	20
2.4.3 Young's Modulus .....	21
2.4.4 Viscoelastic Materials .....	24
2.4.5 Stress Relaxation and Creep .....	26
2.4.6 Dynamic Mechanic Analysis .....	29
2.4.7 Mechanical Properties of the Bladder .....	32
2.5 Shape Memory Alloys .....	34
2.5.1 Shape Memory Effect .....	34
2.5.2 Shape Memory .....	34
2.5.3 Superelasticity .....	35
2.5.4 Shape Memory Training .....	36
2.5.5 Two-Way Shape Memory Effect .....	36
2.5.6 Medical Applications of Shape Memory Alloys .....	37
2.5.7 Other Shape Memory Materials .....	38
2.6 Chapter Summary .....	39

### **Chapter 3 - Frequency Dependant Viscoelastic Properties of *Porcine* Bladder..... 40**

3.1 Introduction .....	40
3.2 Materials and Methods .....	41
3.2.1 General Methods .....	41
3.2.2 Porcine Bladder Pressure Experiment .....	41
3.2.3 Porcine Bladder Pressure Experiment Results .....	45
3.2.4 Uniaxial Testing Methods .....	46
3.2.5 Preliminary Testing .....	50
3.2.6 Final Testing .....	56
3.3 Results .....	57
3.4 Discussion .....	67
3.5 Chapter Summary .....	72

<b>Chapter 4 - Viscoelastic Properties of Human Bladder Tumours.....</b>	<b>73</b>
4.1 Introduction .....	73
4.2 Materials and Methods .....	74
4.2.1 Preliminary Testing Methods .....	74
4.2.2 Preliminary Testing Results .....	77
4.2.3 Final Testing Methods .....	79
4.3 Results.....	83
4.4 Discussion .....	89
4.5 Chapter Summary .....	94
 <b>Chapter 5 - Design of a Surgical Instrument for the Removal of Bladder Tumours..</b>	 <b>95</b>
5.1 Introduction .....	95
5.2 Design Requirements.....	96
5.3 Design Development .....	97
5.3.1 Design Solutions .....	97
5.3.2 Cone Actuation Methods .....	99
5.3.3 Actuation Method Selection .....	103
5.4 Preliminary Nitinol Testing .....	104
5.4.1 One-Way Shape Memory Effect.....	104
5.4.2 Wire Actuation with Loading.....	105
5.4.3 Two-Way Shape Memory Effect .....	106
5.4.4 Nitinol Actuation with Current.....	108
5.4.5 Nitinol Preliminary Testing Findings.....	110
5.5 Final Design.....	111
5.5.1 Detailed Design .....	111
5.5.2 Wiring Configuration .....	112
5.5.3 Risk Assessment .....	115
5.6 Prototype Manufacture .....	118
5.6.1 Nitinol Wire .....	118
5.6.2 Wire Housing .....	119
5.6.3 Polymer Leaves .....	120



5.7 Prototype Testing .....	122
5.7.1 Prototype Actuation.....	122
5.7.2 Fluid Testing Methods.....	123
5.7.3 Fluid Testing Results.....	127
5.8 Discussion .....	129
5.9 Chapter Summary .....	131
 <b>Chapter 6 - Overall Discussion and Conclusions .....</b>	<b>132</b>
 <b>Chapter 7 - Future Work.....</b>	<b>140</b>
7.1 Tissue Testing .....	140
7.2 Instrument Development .....	141
 <b>References .....</b>	<b>143</b>
 <b>Appendix A - Pressure Transducer Calibration .....</b>	<b>158</b>
 <b>Appendix B - Bladder Dimension Schematic .....</b>	<b>159</b>
 <b>Appendix C - Engineering Drawings for Bladder Testing Jigs .....</b>	<b>160</b>
 <b>Appendix D - Wire Housing Engineering Drawing .....</b>	<b>164</b>

## List of Figures

<b>Figure 2.1</b> – Human urinary tract (reproduced with permission from Elsevier (Field et al., 2011)).....	5
<b>Figure 2.2</b> – Anatomy of the urinary bladder (reproduced with permission from John Wiley and Sons (Tortora and Derrickson, 2005)) .....	6
<b>Figure 2.3</b> – Regions and directions of the porcine urinary bladder .....	7
<b>Figure 2.4</b> – Structure of the bladder wall (reproduced with permission from John Wiley and Sons (Peckham, 2011)) .....	8
<b>Figure 2.5</b> – Normal cystometrogram with micturition ‘spikes’ (reproduced with permission from Elsevier (Guyton and Hall, 2006)) .....	9
<b>Figure 2.6</b> – T stages of bladder cancer (reproduced courtesy of an open knowledge project by Cancer Research UK, London, UK).....	11
<b>Figure 2.7</b> – Side view of Olympus OES Pro resectoscope .....	14
<b>Figure 2.8</b> – Transurethral Resection of Bladder Tumours (Copyright <a href="http://bladder.cancercaregiving.com/bladder-cancer-treatment/">http://bladder.cancercaregiving.com/bladder-cancer-treatment/</a> ).....	15
<b>Figure 2.9</b> – Piecemeal removal of bladder cancer (reproduced with permission from John Wiley and Sons (Wiesner et al., 2010)) .....	17
<b>Figure 2.10</b> – Cylindrical rod subjected to a tensile force (F) with cross sectional area (A) highlighted in yellow, original length (L) and change in length ( $\Delta L$ ) .....	20
<b>Figure 2.11</b> – Typical stress strain curve for a metal (adapted from Callister and Rethwisch (2012)). The gradient of the elastic linear portion represents the Young’s modulus of the material, P denotes the proportional limit, $\sigma_y$ the yield strength taken parallel to the elastic slope at 0.002 strain, UTS the ultimate tensile strength and FP the fracture point of the material.....	22
<b>Figure 2.12</b> – Argand diagram of phase lag ( $\delta$ ), dynamic ( $E^*$ ), storage ( $E'$ ) and loss ( $E''$ ) moduli where Im is the imaginary and R is the real axis.....	25
<b>Figure 2.13</b> – Stress strain hysteresis loops for a silicone disc specimen subjected to 8 cycles of loading and unloading. The area highlighted yellow is the energy lost per unit volume....	26
<b>Figure 2.14</b> – Stress (blue) and strain (green) against time during stress relaxation .....	27
<b>Figure 2.15</b> – Stress (blue) and time-dependent strain (green) during creep testing .....	28
<b>Figure 2.16</b> – Sinusoidally varying load input and displacement response for a viscoelastic material. $T_\delta$ is the time lag between the two waves, phase lag ( $\delta$ ) can be calculated from this by multiplying by angular frequency ( $\omega$ ) (i.e. $\delta = \omega T_\delta$ ).....	30

<b>Figure 2.17</b> – Crystal structure change during loading and shape recovery of a shape memory alloy (adapted from Uehara et al. (2009)).....	35
<b>Figure 2.18</b> – One-way (left column) and two-way (right column) shape memory effect. Where a) is the starting martensite shape, b) is the deformed martensite shape, c) is the heated austenite shape and d) is the cooled martensite shape (adapted from Gil and Planell (1998)). .....	37
<b>Figure 3.1</b> – Experimental set up of bladder pressure experiment. a) catheterised porcine bladder; b) syringe used to fill the bladder; c) power pack; d) multimeter; e) interface; f) pressure transducer; g) reference pressure syringe; h) three way valve.....	43
<b>Figure 3.2</b> – Average force (N) against volume (ml) during bladder filling, error bars represent one standard deviation.....	45
<b>Figure 3.3</b> - Initial dissection lines of bladder specimens. Dome region (a), two central regions (b & c) and the trigone region (d). Lines indicate where cuts were made.....	47
<b>Figure 3.4</b> – Fixtures for testing the specimens of bladder (a) looped specimens; (b) rectangular specimens .....	49
<b>Figure 3.5</b> – Storage ( $k'$ ) and loss stiffness ( $k''$ ) against frequency ( $f$ ) for an individual looped specimen. The frequency range tested was 0.01 – 30 – 0.01 Hz. In the key U refers to Up i.e. increasing frequency and D to Down i.e. decreasing frequency.....	51
<b>Figure 3.6</b> – Storage ( $k'$ ) and loss stiffness ( $k''$ ) against frequency ( $f$ ) for an individual looped specimen. The frequency range tested was 30 – 0.01 – 30 Hz. In In the key U refers to Up i.e. increasing frequency and D to Down i.e. decreasing frequency.....	52
<b>Figure 3.7</b> – Storage ( $k'$ ) and loss stiffness ( $k''$ ) against frequency ( $f$ ) for an individual rectangular specimen. The frequency range tested was 0.01 – 10 – 0.01 Hz. In the key U refers to Up i.e. increasing frequency and D to Down i.e. decreasing frequency .....	53
<b>Figure 3.8</b> – Storage ( $k'$ ) and loss stiffness ( $k''$ ) against frequency ( $f$ ) for an individual rectangular specimen. The frequency range tested was 10 – 0.01 – 10 Hz. In the key U refers to Up i.e. increasing frequency and D to Down i.e. decreasing frequency.....	54
<b>Figure 3.9</b> – Storage ( $k'$ ) and loss stiffness ( $k''$ ) against frequency ( $f$ ) for three individual looped specimens. $k'_1$ refers to the data points subjected to the first curve fit of storage stiffness up to 1 Hz (characterised by equation 3.7) and $k'_2$ refers to the data points subjected to the second curve fit of storage stiffness up to the end testing frequency (characterised by equation 3.8). The loss stiffness ( $k''$ ) curve fit is characterised by equation 3.13 .....	61
<b>Figure 3.10</b> – Storage ( $k'$ ) and loss stiffness ( $k''$ ) against frequency ( $f$ ) for three individual rectangular specimens. $k'_1$ refers to the data points subjected to the first curve fit of storage stiffness up to 1 Hz (characterised by equation 3.7) and $k'_2$ refers to the data points	

subjected to the second curve fit of storage stiffness up to the end testing frequency (characterised by equation 3.8). The loss stiffness ( $k''$ ) curve fit is characterised by equation 3.13 .....	62
<b>Figure 3.11</b> – Storage ( $k'$ ) and loss stiffness ( $k''$ ) against frequency ( $f$ ) for looped specimens. Data points represent the average values, with one standard deviation error bars. $k'1$ refers to the data points subjected to the first curve fit of storage stiffness up to 1 Hz (described by equation 3.9) and $k'2$ refers to the data points subjected to the second curve fit of storage stiffness up to the end testing frequency (described by equation 3.10). The loss stiffness ( $k''$ ) curve fit is described by equation 3.14 .....	63
<b>Figure 3.12</b> – Storage ( $k'$ ) and loss stiffness ( $k''$ ) against frequency ( $f$ ) for rectangular specimens. Data points represent the average values, with one standard deviation error bars. $k'1$ refers to the data points subjected to the first curve fit of storage stiffness up to 1 Hz (described by equation 3.11) and $k'2$ refers to the data points subjected to the second curve fit of storage stiffness up to the end testing frequency (described by equation 3.12). The loss stiffness ( $k''$ ) curve fit is described by equation 3.15.....	64
<b>Figure 3.13</b> – Storage ( $E'$ ) and loss modulus ( $E''$ ) against frequency ( $f$ ) for rectangular specimens. Data points represent the average values, with one standard deviation error bars. $E'1$ refers to the data points subjected to the first curve fit of storage stiffness up to 1 Hz (described by equation 3.11) and $E'2$ refers to the data points subjected to the second curve fit of storage stiffness up to the end testing frequency (described by equation 3.12). The loss stiffness ( $E''$ ) curve fit is described by equation 3.15.....	66
<b>Figure 4.1</b> – Compressive DMA set-up for porcine bladder specimens and human bladder tumours .....	76
<b>Figure 4.2</b> – Storage modulus ( $E'$ ) against frequency ( $f$ ) for the three preliminary porcine specimens .....	78
<b>Figure 4.3</b> – Loss modulus ( $E''$ ) against frequency ( $f$ ) for the three preliminary porcine specimens .....	78
<b>Figure 4.4</b> – Human bladder tumour specimens: (a) specimen 2; (b) specimen 3; (c) specimen 6; (d) specimen 7 .....	80
<b>Figure 4.5</b> – Mean storage ( $E'$ ) and loss modulus ( $E''$ ) against frequency ( $f$ ) with 1 standard deviation positive error bars and specimen 3 storage ( $E'$ ) and loss modulus ( $E''$ ) against frequency ( $f$ ) .....	83
<b>Figure 4.6</b> – Storage modulus ( $E'$ ) against log frequency ( $f$ ) for three individual tumour specimens. The curve fit is given by equation 4.5.....	85
<b>Figure 4.7</b> – Mean storage modulus ( $E'$ ) against log frequency ( $f$ ). Error bars represent the 95% confidence intervals for the sample. The mean curve fit for the storage modulus against log frequency is stated in equation 4.6 .....	86

<b>Figure 4.8</b> – Loss modulus ( $E'$ ) against log frequency ( $f$ ) for three individual tumour specimens. The curve fit is given by equation 4.7.....	87
<b>Figure 4.9</b> – Mean loss modulus ( $E''$ ) against log frequency ( $f$ ). Error bars represent 95% confidence intervals for the sample. The mean curve fit for the storage modulus against log frequency is stated in equation 4.8.....	88
<b>Figure 5.1</b> – Closed (a) and open (b) position of the cone concept within the bladder .....	99
<b>Figure 5.2</b> – Transition of a 0.5 mm diameter Nitinol wire from a) deformed martensite to b) austenite (after insertion in boiling water) .....	104
<b>Figure 5.3</b> – M8 nut lifting with 0.5 mm diameter Nitinol wire. a) pre-trained Nitinol wire with no M8 nut, b) deformed Nitinol wire with M8 nut, before heating, c) Nitinol wire with M8 nut returned to original position post heating .....	106
<b>Figure 5.4</b> – Two-Way shape memory effect trial. a) is the pre-trained Nitinol wire at room temperature, b) is the Nitinol wire immediately after being heated past its transformation temperature with a heat gun and c) is the wire after four minutes of cooling .....	107
<b>Figure 5.5</b> – Nitinol wire transition temperature measure set-up. a) Digital thermometer, b) thermocouple, c) crocodile clips, d) Nitinol wire, e) connective wiring and f) power pack ..	109
<b>Figure 5.6</b> – Final design render .....	112
<b>Figure 5.7</b> – Render of prototype including Nitinol wires (dark grey), connective wiring (gold) and wire housing (white). The blue and red wires show the input and output of the electrical connection, respectively.....	113
<b>Figure 5.8</b> – Aluminium wire housing prototype .....	114
<b>Figure 5.9</b> – Prototype circuit diagram.....	115
<b>Figure 5.10</b> – High temperature training jig.....	118
<b>Figure 5.11</b> – Finished cone prototype (left) and aluminium cone onto which the latex was painted (right).....	121
<b>Figure 5.12</b> – Closed (top) and open (bottom) prototype .....	122
<b>Figure 5.13</b> – Instrument dye test set-up. a) simulation irrigation fluid input. b) 50ml syringe for input of dye. c) negative electrical connection. d) positive electrical connection. e) clamp stand and tweezer set-up to insert and remove instrument. f) perspex housing. g) instrument. h) stretched porcine bladder specimen. i) M5 bolt, washer and nut .....	124
<b>Figure 5.14</b> – Bottom of Perspex testing device. a) bottom of Perspex device. b) rubber added on top of the Perspex. c) stretched porcine bladder added on top of the rubber .....	125
<b>Figure 5.15</b> – Closed and open state of the prototype device in fluid. For this test rubber was used at the bottom of the test device.....	127

**Figure 5.16** – Instrument dye tests. Less dense blue dye a – d. Denser blue dye e – h. Where:  
a) & e) are the inserted devices pressed against a sample of porcine bladder wall, b) & f) are  
the dyes being inserted into the device which is where the timing of the test started, c) & g)  
are the device with blue dyes inside once the tubing has been removed and d) & h) are the  
blue dyes escaping once the device is taken out after the 5 minute test had been completed  
.....128

## List of Tables

<b>Table 3.1</b> – Dimensions (mean and standard deviation) of the looped and rectangular specimens. 10 looped and 18 rectangular specimens were tested .....	56
<b>Table 3.2</b> – Testing frequencies for looped and rectangular bladder specimens.....	57
<b>Table 3.3</b> – Curve fit results for average storage and loss stiffness. All coefficients were found to be statistically significant ( $p < 0.05$ ).....	65
<b>Table 4.1</b> – Individual information for the 10 bladder tumour specimens. Three of the specimens used (2, 6 & 7) were from the same individual. SD refers to standard deviation ..	81
<b>Table 4.2</b> – Human bladder tumour testing parameters .....	82
<b>Table 4.3</b> – Curve fit results for storage and loss modulus. All coefficients were found to be statistically significant ( $p < 0.05$ ) .....	88
<b>Table 5.1</b> – Potential cone actuating methods, with their potential advantages and disadvantages .....	100
<b>Table 5.2</b> – Risk assessment for actuating cone device addition to the current resectoscope (Likelihood of Harm; Y – Yes/Very High, Pr – Probable, Po – Possible, R – Remote. Severity of Harm; F – Fatality, Mj – Major, Mn - Minor) .....	116

## Acronyms

BCPP.....	bladder cancer prognosis programme
CFD.....	computational fluid dynamics
CIS .....	carcinoma in situ
DMA.....	dynamic mechanical analysis
EAP.....	electro-active polymer
EDM .....	electrical discharge machining
FEA .....	finite element analysis
FSI .....	fluid structure interaction
MIBC .....	muscle invasive bladder cancer
MRE.....	magnetic resonance elastography
Nitinol .....	nickel titanium naval ordnance laboratory
NMIBC.....	non-muscle invasive bladder cancer
OWSME.....	one-way shape memory effect
SMA.....	shape memory alloy
SMP.....	shape memory polymer
TNM .....	tumour node metastases
TURBT .....	trans-urethral resection of bladder tumours
TWSME .....	two-way shape memory effect
UBC .....	urinary bladder cancer
UTS.....	ultimate tensile strength



# 1 Introduction

The work in this thesis investigates some of the engineering matters associated with bladder cancer. There are problems with the treatments for both muscle invasive bladder cancer (MIBC) and non-muscle invasive bladder cancer (NMIBC). Trans-urethral resection of bladder tumours (TURBT) is the gold standard procedure for NMIBC and suffers from a very high rate of recurrence, up to 61% at year 1 (Sylvester *et al.*, 2006). It is thought that the reasons for this high recurrence rate are associated with TURBT. The treatments for MIBC are partial and radical cystectomy, and these procedures have other problems which include: subsequent tumour relapse, electrolyte imbalance and excess mucus production (Kaufman *et al.*, 2009; Pokrywczynska *et al.*, 2014). This thesis is concerned with decreasing the issues associated with bladder cancer treatment and conducting research that will aid investigations into reducing the complications.

The aims were to investigate the mechanical properties of the urinary bladder and develop a novel instrument for the removal of NMIBC. The specific objectives were to:

- Find the mechanical properties of healthy urinary bladder.
- Acquire the mechanical properties of tumourous bladder tissue.
- Design, prototype and test a novel instrument for the removal of NMIBC that reduces the likelihood of recurrence.

The mechanical properties of bladder tissue are important for the manufacture of more appropriate substitute materials. Also any *autologous* bladder replacements can be compared to the actual tissue mechanical properties and their suitability can be determined.

The differences between normal and malignant tissue can be identified, this is of use for the potential diagnosis of bladder cancer and could be used to inform material properties for surgical trainers. Accurate mechanical properties are also important for computational modelling of the bladder.

Currently in TURBT, tumours are removed piecemeal which facilitates the spread of tumour cells throughout the bladder which can re-implant into the bladder wall and form secondary tumours (Kondas *et al.*, 1999; Bryan *et al.*, 2010). Improving the method of surgery to limit this spread of viable cells and hence lower the high recurrence rate would be of great benefit to patients and hospitals.

Chapter 2 outlines the background information needed to understand the subsequent chapters in the thesis. This includes information on the urinary bladder, bladder cancer, mechanical and viscoelastic properties of materials and shape memory alloys.

Chapter 3 describes a study on the tensile viscoelastic properties of *porcine* bladder rectangular and looped specimens in terms of stiffness. The chapter is based on the work published in the *Journal of the Mechanical Behaviour of Biomedical Materials* titled 'Frequency dependent viscoelastic properties of *porcine* bladder'; 2015, volume 42, pages 168 - 176. This work was also presented at the 2013 *Bose User Conference* in Sheffield. Also included in this chapter are preliminary tests on the pressure volume relationship of the bladder and the effect of increasing or decreasing frequency on the viscoelastic properties of the bladder.

Chapter 4 details a preliminary study on the compressive dynamic properties of *porcine* bladder and then the compressive frequency dependant viscoelastic properties of

human bladder tumours. The work in this chapter is based on the work accepted for publication in the *Journal of the Mechanical Behaviour of Biomedical Materials* titled 'Viscoelastic properties of human bladder tumours'.

Chapter 5 presents the design, prototyping and testing of a novel instrument for the removal of NMIBC. This chapter also outlines the training of the shape memory alloy Nitinol for use as an actuator. The work in this chapter is based on the work accepted for publication in the *Proceedings of the Institution of Mechanical Engineers, Part H: Journal of Engineering in Medicine* titled 'Design of an improved surgical instrument for the removal of bladder tumours'. The work was also presented at the *2015 World Congress on Medical Physics and Biomedical Engineering – Toronto*.

Chapter 6 then provides the overall discussion and conclusions.

## **2 Background**

### **2.1 Chapter Overview**

The aim of this chapter is to provide the background information necessary to understand the subsequent chapters in this thesis. Section 2.2 outlines the urinary bladder and its underlying structure. Section 2.3 describes bladder cancer and the various treatments used to remove it. Section 2.4 defines mechanical properties that will be referred to throughout this thesis. Section 2.5 outlines the shape memory effect for metals and the training required to achieve these effects. Finally section 2.6 summarises the background chapter.

### **2.2 Urinary Bladder**

#### **2.2.1 Human Urinary System**

The human urinary system is comprised of two organs, these are the kidneys and the bladder. The function of the kidneys is to filter blood and remove waste as urine which is then transported to the bladder for storage via the ureters. The bladder is a hollow distensible structure located within the pelvis which functions as the storage organ for urine. Urine is removed from the bladder and out of the body through the urethra; this process is termed micturition (Guyton and Hall, 2010). In males the urethra also passes through a small gland called the prostate. The urinary bladder permits urination or micturition at socially

acceptable times and, hence, correct bladder function is important to a person's independence and quality of life. Figure 2.1 is an illustration of the urinary system.

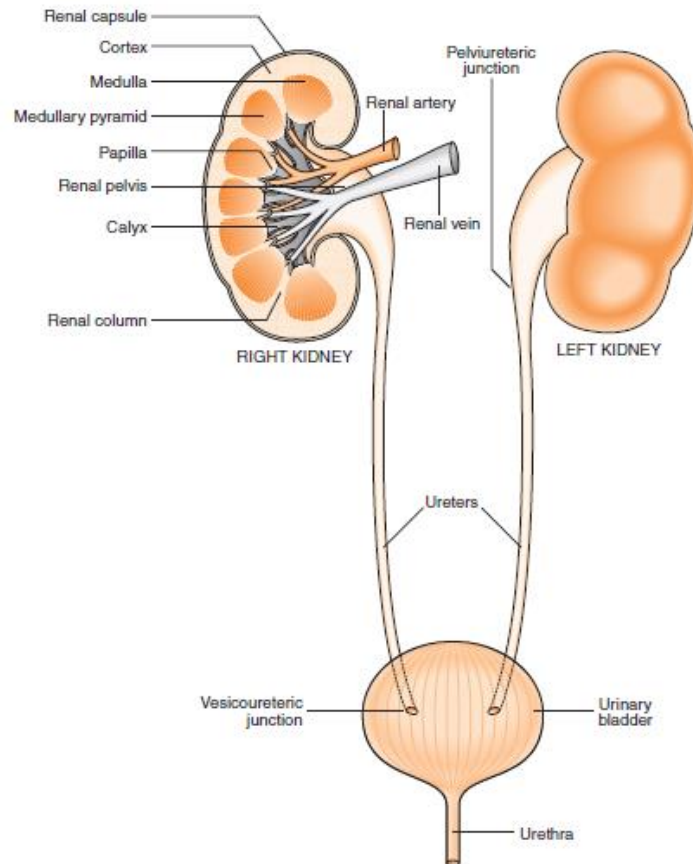


**Figure 2.1 – Human urinary tract (reproduced with permission from Elsevier (Field *et al.*, 2011)).**

### **2.2.2 Anatomy of the Urinary Bladder**

The urinary bladder is made up of different parts or sections which can be seen in figure 2.2. At the bottom of the bladder is the trigone region, which is connected by the

openings of the urethra and the ureters in the bladder. The middle region of the bladder is called the lateral region and the top is the dome.

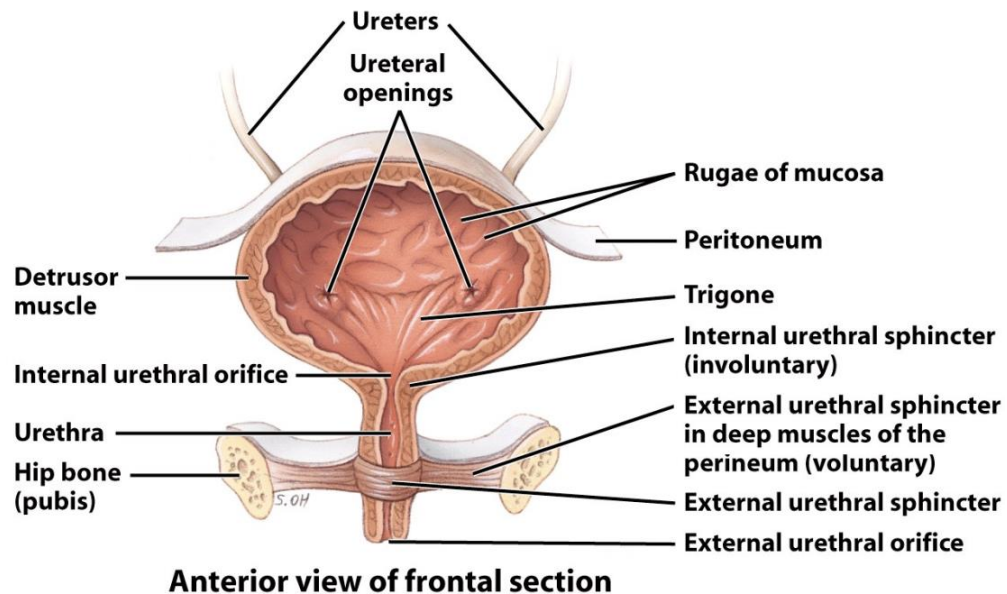


**Figure 2.2 – Anatomy of the urinary bladder (reproduced with permission from John Wiley and Sons (Tortora and Derrickson, 2005)).**

As human bladders are not readily available for testing, the work in this thesis details experiments with *porcine* bladders. *Porcine* bladders display similar tissue mechanics to that of human bladders (Natali *et al.*, 2015). Functionally the detrusor muscle of *porcine* bladders are similar to that of human (Hashitani and Brading, 2003; Rosario *et al.*, 2008). Also, the extracellular matrix of the pig bladder has been used as a xenogeneic scaffold for producing tissue engineered bladders for replacement in humans (Badylak, 2004; Yang *et al.*, 2010). Furthermore, *porcine* bladders are similar anatomically to the human urinary bladder (figure 2.3), as it has a trigone region which makes up the two inlets for the ureters and the outlet

for the urethra. There is also a lateral region further up the bladder and a dome region at the top. In terms of normal volume the human bladder is similar to porcine as Parsons *et al.* (2012) have reported a maximum volume of 450 ml retrieved from pig bladders after slaughter. This is comparable to the fullness a human feels when 400 ml of urine has collected in the bladder (Ganong and Barrett, 1997).

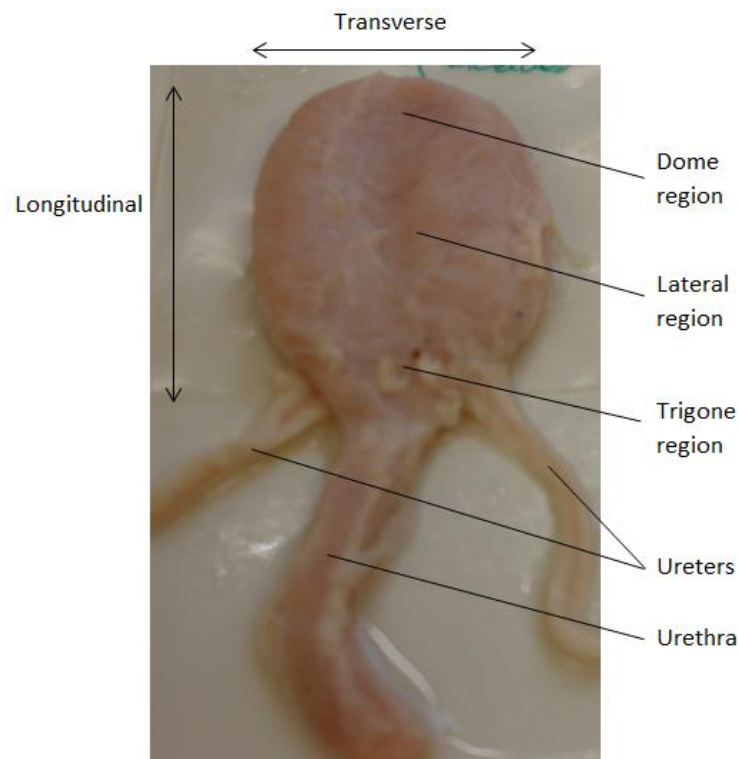


**Figure 2.3 – Regions and directions of the *porcine* urinary bladder.**

### **2.2.3 Structure of the Bladder Wall**

The human urinary bladder wall is comprised of several layers. These layers are, from the inside of the bladder outwards: the mucosa (which includes the transitional epithelium), the submucosa (lamina propria) and the detrusor muscle (muscularis propria) (Peckham,

2011). These layers can be seen in figure 2.4 along with the different orientations of the detrusor muscle through the bladder wall which alternate from longitudinal to transverse to longitudinal. A pig's urinary bladder has a similar structure to that of a human bladder (Dahms *et al.*, 1998; Korossis *et al.*, 2009; Natali *et al.*, 2015).

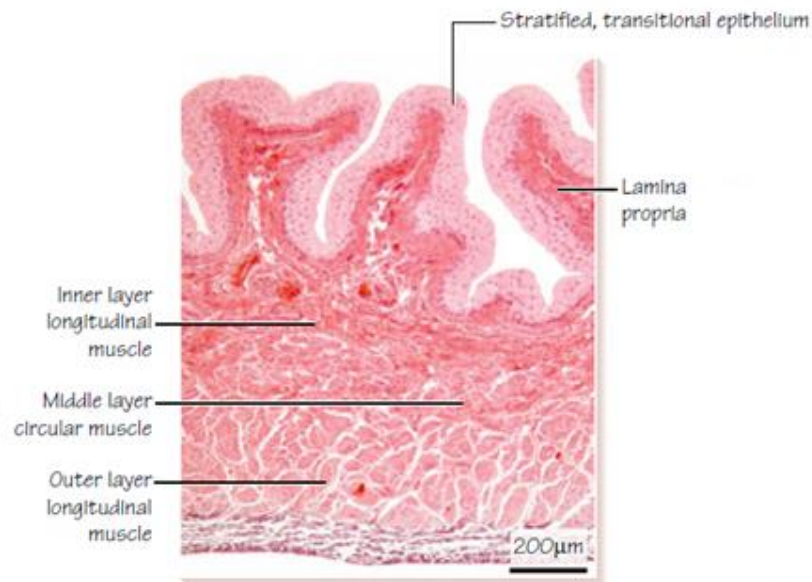


**Figure 2.4 – Structure of the bladder wall (reproduced with permission from John Wiley and Sons (Peckham, 2011)).**

## 2.2.4 Micturition

When the bladder starts to become full, the urge to micturate or urinate starts to be felt. Typically this occurs at around 400 ml (Guyton and Hall, 2010) but can vary depending on a number of factors, including the size of the person. As the bladder continues to fill, stretch receptors in the bladder wall send signals to the sacral part of the spinal column, which return and cause micturition reflexes, in turn causing spikes in intravesical pressure (the pressure within the bladder). These spikes are caused by contractions in the detrusor



muscle, which can be seen in a cystometrogram in figure 2.5, and subside after a few minutes. A cystometrogram is a test of bladder function, during which bladder pressure is measured in response to volumes of liquid being added or taken away (van Mastrigt *et al.*, 1978; Kraklau and Bloom, 1998). As the bladder continues to fill, micturition spikes occur more frequently and become more powerful which causes another reflex; the external sphincter relaxing. The location of the external sphincter can be seen in figure 2.2. The inhibition of the external sphincter, and hence urination, can be stopped voluntarily by signals from the brain. However, the more full the bladder becomes the stronger the consequent inhibition signal which will eventually be able to override the voluntary constriction signals from the brain (Guyton and Hall, 2010).

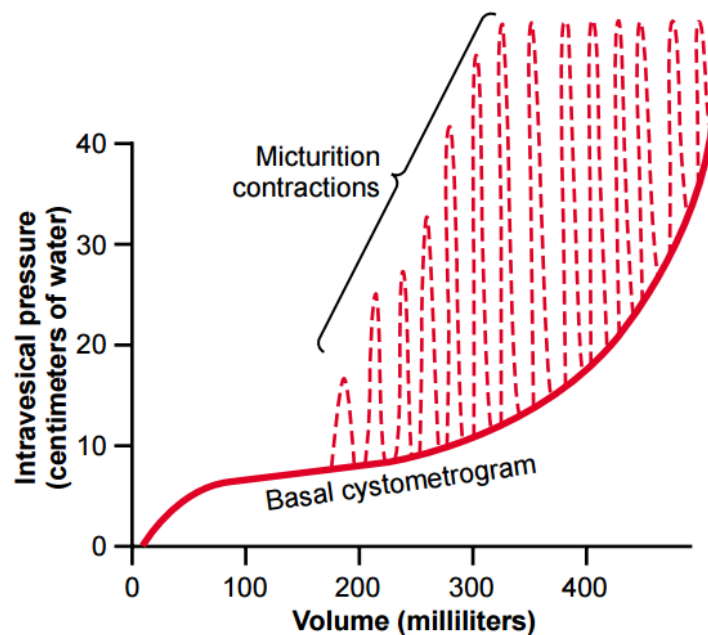


**Figure 2.5 – Normal cystometrogram with micturition ‘spikes’ (reproduced with permission from Elsevier (Guyton and Hall, 2006)).**

It should be noted that the micturition reflex is autonomic and as such generally acts subconsciously. This is in contrast to the conscious decision to prevent micturition which is facilitated by areas in the brain (Guyton and Hall, 2010).

## **2.3 Bladder Cancer**

### **2.3.1 Bladder Cancer Overview**

Urinary bladder cancer is the 4<sup>th</sup> most common cancer in men and the 13<sup>th</sup> most common cancer in women in the UK (Cancer Research UK, 2014). Each year 10,200; 123,135 and 72,570 people are diagnosed with bladder cancer in the UK, EU and USA and with mortality of 5,000; 40,252 and 15,210, respectively (Cancer Research UK, 2014; Burger *et al.*, 2013).

UICC (Union International Contre le Cancer – International Union against Cancer) Tumour, Node, Metastasis (TNM) staging defines the depth of invasion or the other structures that the primary tumour has involved, and also the presence or absence of lymph node and/or distant metastases (Sobin *et al.*, 2009). Figure 2.6 shows a diagram of bladder cancer tumour (T) staging.

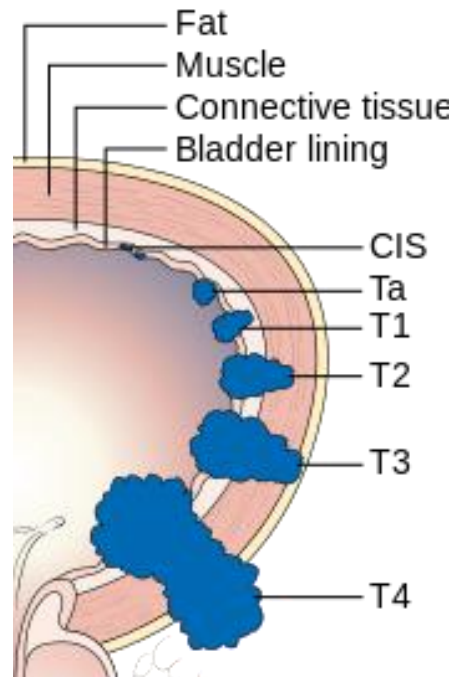


**Figure 2.6 – T stages of bladder cancer (reproduced courtesy of an open knowledge project by Cancer Research UK, London, UK).**

In Western populations, over 90% of bladder cancers are transitional cell carcinomas and at presentation over 75-85% will be Non-Muscle Invasive Bladder Cancer (NMIBC: stages Ta/T1/CIS [carcinoma in situ]), with the remainder being Muscle-Invasive Bladder Cancer (MIBC: stages T2-4) (Wallace *et al.*, 2002; Lorusso and Silvestris, 2005; van Rhijn *et al.*, 2009; Kaufman *et al.*, 2009). Other types of bladder cancer include squamous cell carcinomas (5%) and adenocarcinomas (>2%) (Kaufman *et al.*, 2009).

### **2.3.2 Bladder Cancer Grade and Architecture**

In the Urinary Bladder Cancer (UBC) setting, grade describes the microscopic appearance of the tumour cells and indicates how biologically aggressive the cells are, with grade 1 (G1) being least aggressive and grade 3 (G3) being most aggressive; alternatively,

grade can be described as low or high (Mostofi *et al.*, 1973; Epstein *et al.*, 1998; Kaufman *et al.*, 2009).

The architecture of the tumour is classified by its predominant feature; this can be sessile or papillary (Epstein *et al.*, 1998; Remzi *et al.*, 2009). Papillary (pap) describes a tumour with 'finger like' projections (sometimes likened to a sea anemone), as opposed to sessile in which the tumours are solid and flat (Shirai *et al.*, 1989). Tumours can also exhibit both papillary and sessile (mixed) architecture.

### **2.3.3 Non-Muscle and Muscle Invasive Bladder Cancer**

The cardinal symptom of UBC is painless visible haematuria (presence of blood in the urine), occurring in over 80% of patients at presentation (Wallace *et al.*, 2002; Kaufman *et al.*, 2009). It requires prompt investigation, most often in a 'haematuria clinic' setting (Lynch *et al.*, 1994). Further investigation of patients suspected of having UBC requires multiple diagnostic procedures, including imaging of the upper urinary tract, urine cytology and cystoscopy (Kaufman *et al.*, 2009; Hollenbeck *et al.*, 2010; Babjuk *et al.*, 2011). Briefly, urine cytology is a non-invasive test which involves looking for abnormal cells in a urine sample with the use of a microscope. Urine cystoscopy is an invasive test which makes use of a cystoscope, an instrument with a light and a camera, inserted through the urethra into the bladder to image and inspect the bladder. In most cases the diagnosis is subsequently confirmed following Transurethral Resection of Bladder Tumour (TURBT) (Kaufman *et al.*, 2009; Babjuk *et al.*, 2011).

NMIBC is typified by a high rate of recurrence (15-61% at one year, depending upon risk category (Sylvester *et al.*, 2006)) and so long-term, even lifelong, surveillance with outpatient flexible cystoscopy is the mainstay of subsequent management (Kaufman *et al.*, 2009; Babjuk *et al.*, 2011). Progression to MIBC (Muscle Invasive Bladder Cancer) is also a concern for high-risk NMIBC patients, occurring in up to 17% of patients at one year (Sylvester *et al.*, 2006). Progression to (or presentation with) muscle-invasive disease (stages T2-4) represents the critical step in the disease course, necessitating more radical therapies and carrying a 5-year survival rate of only 27-50% (Wallace *et al.*, 2002; Advanced Bladder Cancer (ABC) Meta-analysis Collaboration, 2005).

#### **2.3.4 Muscle Invasive Bladder Treatment**

Patients who present with, or progress to, MIBC are treated by radiotherapy (Kaufman *et al.*, 2009; Stenzl *et al.*, 2011), chemoradiotherapy (James *et al.*, 2012), partial or radical cystectomy, or neoadjuvant (a therapy given before another treatment which attempts to increase the success of the later treatment (Trimble *et al.*, 1993)) chemotherapy followed by radical cystectomy (Advanced Bladder Cancer (ABC) Meta-analysis Collaboration, 2005; Kaufman *et al.*, 2009; Stenzl *et al.*, 2011; Smith *et al.*, 2014). Radical or partial cystectomy procedures involve removing all or part of the bladder, respectively (Kaufman *et al.*, 2009). Problems and side effects associated with MIBC treatment include: excess mucus production, electrolyte imbalance and subsequent tumour relapse (Kaufman *et al.*, 2009; Pokrywczynska *et al.*, 2014).

### 2.3.5 Non-Muscle Invasive Bladder Treatment

Transurethral Resection of Bladder Tumour (TURBT) is the mainstay of treatment for non-muscle invasive bladder cancer and was first described as suitable surgery by Maximillian Stern and Joseph McCarthy in 1930 (Blandy *et al.*, 2005). It is still considered to be the gold standard today (Wilby *et al.*, 2009). The equipment required for TURBT comprises: a stainless steel outer and inner sheath, an irrigation system, a light source provided via a fibre optic guide from a filament lamp, a rod lens cystoscope attached to a video camera head and a trigger-operated spring-loaded electrically-active wire cutting loop or diathermy loop (figure 2.7). The combination of the cutting loop, the cystoscope and the camera head are termed a 'resectoscope'. There are many resectoscopes on the market made by companies including: Olympus (Tokyo, Japan), Stryker (Kalamazoo, USA), Storz (Tuttlingen, Germany) and Richard Wolf (Knittlingen, Germany).

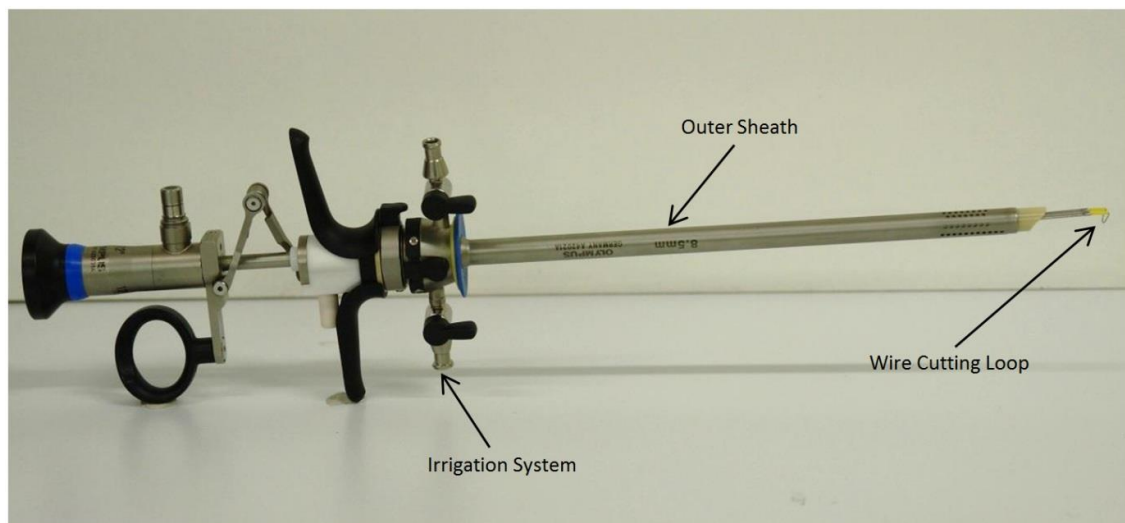


**Figure 2.7 – Side view of Olympus OES Pro resectoscope.**

The method for TURBT procedures is as follows: following a thorough cystoscopy and bimanual examination, the surgeon inserts the resectoscope into the bladder via the urethra. Once inside the bladder, the surgeon will examine the bladder and locate the tumour(s) utilising the high quality video camera attached to the cystoscope. The TURBT will then commence utilising the diathermy cutting loop. The diathermy loop is used to cut into the tumour to remove it in slices or 'chips' (Blandy *et al.*, 2005; Wilby *et al.*, 2009), this method can be seen in figure 2.8.

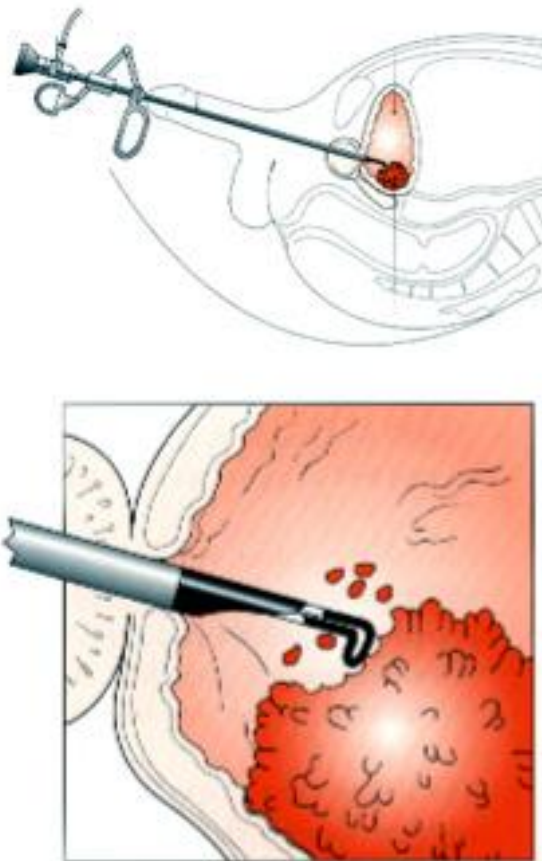


**Figure 2.8 – Transurethral Resection of Bladder Tumours (Copyright**

<http://bladder.cancercaregiving.com/bladder-cancer-treatment/>).

Irrigation into and out of the bladder via the sheath is used throughout the procedure to distend the bladder (which smooths its mucosal surface as it is otherwise folded when the bladder is empty) and to wash away blood and smaller pieces of tumour debris (to maintain good vision). The larger pieces of tumour or 'chips' are either drained out of the bladder by simply removing the resectoscope from the outer sheath, or are washed out by the use of an Ellik bladder evacuator or similar. These evacuators are made from flexible polymers which are connected to the resectoscope and, when squeezed and released, create back pressure forcing irrigating solution and the pieces of tumour out of the bladder and into the evacuator. The surgeon will repeat this process until all of the tumour has been visually removed. The diathermy cutting loop, or alternatively a diathermy 'roly-ball', will then be used to cauterise bleeding vessels and healthy-looking bladder mucosa immediately surrounding the base of the tumour to achieve a 'negative margin'. Negative margin refers to a margin of normal healthy tissue around the base of the tumour to improve confidence in complete tumour removal and to reduce the risk of tumour recurrence (Blandy *et al.*, 2005; Ray and O'Brien, 2007; Wilby *et al.*, 2009).

There are two different types of energy that can be used for wire loop TURBT, these are monopolar and bi-polar. Monopolar describes electrical current coming into contact with the bladder through the wire loop and then leaving the body through a metallic plate attached to the patient's leg. Bi-polar describes the electrical current entering, coming into contact with and leaving the bladder via the cutting loop. The irrigating solution in a TURBT is dependent on the type of energy source being used, for bi-polar resection an isotonic solution such as saline is required, whereas monopolar resection makes use of hypotonic solutions such as glycine or water (Cauberg *et al.*, 2009).



### 2.3.6 Non-Muscle Invasive Bladder Treatment Problems

The main problem with the use of TURBT for tumour resection is that tumours are removed piecemeal; this can be seen in figure 2.9.

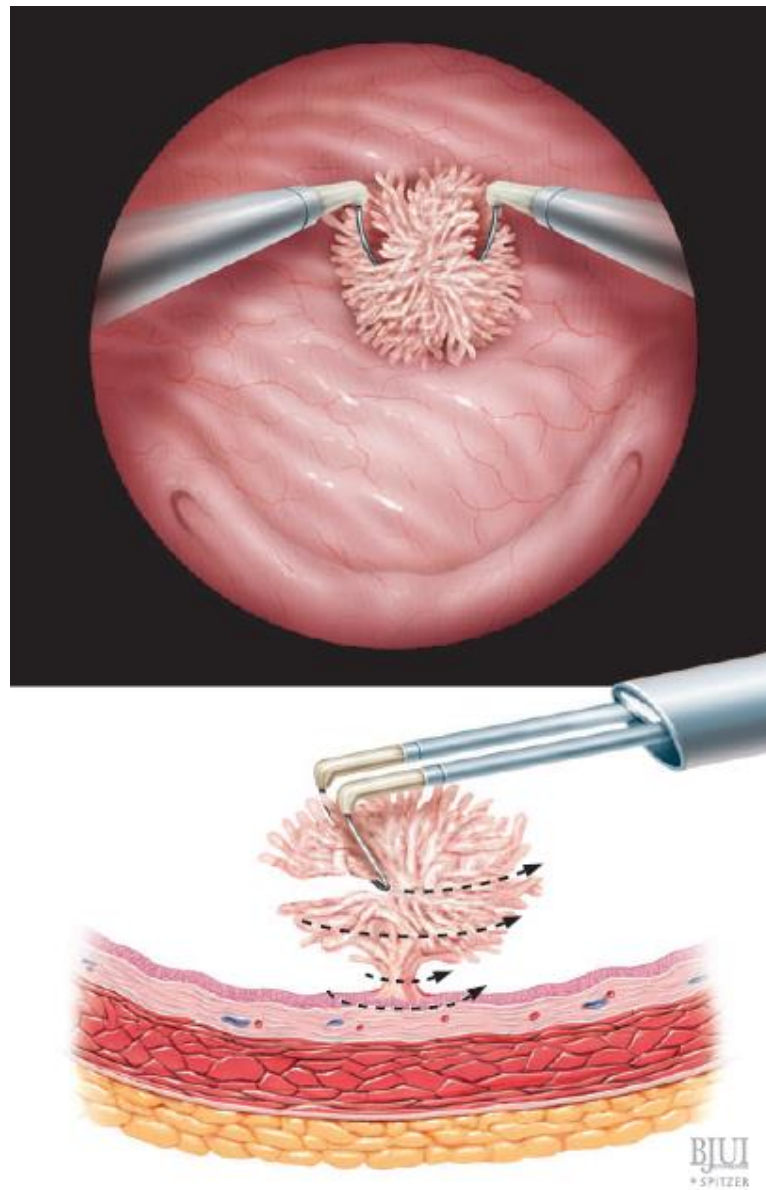


**Figure 2.9 – Piecemeal removal of bladder cancer (reproduced with permission from John Wiley and Sons (Wiesner *et al.*, 2010)).**

This is contrary to basic principles of surgical oncology whereby tumours should be removed *en bloc* (Wilby *et al.*, 2009; Ray and O'Brien, 2007); therefore, a negative lateral or deep margin cannot be guaranteed. Ray and O'Brien (2007) state that for any other tumour apart from tumours in the bladder, piecemeal resection "would be considered oncological madness". Moreover, resecting the tumour whilst irrigating the bladder creates a solution of potentially viable tumour cells within the bladder. These cells can subsequently re-implant at the tumour site or elsewhere within the entirety of the bladder (Bryan *et al.*, 2010; Kondas *et al.*, 1999). *En bloc* resection with a negative margin would be ideal as it would prevent the scattering of tumour cells and would ensure that only normal tissue is present in the bladder post resection (Ray and O'Brien, 2007).

The mechanisms of recurrence of NMIBC were described by Kondas *et al.* (1999) as: (i) incomplete resection of the primary urothelial cancer; (ii) tumour cell re-implantation; (iii) growth of microscopic tumours present at the time of the previous resection and (iv) new tumour formation. Utilising alternative optical technologies (such as narrow band imaging and photodynamic diagnosis (Patel *et al.*, 2011)) may reduce the positive margin rate (incomplete resection). It may also identify small tumours otherwise missed by conventional white light cystoscopy; however, these approaches have not been universally-adopted and do not change the fundamental principles of the procedure. Thus, surgical failure is considered to be an important contributor to the high recurrence rates observed in patients with NMIBC (Bryan *et al.*, 2010). Recurrence rates vary from 15 – 61 % at year 1 and 31 – 78 % at 5 years depending on risk factors such as: number of tumours, size of tumour(s), prior recurrence, T stage and grade (Sylvester *et al.*, 2006). These rates are considered to be unacceptably high (Wilby *et al.*, 2009; Sylvester *et al.*, 2006), and result in repeated TURBTs

which are both burdensome to patients and expensive for healthcare providers (Sangar *et al.*, 2005; Svatek *et al.*, 2014).

### **2.3.7 Bladder Cancer Summary**

Due to the relatively high incidence and high recurrence of bladder cancer it has become expensive for healthcare providers to treat (Bryan *et al.*, 2014). In the United States of America in 2001 the accumulated cost of bladder cancer was \$3.7 billion (Lotan *et al.*, 2009). Despite this, there is only modest research funding for UBC compared to other malignancies (Lotan *et al.*, 2009). As a result there has been a lack of scientific advancement in the field (Lotan *et al.*, 2009; Kaplan *et al.*, 2014).

There has been research into tissue engineering of bladders (Badylak, 2004) which could be useful as whole or partial bladder replacements for MIBC (Orabi *et al.*, 2013). Also, research is underway to investigate how to remove NMIBC *en bloc* and whether novel imaging techniques for TURBT are sufficient to find smaller tumours (Bach *et al.*, 2015). However, little has been done to reduce the scattering effect of TURBT (Wilby *et al.*, 2009).

## **2.4 Mechanical Properties of Materials**

### **2.4.1 Introduction**

The mechanical properties of a material describe how a material will behave when subjected to a load. The type of mechanical property depends on how the material is loaded. In the following section both elastic and viscoelastic properties are described. Elastic material properties assume no time dependant behaviour, whereas viscoelastic properties

assume differences in mechanical properties depending on strain or loading rate.

Throughout this thesis mechanical properties are used to quantify and describe tissues.

### 2.4.2 Stiffness

Stiffness ( $k$ ) is a measure of the rigidity of an object. Stiffness measures the resistance of a structure to an applied load and is calculated using equation 2.1.

$$k = \frac{F}{\Delta L} \quad (2.1)$$

where  $F$  is the applied force and  $\Delta L$  the change in length of the structure, which can be seen in figure 2.10.

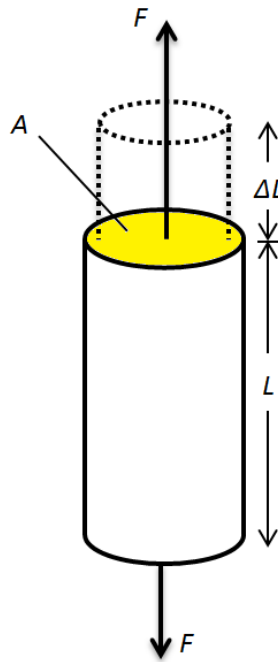


**Figure 2.10 – Cylindrical rod subjected to a tensile force ( $F$ ) with cross sectional area ( $A$ ) highlighted in yellow, original length ( $L$ ) and change in length ( $\Delta L$ ).**

Stiffness is a structural property and as such is influenced by variations in specimen geometry and the materials of which it is comprised. Stiffness can be used to decide whether a structure, such as a spring, is rigid enough to support a given load for a specific application. This is in contrast to a Young's modulus ( $E$ ) (described in section 2.4.3) which accounts for specimen geometry; a specimen of any size composed of the same material will return the same modulus (Millard *et al.*, 2011).

### 2.4.3 Young's Modulus

Young's modulus ( $E$ ) is a material property which is measured in Pascals (Pa). It can be described as the ratio of the stress ( $\sigma$ ) induced in a material to the strain ( $\epsilon$ ), as shown in equation 2.2.

$$E = \frac{\sigma}{\epsilon} \quad (2.2)$$

Young's modulus is a measure of rigidity, in terms of area, and measured per unit length. It is used to compare materials. The engineering stress ( $\sigma$ ) that is induced in a material is equal to the force ( $F$ ) applied on the materials divided by its initial cross sectional area ( $A$ ) (equation 2.3).

$$\sigma = \frac{F}{A} \quad (2.3)$$

The engineering strain ( $\epsilon$ ) that is experienced by a material is equal to the change in length ( $\Delta L$ ) divided by its original length ( $L$ ) and as such is dimensionless (equation 2.4).

$$\epsilon = \frac{\Delta L}{L} \quad (2.4)$$

Figure 2.10 shows a cylindrical rod tensile test schematic which can be used to determine Young's modulus. An example of a material with a low modulus is silicone which has a Young's modulus of 8 – 30 MPa (Granta Design Ltd, 2013). An example of a material with a high modulus is medium carbon steel which has a Young's modulus of 207 GPa (Callister and Rethwisch, 2012). Young's modulus is measured using a tensile ramp test to 'pull' a material apart to failure. Whilst this test is taking place load and displacement measurements are recorded and used to calculate stress and strain using equations 2.3 and 2.4 (ASTM International, 2010). Figure 2.11 shows a typical metal stress strain curve for the test.

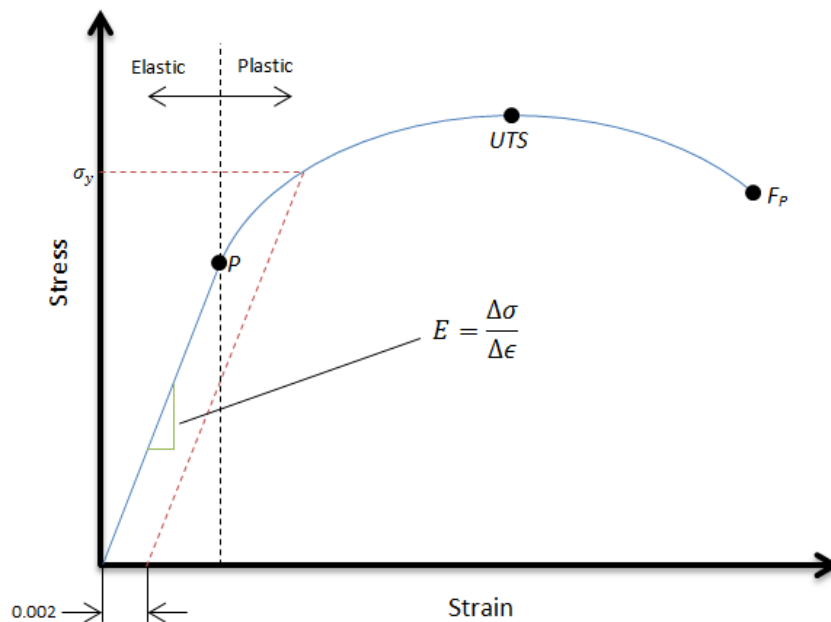


**Figure 2.11 – Typical stress strain curve for a metal (adapted from Callister and Rethwisch (2012)). The gradient of the elastic linear portion represents the Young's modulus of the material,  $P$  denotes the proportional limit,  $\sigma_y$  the yield strength taken parallel to the elastic slope at 0.002 strain,  $UTS$  the ultimate tensile strength and  $F_P$  the fracture point of the material.**

There are two regions that can be seen in figure 2.11: the elastic and plastic regions. The elastic part of the curve is the region where the material has been deformed but is able to return to its original shape; whereas, the plastic region defines the later part of the curve where the material will not return to its original shape when unloaded. The Young's modulus is taken from the slope of the curve before the elastic limit. As it is difficult to accurately measure where the elastic limit occurs there is a convention that the yield stress ( $\sigma_y$ ) is taken from a parallel slope to the origin to proportional limit slope, at 0.002 strain. For materials such as rubbers, which exhibit non-linear elastic behaviour, different types of moduli are used to characterise their material properties. For example, a secant modulus takes the slope of the curve from the origin to any point on the curve; instead, a tangent modulus takes the slope from a tangential line at any point on the curve (Callister and Rethwisch, 2012). There are, however, issues with these moduli: a secant modulus assumes linear behaviour when, in all likelihood, the behaviour is not linear. A tangent modulus varies depending on the stress or strain value at which it is taken.

Another phenomenon that can be seen during the deformation of a material, such as in the tensile test shown in figure 2.10, is the shortening of the transverse diameter whilst the longitudinal length increases. This effect is described by the Poisson's ratio ( $\nu$ ) which is calculated as the negative ratio of the transverse strain to the longitudinal strain (equation 2.5) (Callister and Rethwisch, 2012).

$$\nu = -\frac{\varepsilon_t}{\varepsilon_l} \quad (2.5)$$

where  $\varepsilon_t$  is the transverse strain which is positive when the transverse length of the test specimen is increasing.  $\varepsilon_l$  is the longitudinal strain which is positive when the length of the

longitudinal length is increasing. Some typical values for Poisson's ratio are 0.49 for rubber and 0.3 for steel (Granta Design Ltd, 2013). If a material is linearly elastic and is homogenous and isotropic (i.e. displays the same mechanical properties independent of direction), then the Young's modulus ( $E$ ) and Poisson's ratio ( $\nu$ ) can determine the strain of the material to an applied stress in any direction and *vice versa*, provided the material is not stressed past its yield strength ( $\sigma_y$ ) (Callister and Rethwisch, 2012).

#### **2.4.4 Viscoelastic Materials**

Viscoelastic materials can be defined as materials that exhibit both elastic and viscous behaviour. The strain response of a perfectly elastic material to an induced stress is instantaneous. This is in contrast to materials with a viscous element where the response is time dependant. The elastic and viscous properties of a material can be characterised by storage ( $E'$ ) and loss modulus ( $E''$ ), respectively. Dynamic modulus ( $E^*$ ) is a complex number which is made up of real and imaginary components where  $E'$  lies on the real axis and  $E''$  on the imaginary axis (Hukins *et al.*, 1999). Some examples of viscoelastic materials include biological tissues, natural and synthetic polymers (Menard, 2008). The relationship between  $E'$ ,  $E''$ , and phase lag ( $\delta$ ) are shown in figure 2.12.



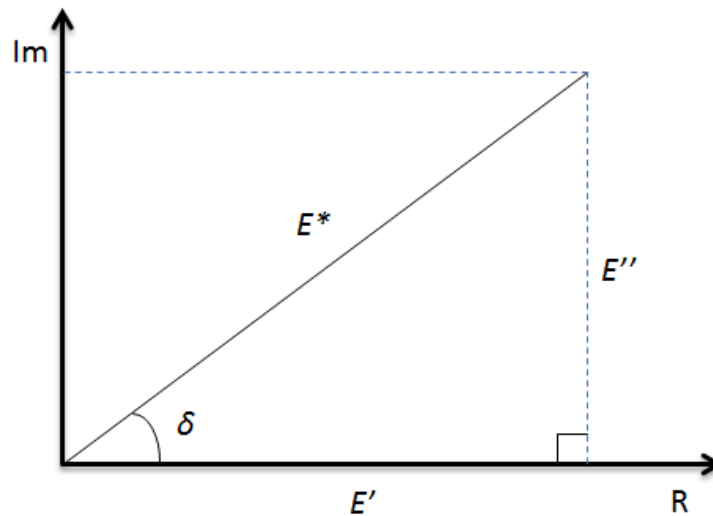


**Figure 2.12 – Argand diagram of phase lag ( $\delta$ ), dynamic ( $E^*$ ), storage ( $E'$ ) and loss ( $E''$ ) moduli where Im is the imaginary and R is the real axis.**

The storage modulus refers to the rigidity of a material. It characterises the ability of a material to store energy, used for the elastic response when a stress is removed from a viscoelastic material. The loss modulus characterises the ability of a material to dissipate energy due to friction and internal motions. Rigidity is related to work done when deforming a material and hence the amount of energy a material can potentially store and lose. The energy loss of a viscoelastic material can be seen in a hysteresis loading-unloading loop (figure 2.13) where the energy dissipated is given by the area within the loop (Menard, 2008).

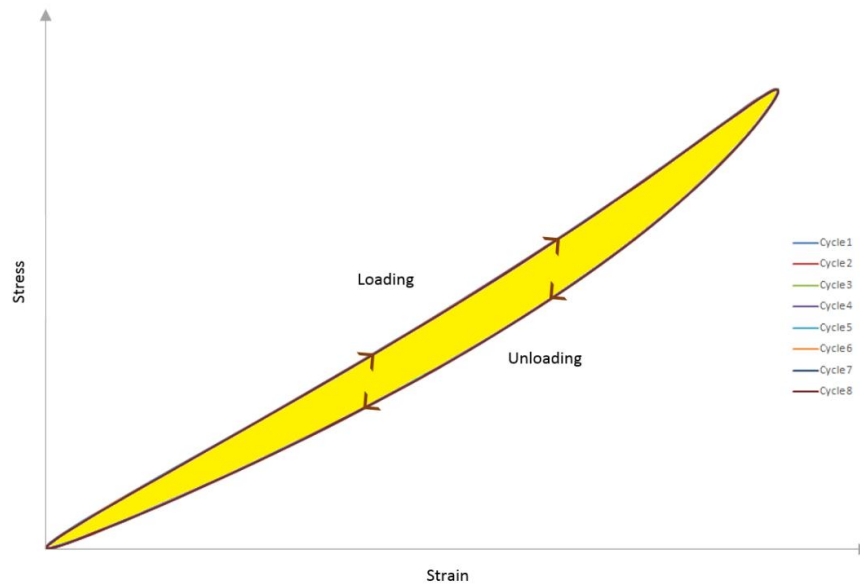


**Figure 2.13 – Stress strain hysteresis loops for a silicone disc specimen subjected to 8 cycles of loading and unloading. The area highlighted yellow is the energy lost per unit volume.**

The dynamic modulus at a given angular frequency,  $E^*(\omega)$ , is analogous to Young's modulus at the equivalent loading rate. However, they are difficult to compare as  $E^*$  is a dynamic property whereas Young's modulus is taken from one test potentially up to failure.  $E^*$  can be determined following multiple loading cycles or from a stress relaxation or creep tests. When a material is subjected to a sinusoidally varying stress or strain  $E^*$  also takes into account the unloading of a material which is in contrast to Young's modulus, which is typically calculated from the loading slope only.

### 2.4.5 Stress Relaxation and Creep

Viscoelastic materials exhibit stress relaxation and creep. Stress relaxation describes the decrease in stress that is observed when a viscoelastic material is held at a given strain

for a certain length of time. A graph of stress and strain against time representing stress relaxation can be seen in figure 2.14 (Ward and Sweeney, 2004).

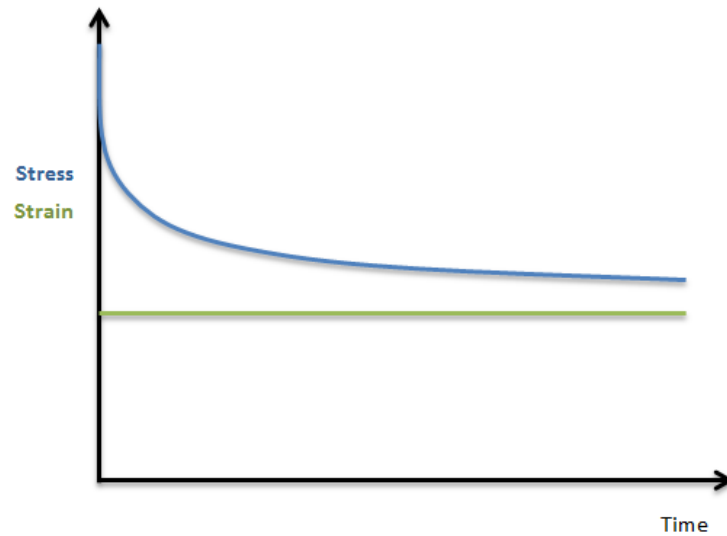


**Figure 2.14 – Stress (blue) and strain (green) against time during stress relaxation.**

Creep describes the increase in strain that is observed over time when the stress induced in a viscoelastic material is held constant. An illustration of this can be seen in figure 2.15 (Ward and Sweeney, 2004).

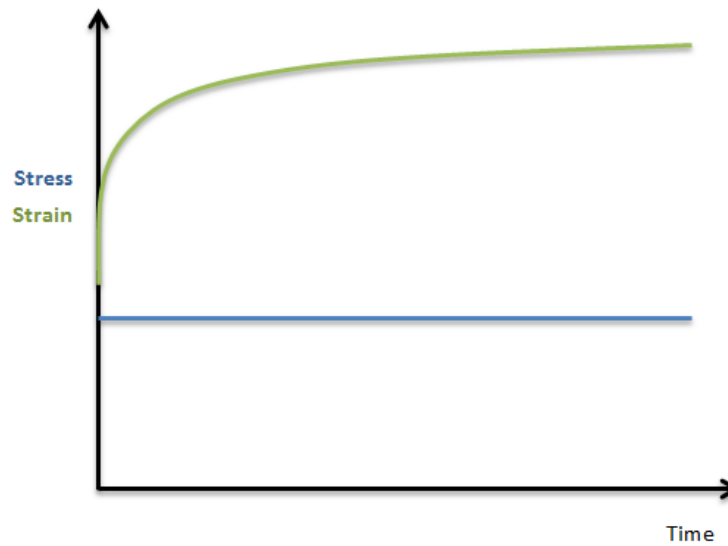


**Figure 2.15 – Stress (blue) and time-dependent strain (green) during creep testing.**

Briefly, the storage and loss moduli of viscoelastic materials, derived from  $E^*$ , can be calculated from creep and stress relaxation curves using equation 2.6 (Arridge and Barham, 1986; Aspden, 1991; Holmes and Hukins, 1996).

$$E^*(f) = E_R + 2\pi if \int_0^{\infty} \{E(t) - E_R\} \exp(2\pi ift) dt \quad (2.6)$$

where  $E_R$  is the theoretical equilibrium value that the modulus will tend toward after such a time that all stress relaxation or creep are complete and  $E(t)$  is the value of modulus at time,  $t$ . The stress relaxation or strain increase (creep) exponential curves are analysed using Fourier transforms from which storage and loss modulus are calculated (Aspden, 1991; Holmes and Hukins, 1996).

#### 2.4.6 Dynamic Mechanic Analysis

Dynamic Mechanical Analysis (DMA) is another method of measuring the viscoelastic properties of a material. DMA can be used to characterise both the elastic and viscous parts of a material with storage ( $E'$ ) and loss ( $E''$ ) moduli, respectively. DMA enables properties of viscoelastic materials to be found at a variety of frequencies. It is useful because it enables the short term effects of loading on viscoelastic properties to be found. This is in contrast to stress relaxation and creep tests which are useful for determining longer term effects on viscoelastic materials (Menard, 2008).

DMA measures the time dependant response of a viscoelastic material as a phase lag, which is measured in degrees ( $^{\circ}$ ). This is different to creep and stress relaxation tests where an equilibrium modulus is used. A perfectly elastic material has a phase lag ( $\delta$ ) of  $0^{\circ}$  and a perfectly viscous material has a phase lag ( $\delta$ ) of  $90^{\circ}$  (Menard, 2008).

DMA involves applying a known oscillating load, or displacement, to a structure in the form of a sinusoidal wave and then measuring the response. A representation of this can be seen in figure 2.16 where a sinusoidal load has been applied and the subsequent sinusoidal displacement has been measured.

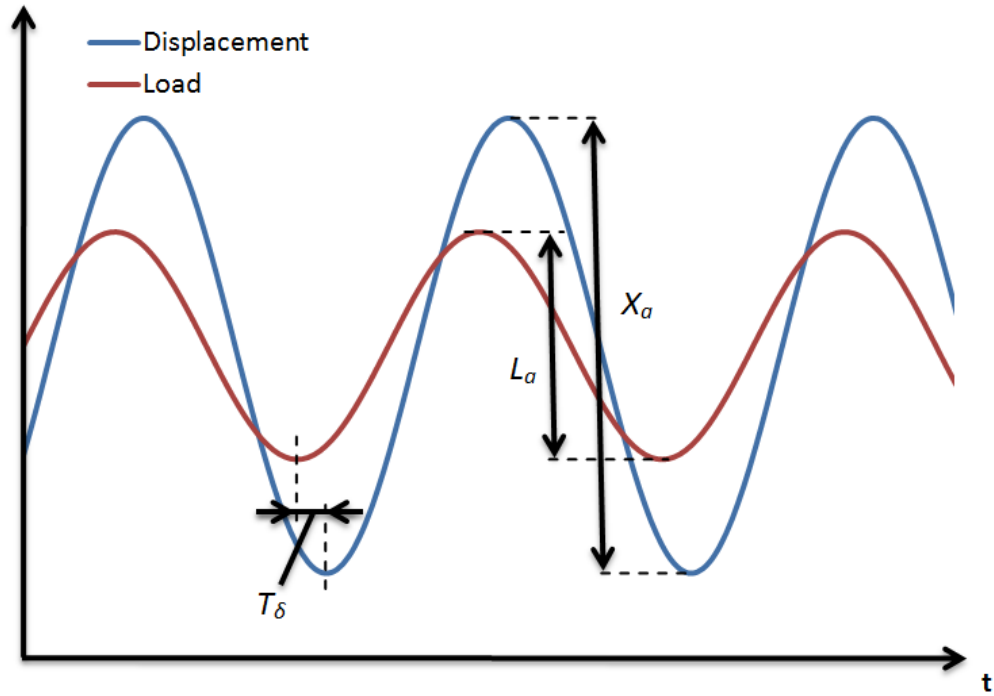


**Figure 2.16 – Sinusoidally varying load input and displacement response for a viscoelastic material.  $T_\delta$  is the time lag between the two waves, phase lag ( $\delta$ ) can be calculated from this by multiplying by angular frequency ( $\omega$ ) (i.e.  $\delta = \omega T_\delta$ ).**

Fourier analysis is then used to determine the fundamental frequencies and amplitudes of both the input and the response waveforms. The amplitude is from the peak to the trough of the waveform. The dynamic stiffness ( $k^*$ ) is then calculated using the load ( $L_a$ ) and the displacement amplitude ( $X_a$ ), see figure 2.16.

$$k^* = L_a / X_a \quad (2.7)$$

The phase lag ( $\delta$ ) is calculated using the fundamental frequency waves found from the Fourier analysis. The time lag between the two waves ( $T_\delta$ ) is multiplied by the angular frequency ( $\omega$ ) which converts time to degrees and gives the phase lag ( $\delta$ ).

$$\delta = \omega T_{\delta} \quad (2.8)$$

With values for dynamic stiffness ( $k^*$ ) and phase lag ( $\delta$ ), storage ( $k'$ ) and loss stiffness ( $k''$ ) can then be found using the following formulae:

$$k' = k^* \cos \delta \quad (2.9)$$

$$k'' = k^* \sin \delta \quad (2.10)$$

These formulae are derived from the relationship shown in figure 2.10. These stiffness values can be converted to moduli ( $E^*$ ,  $E'$  or  $E''$ ) using a shape factor ( $S$ ). For example, the shape factor for rectangular samples can be calculated from:

$$S = wd/h \quad (2.11)$$

where  $w$  is width,  $d$  is depth and  $h$  is height of the specimen (Menard, 2008).

Both storage ( $k'$ ) and loss ( $k''$ ) stiffness can be converted to storage ( $E'$ ) and loss ( $E''$ ) moduli by dividing by shape factor ( $S$ ) (Fulcher *et al.*, 2009).

$$E' = k'/S \quad (2.12)$$

$$E'' = k''/S \quad (2.13)$$

The main advantage of DMA is that it can determine viscoelastic properties quickly as opposed to creep and stress relaxation tests. The DMA software used in this thesis acquired data at varying rates from the sine waves depending on the value of the frequency so that

the entire sinusoidal waveform was accounted for in the data acquisition, i.e. at higher frequencies the data sampling rate was higher. Another issue with creep testing is that very high resolution data acquisition is required for the user to be able to calculate equivalent dynamic moduli at high frequencies. DMA is useful as variables such as frequency or temperature can be changed during testing (Menard, 2008).

#### **2.4.7 Mechanical Properties of the Bladder**

The mechanical properties of *porcine* and human longitudinal rectangular specimens of bladder, in terms of ultimate tensile strength and elastic modulus, have been shown to be similar by Dahms *et al.* (1998). The study reported ultimate tensile strength (UTS) values of 0.32 MPa and 0.27 MPa, and also elastic moduli of 0.26 MPa and 0.25 MPa for *porcine* and human bladder, respectively. The study also investigated *murine* bladder using the same techniques and reported an ultimate tensile strength of 0.72 MPa and a modulus of 0.76 MPa.

Other uniaxial tests on *porcine* bladder rectangular specimens have been reported by Korossis *et al.* (2009), Zanetti *et al.* (2012) and Natali *et al.* (2015). The study by Korossis *et al.* (2009) found that in all regions of the bladder the ultimate tensile stresses exhibited by the longitudinal specimens was higher than that of the transverse specimens. For example, in the lateral region the longitudinal UTS was 1.6 MPa as opposed to 0.8 MPa in the transverse direction. Also using ramp tests they reported higher stiffnesses in the longitudinal direction for every region tested. Zanetti *et al.* (2012) reported on the differences in mechanical properties of the *porcine* bladder depending on the number of



cycles in terms of the secant modulus. This study also investigated the dynamic modulus calculated from stress relaxation. Natali *et al.* (2015) used cyclic tests at different strain rates to determine the stress-strain behaviour of *porcine* bladder rectangular strips and found higher stiffnesses in the transverse direction.

In addition, other uniaxial tests on the bladder have been reported. Alexander (1971) identified three mechanical components of rat, cat and rabbit bladders during deformation, these were a rapid viscoelastic element, a slow plastoelastic element and a slow creep. Another study by Alexander (1976) investigated series elasticity of looped rat bladder specimens during stress relaxation and found that contractile cross bridges did not affect the elasticity measured. Work by van Mastrigt *et al.* (1978) investigated stress relaxation, pulsing and force extension of pig and dog bladders. They found that dog bladders exhibited “mainly passive properties” whereas “pig bladders showed more active properties”. Griffiths *et al.* (1979) measured the active properties of pig bladder strips subjected to electrical stimulation and found a linear increase in the force exerted (against time) by a “pre-stretched” strip which rose to a maximum steady value and then decreased. Finkbeiner and O’Donnell (1990) “stretched” guinea pig and rat bladder strips and found that the tension generated depended on the loading rate.

There have also been studies which have investigated biaxial mechanical properties. Gilbert *et al.* (2008) found that the pig bladder specimens they tested were stiffer in the longitudinal direction. Chen *et al.* (2013) also found that *murine* bladder exhibited higher stiffness in the longitudinal direction. Gloeckner *et al.* (2002) found that inactive spinal cord injured rat bladders (tested 10-14 days after injury) were consistently more compliant than

normal rat bladders. Finally, Nagatomi *et al.* (2004) investigated the stress relaxation of rat bladder also following spinal cord injury and found less stress relaxation in the spinal cord injured rats compared to control non spinal cord injured bladders.

## **2.5 Shape Memory Alloys**

### **2.5.1 Shape Memory Effect**

A shape memory alloy is a material which exhibits a shape memory effect. The material can 'remember' a pre-set shape and, depending on the specific composition of the alloy, after deformation it will return to this shape either with heating or spontaneously. Heat recoverable strains exhibit shape memory and spontaneous recovery superelasticity. The most well known shape memory alloy, nickel titanium, was discovered at the US Naval Ordnance Laboratory and reported in 1963, hence the acronym Nitinol (Buehler *et al.*, 1963; Gil and Planell, 1998; Otsuka and Wayman, 1999; Morgan and Broadley, 2004).

### **2.5.2 Shape Memory**

A shape memory alloy (SMA) such as Nitinol, has the ability to 'remember' a pre-set shape and because of this can be trained to return to a particular shape when heated. This is due to the two solid phases that shape memory alloys have: martensite and austenite. When the SMA is at a lower temperature than its transition temperature it is in the martensite phase and has a specific crystal structure; these can be seen in figure 2.17 during the martensite states. Then, when the material is heated past its transition temperature, the crystal structure of the SMA changes to austenite. This crystal structure change is also called

a phase change and provides the means for the material to return to a set high temperature shape. Subsequently, when the material cools after heating, the crystal structure reverts to martensite. This phase change is also referred to as the one-way shape memory effect (Gil and Planell, 1998; Otsuka and Wayman, 1999).

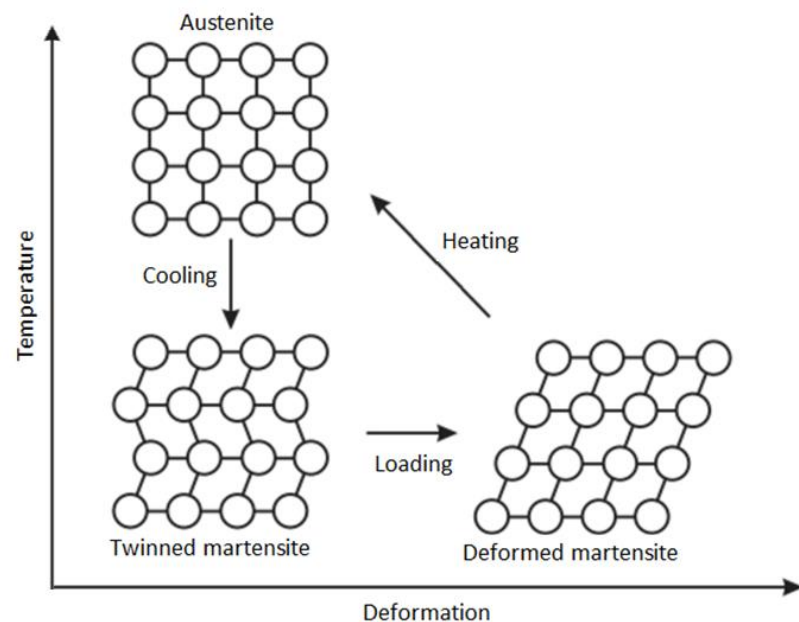


**Figure 2.17 – Crystal structure change during loading and shape recovery of a shape memory alloy (adapted from Uehara *et al.* (2009)).**

### 2.5.3 Superelasticity

The superelasticity phenomena exhibited by shape memory alloys can be defined as a material that will recover from an induced strain by just releasing the load applied to it. This is due to the material's Austenite finish ( $A_f$ ) temperature being below the temperature

to which the material is being exposed. It is on this principle that shape memory alloy medical devices such as stents work (Gil and Planell, 1998; Otsuka and Wayman, 1999).

#### **2.5.4 Shape Memory Training**

This high temperature shape is trained into the material by fixing it in a desired position and heating it to a high temperature, somewhere in the range of 450 – 550 °C, for a time ranging from 5 to 25 minutes. These parameters are variable depending on the specific composition of the Nitinol and the transition temperature that is desired. When the alloy is below the transition temperature it can be deformed to any shape and when heated past the transition temperature it will return to the trained high temperature shape, hence, demonstrating the one-way shape memory effect (Otsuka and Wayman, 1999; Morgan and Broadley, 2004).

#### **2.5.5 Two-way Shape Memory Effect**

The two-way shape memory is another phenomena exhibited by shape memory alloys. Effectively both high and low temperature (austenite and martensite) shapes can be trained into the material. The difference from the one-way shape memory effect is that with the two-way effect, when cooling from the austenite phase to the martensite, the material changes shape rather than just remaining in the same austenite shape (Gil and Planell, 1998). The difference can be seen in figure 2.18.

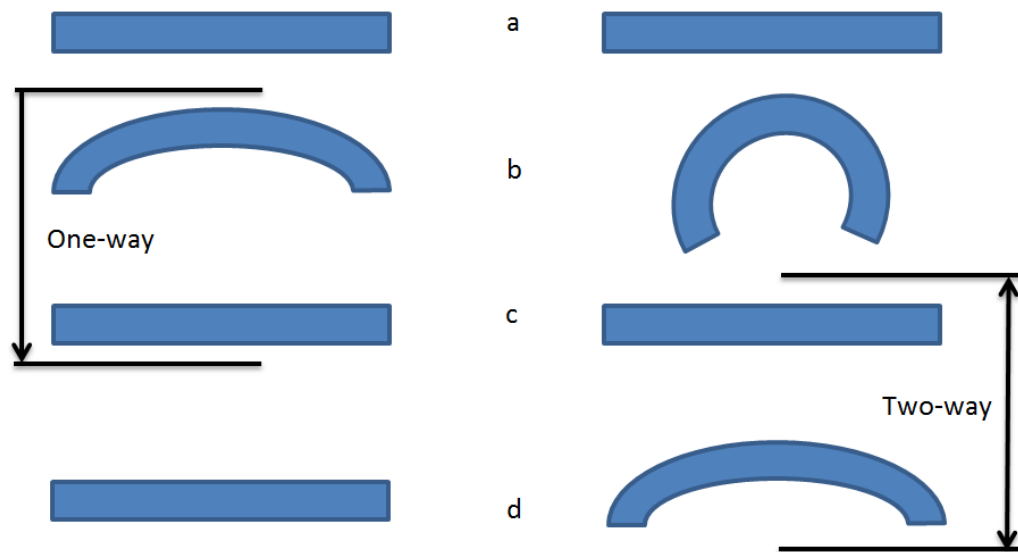


**Figure 2.18 – One-way (left column) and two-way (right column) shape memory effect. Where a) is the starting martensite shape, b) is the deformed martensite shape, c) is the heated austenite shape and d) is the cooled martensite shape (adapted from Gil and Planell (1998)).**

The two way shape memory effect can be trained into a shape memory alloy by deforming the material, when cooling from austenite to martensite, to a desired shape. This two-way training needs to be repeated multiple times for the material to effectively conform to a low temperature shape without external forces (Gil and Planell, 1998; Luo and Abel, 2007; Fortini *et al.*, 2014).

### **2.5.6 Medical Applications of Shape Memory Alloys**

Nitinol is the shape memory alloy that is predominantly used in medical applications. Although Nitinol alloys are more expensive than stainless steels, they are attractive for use within the body. They are non-magnetic, they possess physical properties which more

accurately mimic the mechanical behaviour of human tissues and bones, they are bio-compatible, they exhibit high corrosion resistance (better than stainless steel) and they can be manufactured to respond to body temperature (Machado and Savi, 2003; Mohd Jani *et al.*, 2014).

After discovery in 1962, the first main medical application of Nitinol was in superelastic orthodontic braces. One of the most popular uses of shape memory alloys are in cardiovascular devices such as stents. Shape memory stents are preferable to stainless steel as they can exert an outward force and are more compliant so can bend to the contours of blood vessels. Shape memory alloys are also used in medical devices such as bone plates, medical tweezers, anchors, implants, eyeglass frames and guide wires (Machado and Savi, 2003; Mohd Jani *et al.*, 2014). Nitinol devices such as stents and graspers for kidney stones (Kourambas *et al.*, 2000) are ideal for use in the body as they can be inserted through small incisions or through orifices via catheters and expand once positioned in the correct place.

### **2.5.7 Other Shape Memory Materials**

Certain polymers, such as: polynorbornene, poly(*trans*-isoprene), styrene-butadiene copolymers and polyurethane elastomers, can also exhibit the shape memory effect. In comparison to Nitinol, which can recover strains up to 8% (van Humbeeck, 1999; Liu *et al.*, 2007), shape memory polymers (SMPs) allow for deformations of up to 400% (Lendlein and Langer, 2002). SMPs are also cheaper than SMAs, are less dense and can be biodegradable in addition to biocompatible (Liu *et al.*, 2007).

Lendlein and Langer (2002) have described a biodegradable, biocompatible suture which is able to provide tension to hold together the edges of an incision or wound to aid the healing process. SMPs do however, depending on the specific polymer, have slower return speeds and, as would be expected, have lower Young's moduli (Liu *et al.*, 2007) which will prevent use in certain structural applications.

## 2.6 Chapter Summary

This background chapter can be summarised as follows:

- The urinary bladder is part of the urinary system and is responsible for the storage and release of urine.
- Non-muscle invasive bladder cancer has a high recurrence rate which is, in part at least, caused by the dated gold standard method of surgery used for treatment, transurethral resection of bladder tumours (TURBT).
- Dynamic mechanical analysis is a dynamic method which can be used to measure the viscoelastic properties of a material.
- Shape memory alloys have the ability to 'remember' a pre-set shape or shapes. Transformation to a pre-set shape can be induced using heat.

## 3 Frequency Dependant Viscoelastic Properties of *Porcine* Bladder

### 3.1 Introduction

The aim of this chapter was to use Dynamic Mechanical Analysis (DMA) to measure the viscoelastic properties of *porcine* bladder tissue. Bladder tissue is a viscoelastic material, but the exact bladder tissue stiffness response to a frequency sweep is unknown. Viscoelastic structures can be defined by storage ( $k'$ ) and loss stiffness ( $k''$ ). Storage stiffness characterises the structure's ability to elastically store energy and loss stiffness characterises the structure's ability to dissipate energy that is lost due to the viscous processes occurring in the structure, viscoelastic materials are described in section 2.4.4. Previous studies on the bladder have investigated stress relaxation (van Mastrigt and Nagtegaal, 1981), elastic modulus (Dahms *et al.*, 1998) and also the cyclic stress-strain properties (Zanetti *et al.*, 2012). However, none have measured the viscoelastic properties, in terms of storage and loss stiffness, over a frequency range. A detailed understanding of bladder viscoelasticity is vital for developing accurate computational models of the bladder, for the development of replacement materials and to test the suitability of current autograft techniques, such as the creation of a 'neobladder' from part of the patient's bowel (Pokrywczynska *et al.*, 2014).

This chapter describes the DMA testing of *porcine* bladder tissue. Section 3.2 describes the materials and methods used to find the viscoelastic properties of porcine bladder tissue and the preliminary testing that was conducted. Section 3.3 details the results



found from the DMA. Section 3.4 discusses the significance of the results found and section 3.5 outlines the general conclusions.

## **3.2 Materials and Methods**

### **3.2.1 General Methods**

*Ex vivo* whole *porcine* bladders were supplied by Fresh Tissue Supplies (East Sussex, UK). The bladders were of mixed sex from pigs all under a year old. Hashitani and Brading (2003) have concluded that, “pig bladders provide a suitable model to investigate human bladder function” when looking at the function of the detrusor muscles. Once received the specimens were wrapped in tissue paper, soaked in Ringer’s solution (Oxoid Ltd, Basingstoke, UK), placed in heat sealed plastic bags and stored in a freezer at -40°C. Previous studies have shown that freezing and thawing does not affect the mechanical properties of biological tissues such as: vocal tissue (Chan and Titze, 2003), ligaments (Woo *et al.*, 1986) and articular cartilage (Szarko *et al.*, 2010). When specimens were required for testing, bladders were defrosted at room temperature, soaked in Ringer’s solution for around three hours and then dissected. All subsequent testing was carried out in a controlled environment at room temperature, 20°C.

### **3.2.2 Porcine Bladder Pressure Experiment**

To evaluate the typical loads that a porcine bladder would experience, a pressure volume experiment was conducted. Eight porcine bladders were catheterised using clear tubing (inside diameter of 3.5 mm and outside diameter of 5.5 mm) and cable ties. The

tubing was inserted through the urethra until the start of the tubing is at the base of the trigone region, then two cable ties were fastened around the urethra and tubing (both Fischer Scientific, UK). The tubing was then connected to a differential pressure transducer (Gaeltec Devices Ltd, Dunvegan, UK) and filled 50 ml at a time with water using a three way valve and a 60 ml syringe (both Fischer Scientific, UK). The catheterised bladders were set up in a funnel at the same height as the reference pressure to give a zero reading. The pressure transducer required a 3 V, 0.1 A direct current power supply (RS Components, UK) and pressure readings were measured using a multimeter (Fischer Scientific, UK) in mV. Prior to the study the pressure transducer was calibrated using the same equipment and supply against pressure head calculations which can be found in appendix A. It should be noted that the mean voltage against pressure head graph included in appendix A does include 1 standard deviation vertical error bars, however, they are difficult to see as they were small. The equation below shows the conversion of voltage ( $V$ ) to pressure ( $P$ ):

$$P = \frac{V - 0.8788}{0.0242} \quad (3.1)$$

The test setup can be seen in figure 3.1.

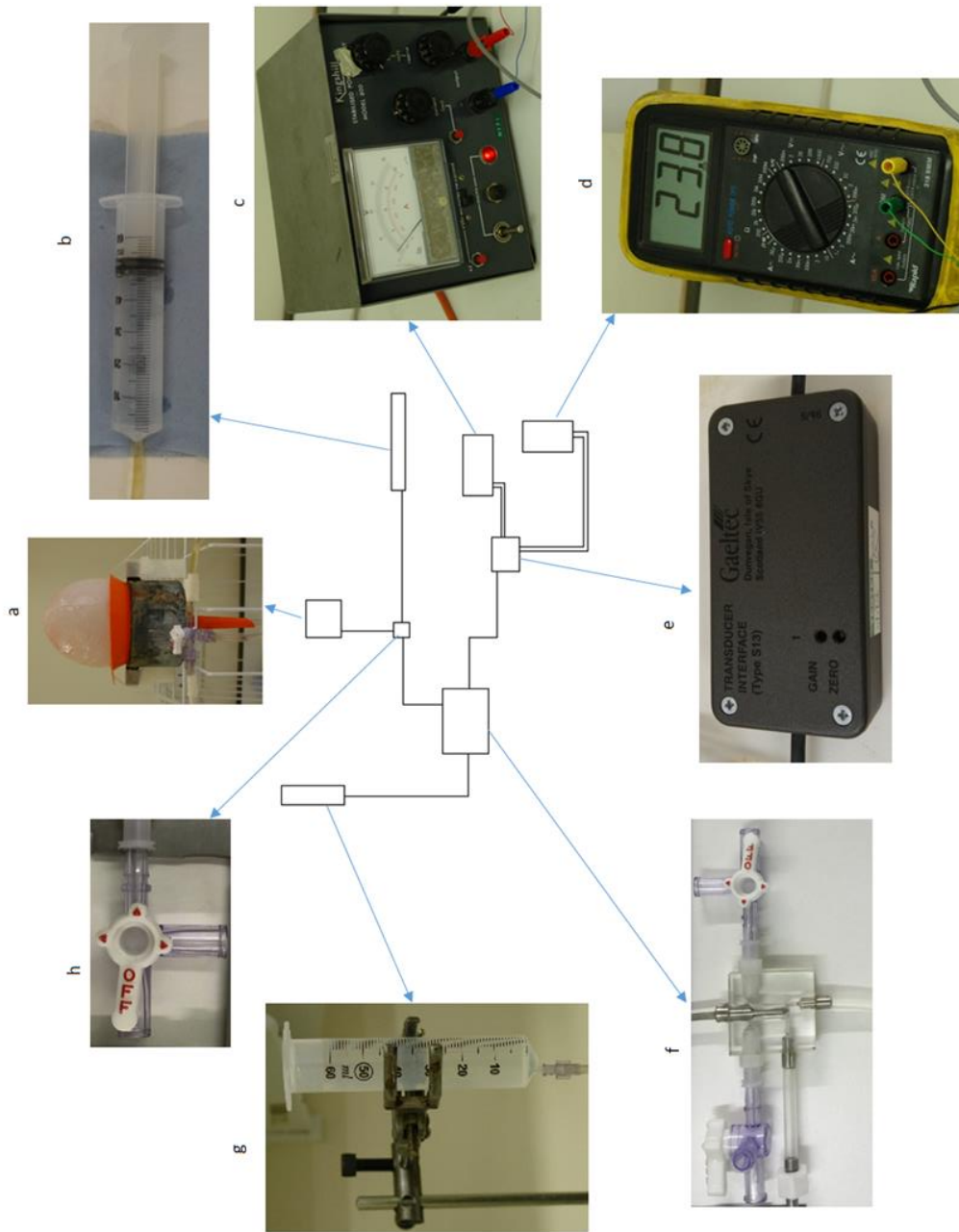


Figure 3.1 – Experimental set up of bladder pressure experiment. a) catheterised porcine bladder; b) syringe used to fill the bladder; c) power pack; d) multimeter; e) interface; f) pressure transducer; g) reference pressure syringe; h) three way valve.

The maximum diameter of the filled bladder was also measured for each volume using Vernier callipers (Fischer Scientific, UK). By approximating the shape of the bladder to a sphere this enabled the calculation of the inner surface area ( $A$ ) of the bladder. The thickness change during filling was assumed to be negligible. The inner surface area,  $A$ , was calculated using:

$$A = 4\pi r_i^2 \quad (3.2)$$

where  $r_i$  is the horizontal inner radius of the bladder.

To get the value for the horizontal inner radius ( $r_i$ ) of the bladder the following equation was used:

$$r_i = \frac{(D_o - (2t))}{2} \quad (3.3)$$

where  $t$  is the bladder wall thickness. A schematic of the bladder and the associated geometries that are used can be found in appendix B.

The average bladder wall thickness was measured from 28 specimens as 5.0 mm with a standard deviation of 1.1 mm. This value was used for  $t$  for all volumes. The force,  $F$ , on the bladder wall at specific points could then be calculated from:

$$F = PA \quad (3.4)$$

where  $P$  is pressure.

### 3.2.3 Porcine Bladder Pressure Experiment Results

Stress or pressure relaxation was observed. Each time the Bladder was filled with 50 ml of water initially a high mV reading was seen which steadily decreased. This relaxation was no longer noticeable after around 120 s. Therefore, the pressure was allowed to stabilise for around 120 s, after which the pressure was recorded. The average force results at different volumes can be seen in figure 3.2.

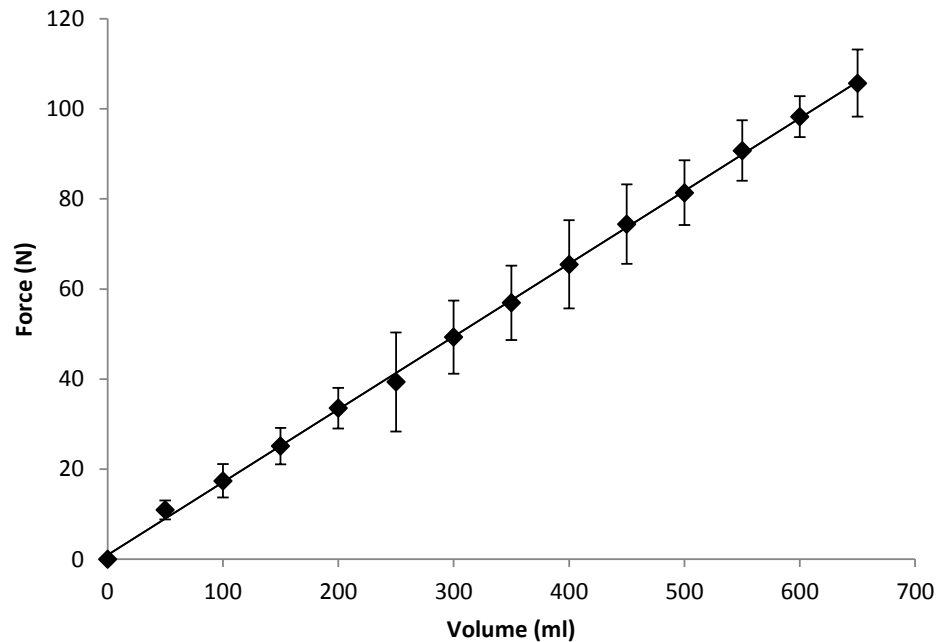


**Figure 3.2 – Average force (N) against volume (ml) during bladder filling, error bars represent one standard deviation.**

A force range of 10 – 110 N was seen for the entire bladder. During preliminary uniaxial testing of bladder specimens it was found that only the lower end of these forces could be reached due to the low stiffness of the material and the low travel of the uniaxial testing machine that was used. This was expected as the bladder specimens being used were only a proportion of the entire bladder. Furthermore Ganong and Barrett (1997) state that the bladder feels full at around 400 ml and the first urge to micturate is felt at 150 ml. This corresponds with the lower end of the forces found in figure 3.2.

### **3.2.4 Uniaxial Testing Methods**

Two methods of tensile DMA were used in this study; the first made use of looped bladder specimens and the second rectangular specimens. The rectangular specimens made use of grips that are standard in biological material mechanical testing; however, a problem with this type of testing is slipping of the specimen out of the grips during loading. Therefore, looped specimens were also incorporated into the study to identify whether there was a difference between the two. The specimens were initially prepared by dissecting the bladders using three cuts (figure 3.3), made using surgical scissors (Fischer Scientific, UK). The dissection resulted in four areas of bladder: two looped central areas of the bladder, the dome region and the trigone region with ureters and urethra attached.

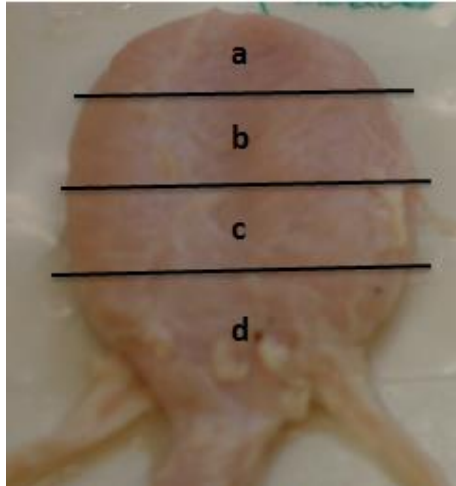


**Figure 3.3 - Initial dissection lines of bladder specimens. Dome region (a), two central regions (b & c) and the trigone region (d). Lines indicate where cuts were made.**

Experimental specimens were obtained from the two central regions of the bladder (areas b and c in figure 3.3). These were the regions where looped specimens were easily obtainable. Rectangular specimens were also obtained from this region to preserve consistency in the method of testing. For the rectangular specimens the central looped regions were dissected again with two more cuts, to create two strips from one looped specimen. These cuts were always in the same anatomical location, laterally aligned to the ureters.

The viscoelastic properties of the bladder specimens were determined from DMA using a Bose Electroforce 3200 testing machine coupled with WinTest DMA software (Bose Corporation, Electroforce Systems Group, Minnesota, USA). Patel *et al.* (2008) have given full details of the Bose Electroforce 3200 testing machine including maximum errors of the 225 N load cell and the 6.5 mm displacement transducer which are 0.21 % and 0.49 % of their respective full scales. Previously Bose testing machines have been used for tensile testing of

biological materials including heart chordae and bladder (Millard *et al.*, 2011; Zanetti *et al.*, 2012).

Custom-designed fixtures were manufactured to enable the testing of both looped and rectangular specimens; the engineering drawings for these jigs can be seen in appendix C. Each fixture consisted of two identical but separate parts to fasten the bladder specimens to the base and actuator of the testing machine (figure 3.4). The fixtures for the looped specimens consisted of two horizontal cylinders that the loops were secured around. The rectangular fixtures consisted of two horizontal grips that were supplemented with fine sandpaper to prevent slippage. The grips were fastened to the specimen by turning two horizontal screws, creating a compressive force on the top and bottom of the specimen.

Tensile preloads of approximately 10 N and 20 N were applied to the rectangular and looped specimens, respectively. These were achieved by attaching the specimens to the jigs and then moving the base stage of the testing machine downwards, loading the specimen. Double the preload was exerted on the looped specimens as there were two load bearing structures as opposed to one for the rectangular specimens. These preloads were necessary to ensure that specimens remained on the fixtures during testing. The specimens were then allowed to relax for 2 minutes as this was the previously observed time when any stress relaxation stopped (section 3.2.3). The preloaded specimens of bladder were covered with tissue paper soaked in Ringer's solution so that the specimen did not dehydrate during testing. This is consistent with procedures previously described by Öhman *et al.* (2009) and Wilcox *et al.* (2014) for testing tendons and heart chordae, respectively.



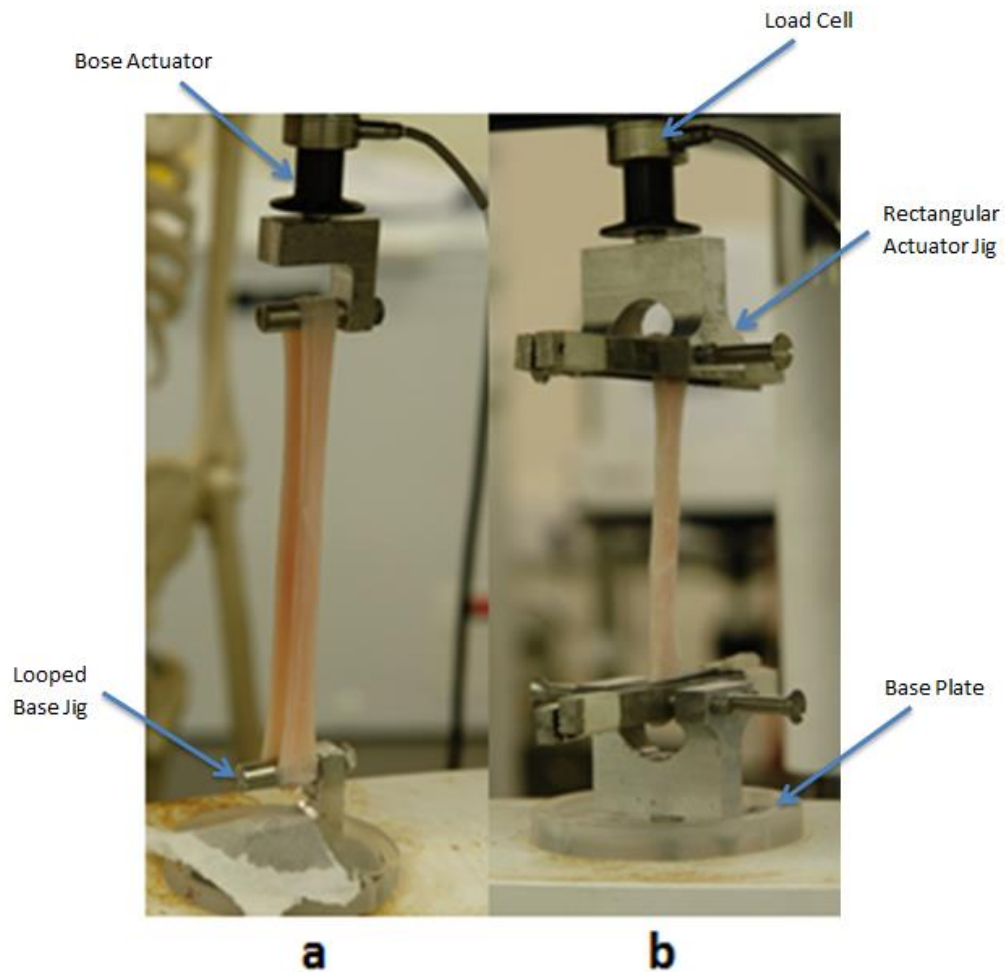


**Figure 3.4 - Fixtures for testing the specimens of bladder (a) looped specimens; (b) rectangular specimens.**

The WinTest software uses readings of force and displacement from the load cell and displacement transducer and from this dynamic stiffness ( $k^*$ ) and the phase lag ( $\delta$ ) are calculated. Dynamic stiffness was found using Fourier analysis to determine the ratio of load to displacement. The phase lag was also found using Fourier analysis to determine the phase difference between the load and displacement. The method the software used is described in detail in section 2.4.6. Storage ( $k'$ ) and loss stiffness ( $k''$ ) were then calculated from:

$$k' = k^* \cos \delta \quad (3.5)$$

$$k'' = k^* \sin \delta \quad (3.6)$$

### 3.2.5 Preliminary Testing

Due to the high stress relaxation of bladder tissue, load controlled DMA testing was not possible and therefore displacement control was used. A sinusoidally varying displacement was applied to the specimens between 2.5 mm and 5.5 mm; this corresponded to the lower end of the force range found in section 3.2.3.

The looped specimens were initially tested in the range of 0.01 – 30 Hz. Four specimens were tested from 0.01 – 30 – 0.01 Hz; a separate four specimens were tested from 30 – 0.01 – 30 Hz. The rectangular specimens were tested in the same manner but in the range 0.01 – 10 Hz as the specimens were slipping in the grips at the higher frequencies. There were 13 test frequencies in the stated ranges with a dwell time of 10 seconds in between each frequency. The specimens were tested in these orders to investigate whether the order of the frequency sweep altered storage stiffness ( $k'$ ) and loss stiffness ( $k''$ ) and whether pre-cycling would be necessary. Typical results for each of the four test parameters can be seen in figures 3.5 to 3.8.

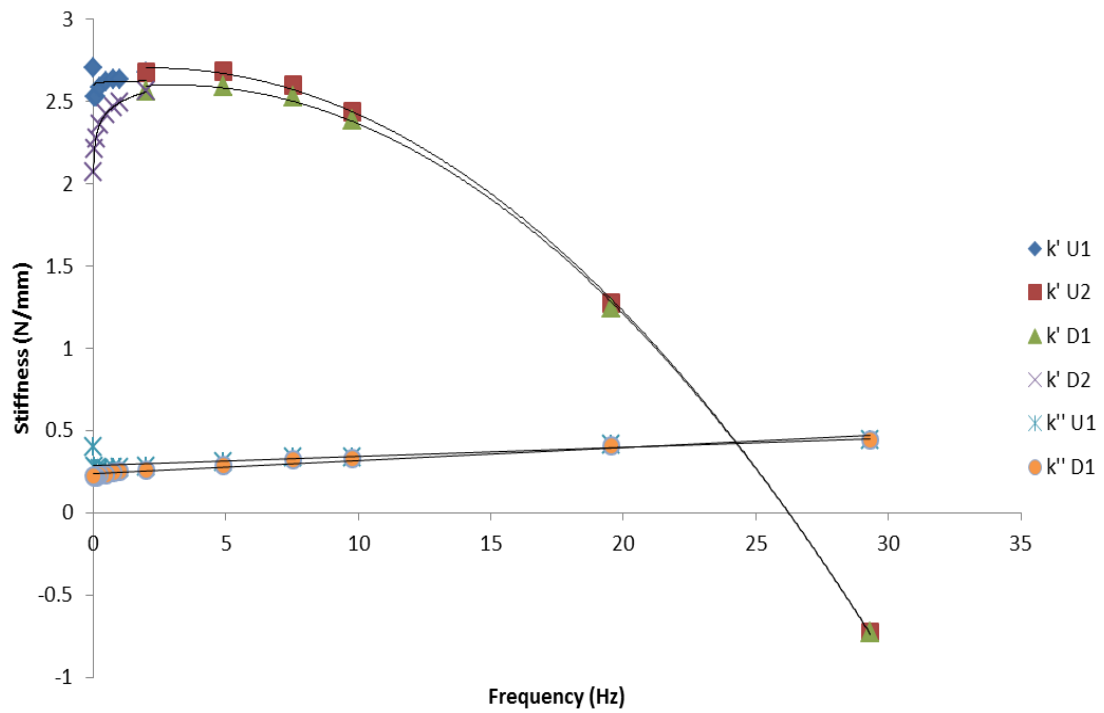


**Figure 3.5 - Storage ( $k'$ ) and loss stiffness ( $k''$ ) against frequency ( $f$ ) for an individual looped specimen. The frequency range tested was 0.01 – 30 – 0.01 Hz. In the key U refers to Up i.e. increasing frequency and D to Down i.e. decreasing frequency.**

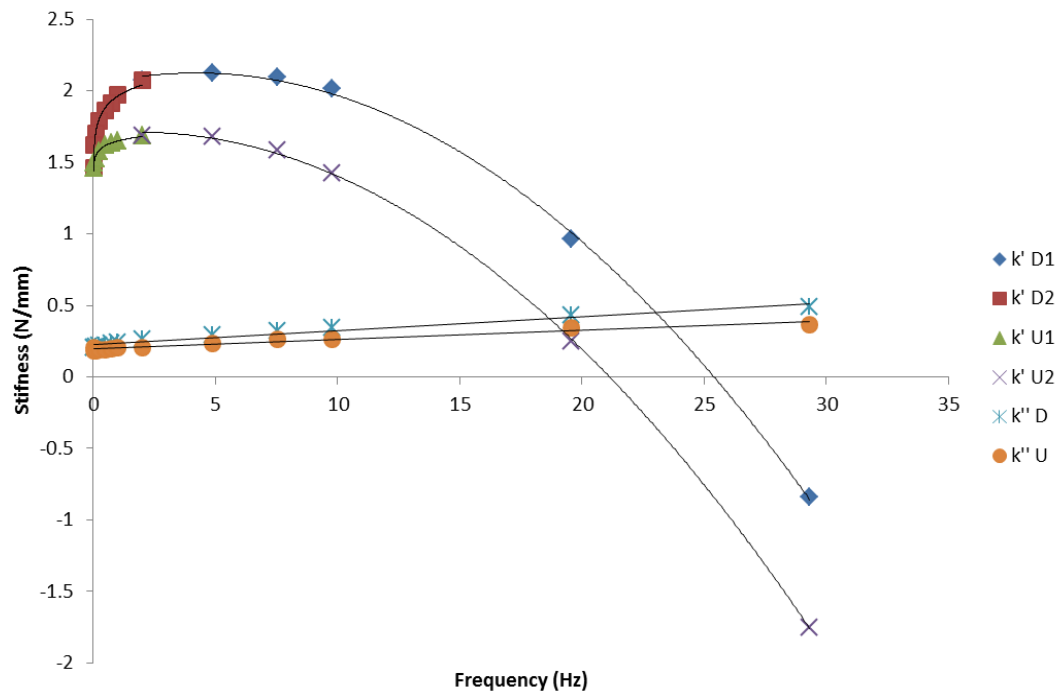


**Figure 3.6 - Storage ( $k'$ ) and loss stiffness ( $k''$ ) against frequency ( $f$ ) for an individual looped specimen. The frequency range tested was 30 – 0.01 – 30 Hz. In the key U refers to Up i.e. increasing frequency and D to Down i.e. decreasing frequency.**

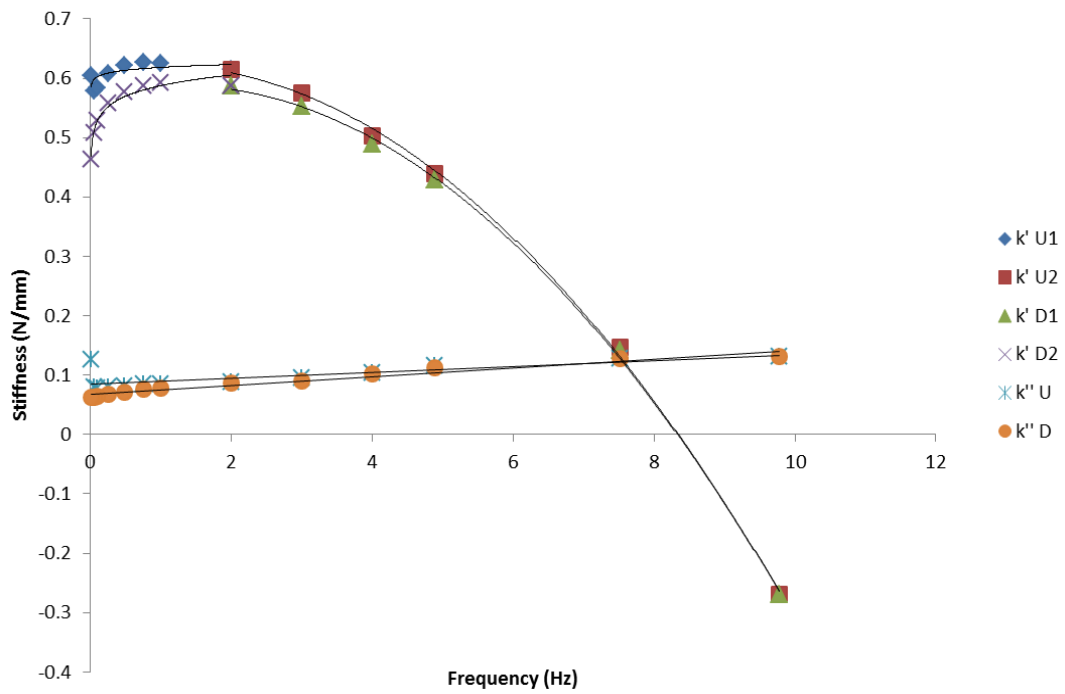


**Figure 3.7 - Storage ( $k'$ ) and loss stiffness ( $k''$ ) against frequency ( $f$ ) for an individual rectangular specimen. The frequency range tested was 0.01 – 10 – 0.01 Hz. In the key U refers to Up i.e. increasing frequency and D to Down i.e. decreasing frequency.**

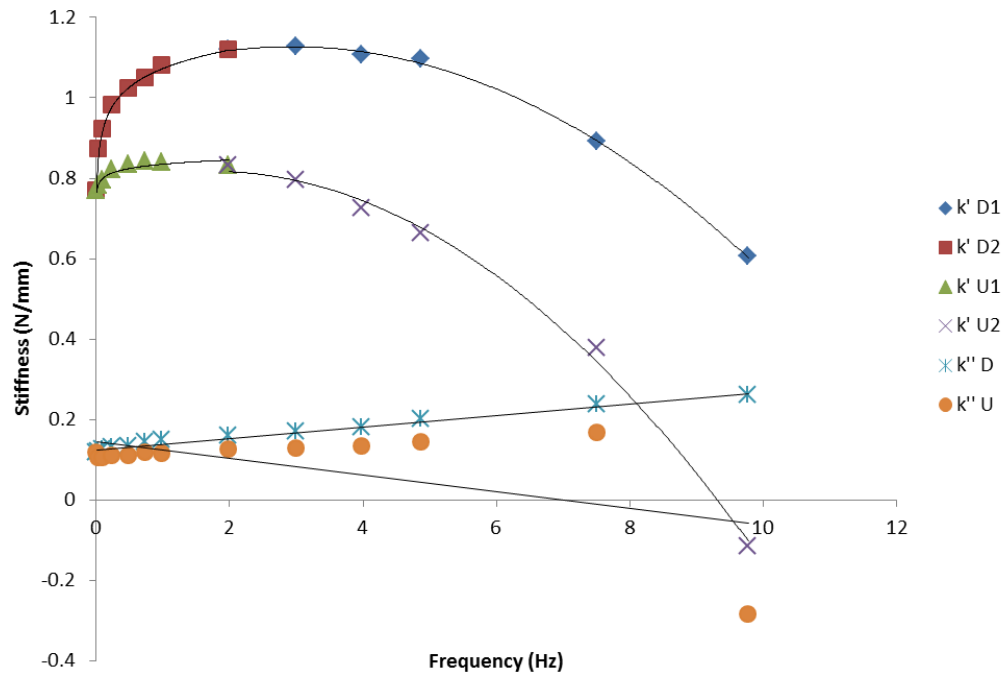


**Figure 3.8 - Storage ( $k'$ ) and loss stiffness ( $k''$ ) against frequency ( $f$ ) for an individual rectangular specimen. The frequency range tested was 10 – 0.01 – 10 Hz. In the key U refers to Up i.e. increasing frequency and D to Down i.e. decreasing frequency.**

It was seen that pre-cycling did affect the tests as the first results for storage and loss stiffness on figure 3.5 and figure 3.7 differed from the general trend. In figure 3.6 and figure 3.8 the increasing curve fits of the storage stiffness from 0 to 2.5 Hz showed repeatable trends with high  $R^2$  values for logarithmic curve fits ( $R^2 > 0.85$ ), this was put down to the effect of pre-cycling from earlier frequencies. With pre-cycling, in the form of earlier frequencies, repeatable trends were seen whether the frequency was increasing or decreasing.

Preliminary testing showed that the results were similar whether the frequency started at 0.01 Hz and was increased, or started at 5 or 10 Hz and decreased. It was decided that for the actual tests increasing frequencies would be used as this is a standard approach in frequency sweep DMA studies (Wilcox *et al.*, 2014; Fulcher *et al.*, 2009). Negative stiffnesses were observed in all of the preliminary tests (figures 3.5 to 3.8). This was due to lateral vibration of the specimens and was used to identify the frequency limits of the test. Therefore, a frequency range with only positive stiffness values was selected for the actual tests.

### 3.2.6 Final Testing

The length, width and thickness of each specimen were measured with Vernier callipers (Fischer Scientific, UK) by taking three measurements. Table 3.1 shows the mean and standard deviation of the dimensions of the prepared specimens.

**Table 3.1 - Dimensions (mean and standard deviation) of the looped and rectangular specimens. 10 looped and 18 rectangular specimens were tested.**

	Loop			Rectangular		
	Length (mm)	Width (mm)	Thickness (mm)	Length (mm)	Width (mm)	Thickness (mm)
<b>Mean</b>	54.5	24.0	4.7	59.3	25.6	5.0
<b>Std Deviation</b>	4.8	2.8	1.1	9.9	3.9	1.1

A sinusoidally varying displacement was applied to the specimens between 2.5 mm and 5.5 mm. Both types of specimens were tested in 11 steps with increasing frequencies: between 0.01 and 10 Hz (looped specimens) and between 0.01 and 5 Hz (rectangular specimens), as shown in Table 3.2. Both the rectangular and looped specimens were also subjected to 120 seconds of precycling at 5 and 10 Hz, respectively. The same dwell time of 10 seconds was used in between frequencies. The same displacement of between 2.5 and 5.5 mm was used during the precycling. Therefore, the specimens were preconditioned before testing. This is consistent with testing of other soft tissues (Öhman *et al.*, 2009; Wilcox *et al.*, 2014).



**Table 3.2 - Testing frequencies for looped and rectangular bladder specimens.**

Testing Order	Looped Specimens (Hz)	Rectangular Specimens (Hz)
1	0.01	0.01
2	0.05	0.05
3	0.1	0.1
4	0.25	0.25
5	0.5	0.5
6	0.75	0.75
7	1	1
8	2.5	2
9	5	3
10	7.5	4
11	10	5

All statistical analysis of the data was undertaken using Minitab (Version 15.1.20.0, Minitab Inc., Pennsylvania, USA). The significance of the curve fits generated for storage and loss stiffness was tested using regression analysis to generate  $p$ -values. If the  $p$ -value was less than 0.05, the curve fit of the relationship was significant (Reilly, 2015).

### **3.3 Results**

Figures 3.9 and 3.10 show three specimen results from the looped and rectangular tests, respectively. All the storage stiffness results follow the same trend, with initially increasing storage stiffness with frequency and then a decrease at higher frequencies. The loss stiffness results follow the same shallow gradient linear increase with increasing frequency.

Figures 3.11 and 3.12 show the average results for looped and rectangular specimens, respectively. In figure 3.11 (loop) the storage stiffness increased up to a stiffness of around 2 N/mm and then decreased at higher frequencies. The loss stiffness increased from 0.25 to 0.30 N/mm over the frequency range. In figure 3.12 (rectangular) the storage stiffness increased up to a stiffness of around 0.80 N/mm and then decreased at higher frequencies. The loss stiffness increases from 0.10 to 0.13 N/mm over the frequency range. The loss stiffness was lower than storage stiffness for all frequencies tested.

The trends for storage stiffness were described by two curve fits: a logarithmic fit (equation 3.7) from 0.01 to 1 Hz and a second order polynomial fit (equation 3.8) for the remainder of the frequency sweep. No fitting of physical models, such as spring mass damper systems, was attempted as storage and loss modulus do not necessarily inform spring or damping coefficients. The values for coefficients  $A$ ,  $B$ ,  $C$ ,  $D$  and  $E$  can be found in table 3.3. These curve fits showed a strong correlation with  $R^2$  values of 0.77 and above (most between 0.9 and 1) and all had p-values of less than 0.05 showing that they were significant.

$$k' = A \ln(f) + B \quad \text{for } 0.01 < f \leq 1 \quad (3.7)$$

$$k' = C(f^2) + D(f) + E \quad \text{for } f \geq 1 \quad (3.8)$$

where  $k'$  is the storage stiffness and  $f$  is the frequency.

The average storage stiffness curve fits for the looped specimens were:

$$k' = 0.0455\ln(f) + 1.951 \quad \text{for } 0.01 < f \leq 1 \quad (3.9)$$

$$k' = -0.0073(f^2) + 0.0529(f) + 1.9207 \quad \text{for } 1 \leq f < 10 \quad (3.10)$$

The average storage stiffness curve fits for the rectangular specimens were:

$$k' = 0.0202\ln(f) + 0.7912 \quad \text{for } 0.01 < f \leq 1 \quad (3.11)$$

$$k' = -0.0129(f^2) + 0.0293(f) + 0.7733 \quad \text{for } 1 \leq f < 5 \quad (3.12)$$

Both types of specimen also exhibited the same trends for loss stiffness, which has been described by a linear fit (equation 3.13). The coefficients  $F$  and  $G$  can be found in table 3.3. These linear fits showed strong correlation with  $R^2$  values of 0.63 and above (most between 0.85 and 0.93) and all had  $p < 0.05$  showing that they were significant.

$$k'' = F(f) + G \quad (3.13)$$

where  $k''$  is the loss stiffness and  $f$  is the frequency.

The average loss stiffness curve fits for the looped (equation 3.14) and rectangular specimens (equation 3.15) were:

$$k'' = 0.009(f) + 0.226 \quad \text{for } 0.01 < f < 10 \quad (3.14)$$

$$k'' = 0.0093(f) + 0.0984 \quad \text{for } 0.01 < f < 5 \quad (3.15)$$

Storage ( $E'$ ) and loss moduli ( $E''$ ) can also be used to describe materials and they are calculated by dividing the relevant stiffness by a shape factor (Fulcher *et al.*, 2009). The shape factor for rectangular specimens was calculated from:

$$S = wd/h \quad (3.16)$$

where,  $w$  is width,  $d$  is depth and  $h$  is height (Menard, 2008).

For example, the storage stiffness of specimen 13 at 0.01 Hz is 0.44 N/mm and the equivalent storage modulus ( $E'$ ) is 0.21 MPa. The mean storage and loss modulus of the rectangular specimens can be seen in figure 3.13. However, stiffness is used to compare the results in this study as no appropriate shape factor approximation for looped specimens was found.

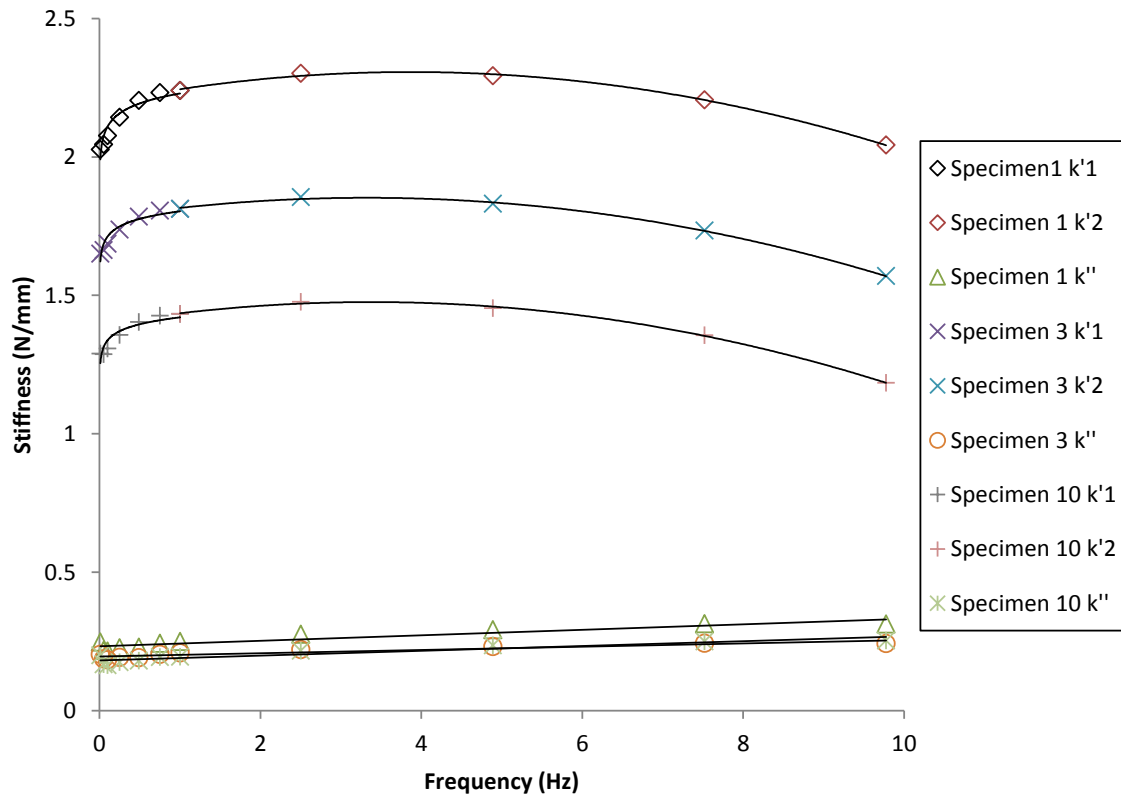
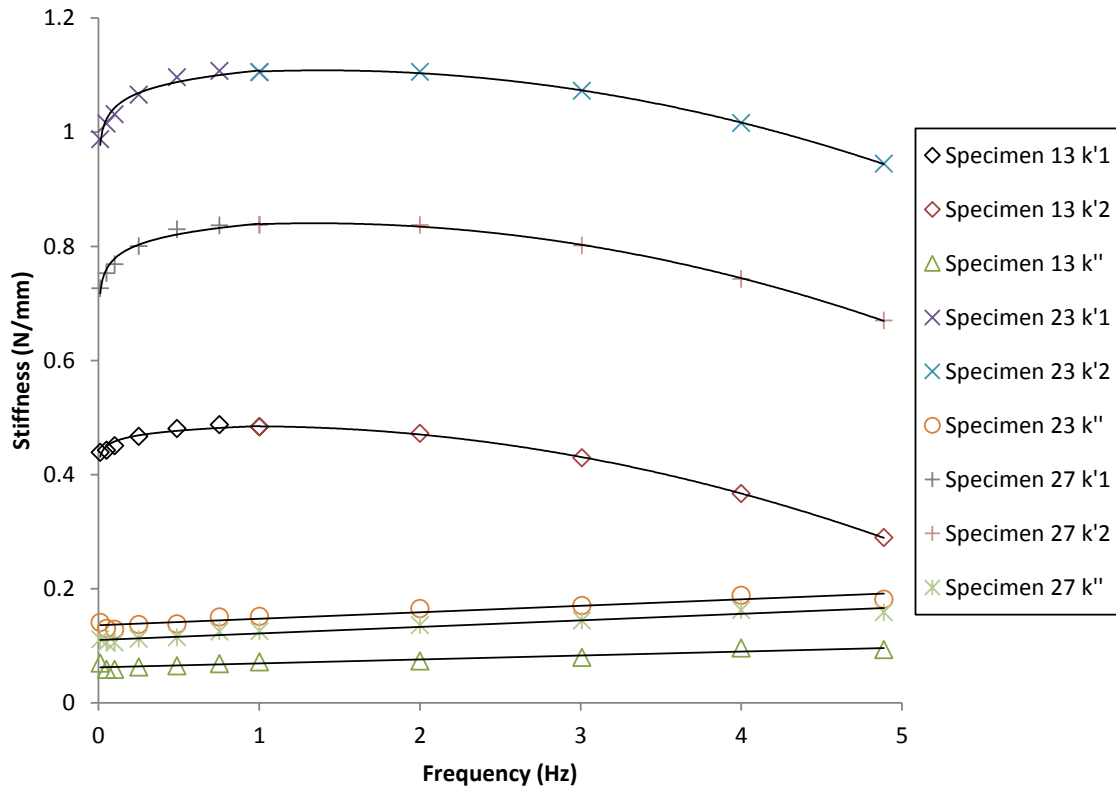


Figure 3.9 - Storage ( $k'$ ) and loss stiffness ( $k''$ ) against frequency ( $f$ ) for three individual looped specimens.  $k'1$  refers to the data points subjected to the first curve fit of storage stiffness up to 1 Hz (characterised by equation 3.7) and  $k'2$  refers to the data points subjected to the second curve fit of storage stiffness up to the end testing frequency (characterised by equation 3.8). The loss stiffness ( $k''$ ) curve fit is characterised by equation 3.13.



**Figure 3.10 - Storage ( $k'$ ) and loss stiffness ( $k''$ ) against frequency ( $f$ ) for three individual rectangular specimens.  $k'1$  refers to the data points subjected to the first curve fit of storage stiffness up to 1 Hz (characterised by equation 3.7) and  $k'2$  refers to the data points subjected to the second curve fit of storage stiffness up to the end testing frequency (characterised by equation 3.8). The loss stiffness ( $k''$ ) curve fit is characterised by equation 3.13.**

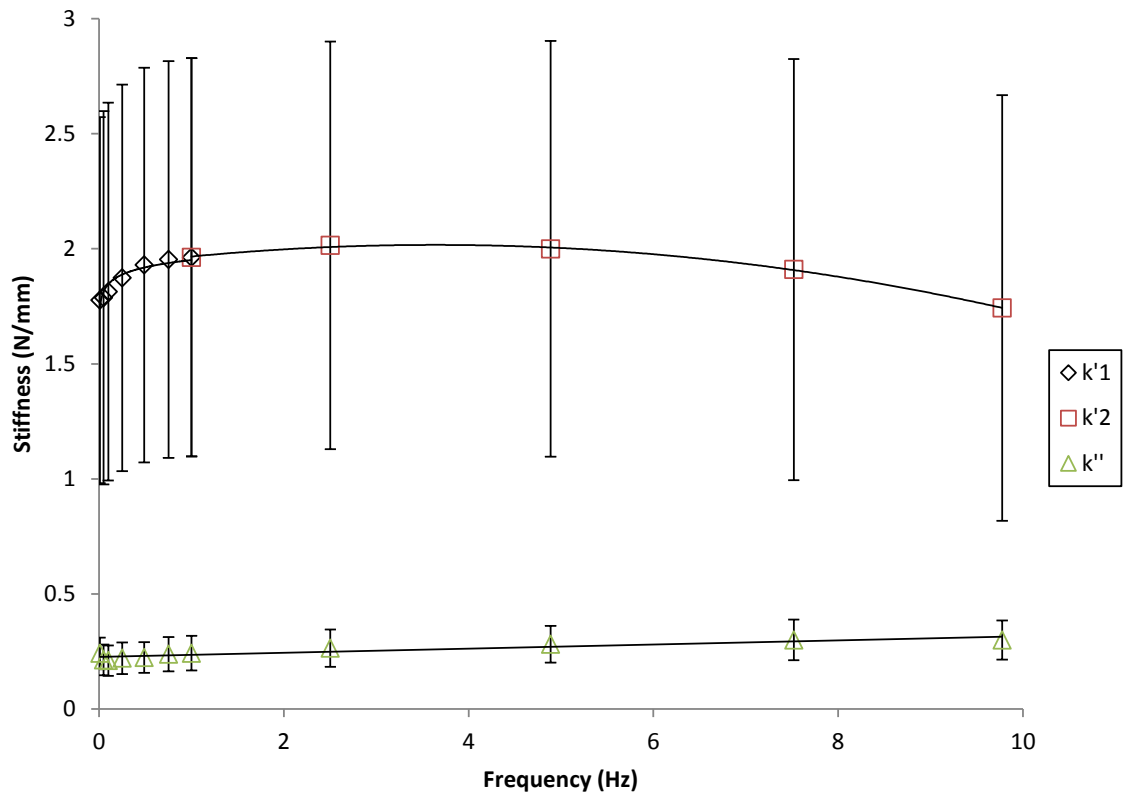
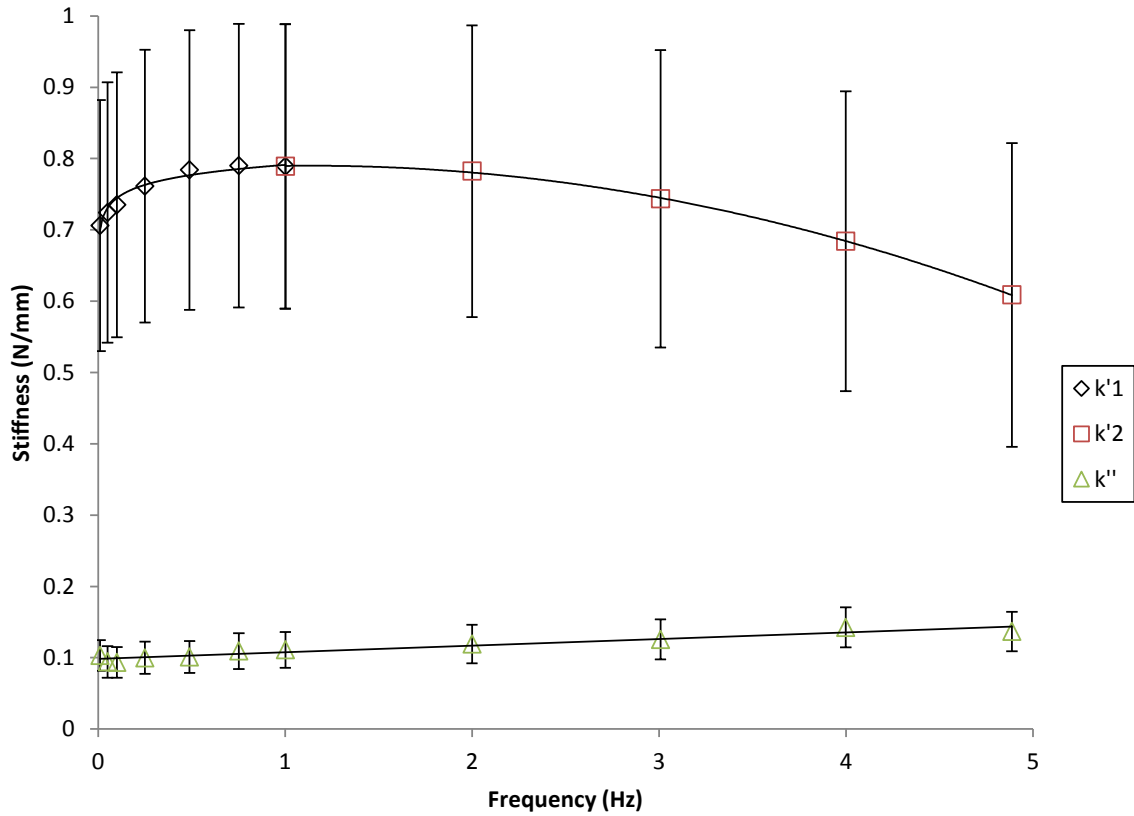


Figure 3.11 - Storage ( $k'$ ) and loss stiffness ( $k''$ ) against frequency ( $f$ ) for looped specimens.

Data points represent the average values, with one standard deviation error bars.  $k'1$  refers to the data points subjected to the first curve fit of storage stiffness up to 1 Hz (described by equation 3.9) and  $k'2$  refers to the data points subjected to the second curve fit of storage stiffness up to the end testing frequency (described by equation 3.10). The loss stiffness ( $k''$ ) curve fit is described by equation 3.14.



**Figure 3.12 - Storage ( $k'$ ) and loss stiffness ( $k''$ ) against frequency ( $f$ ) for rectangular specimens. Data points represent the average values, with one standard deviation error bars.  $k'1$  refers to the data points subjected to the first curve fit of storage stiffness up to 1 Hz (described by equation 3.11) and  $k'2$  refers to the data points subjected to the second curve fit of storage stiffness up to the end testing frequency (described by equation 3.12).**

**The loss stiffness ( $k''$ ) curve fit is described by equation 3.15.**



Table 3.3 – Curve fit results for storage and loss stiffness. All coefficients were found to be statistically significant ( $p < 0.05$ ).

Specimen number	Specimen type	Frequency range (Hz)	Storage stiffness ( $k'$ ) curve fit					Loss stiffness ( $k''$ ) curve fit				
			0.01 to 1 Hz ( $k' = A \ln(f) + B$ )					1 Hz to end frequency ( $k' = C f^2 + D f + E$ )				
			A	B	R <sup>2</sup>	C	D	E	R <sup>2</sup>	F	G	R <sup>2</sup>
1	Loop	0.01 to 10	0.052	2.23	0.92	-0.0076	0.058	2.19	0.99	0.0099	0.23	0.86
2	Loop	0.01 to 10	0.039	1.44	0.91	-0.0070	0.047	1.41	0.99	0.0095	0.18	0.89
3	Loop	0.01 to 10	0.040	1.80	0.91	-0.0068	0.045	1.78	0.99	0.0059	0.20	0.85
4	Loop	0.01 to 10	0.031	1.41	0.8	-0.0067	0.042	1.39	0.99	0.0069	0.17	0.85
5	Loop	0.01 to 10	0.090	4.28	0.94	-0.0088	0.086	4.23	0.99	0.0143	0.40	0.84
6	Loop	0.01 to 10	0.042	1.65	0.89	-0.0071	0.049	1.62	0.99	0.0088	0.21	0.87
7	Loop	0.01 to 10	0.048	2.09	0.89	-0.0076	0.057	2.06	0.99	0.0100	0.28	0.86
8	Loop	0.01 to 10	0.041	1.60	0.9	-0.0071	0.048	1.57	0.99	0.0087	0.21	0.88
9	Loop	0.01 to 10	0.039	1.59	0.9	-0.0070	0.047	1.56	0.99	0.0074	0.19	0.84
10	Loop	0.01 to 10	0.036	1.42	0.86	-0.0071	0.048	1.39	0.99	0.0087	0.18	0.85
11	Rectangular	0.01 to 5	0.011	0.59	0.77	-0.0122	0.021	0.58	1.00	0.0071	0.08	0.63
12	Rectangular	0.01 to 5	0.011	0.69	0.84	-0.0125	0.022	0.68	1.00	0.0073	0.08	0.90
13	Rectangular	0.01 to 5	0.012	0.49	0.91	-0.0125	0.023	0.47	1.00	0.0069	0.06	0.90
14	Rectangular	0.01 to 5	0.012	0.44	0.95	-0.0112	0.015	0.44	0.99	0.0070	0.05	0.93
15	Rectangular	0.01 to 5	0.019	0.78	0.96	-0.0139	0.033	0.75	1.00	0.0102	0.11	0.92
16	Rectangular	0.01 to 5	0.023	0.78	0.96	-0.0133	0.035	0.76	1.00	0.0120	0.11	0.93
17	Rectangular	0.01 to 5	0.022	0.76	0.98	-0.0127	0.030	0.74	1.00	0.0103	0.10	0.92
18	Rectangular	0.01 to 5	0.021	0.80	0.98	-0.0129	0.027	0.79	1.00	0.0087	0.11	0.94
19	Rectangular	0.01 to 5	0.018	0.69	0.97	-0.0130	0.028	0.68	1.00	0.0088	0.09	0.93
20	Rectangular	0.01 to 5	0.017	0.61	0.97	-0.0125	0.025	0.60	1.00	0.0087	0.08	0.93
21	Rectangular	0.01 to 5	0.019	0.86	0.96	-0.0119	0.022	0.85	0.99	0.0087	0.11	0.89
22	Rectangular	0.01 to 5	0.021	0.76	0.97	-0.0132	0.029	0.74	1.00	0.0085	0.09	0.90
23	Rectangular	0.01 to 5	0.028	1.11	0.97	-0.0135	0.037	1.08	1.00	0.0113	0.14	0.91
24	Rectangular	0.01 to 5	0.029	1.03	0.98	-0.0135	0.038	1.01	1.00	0.0106	0.12	0.93
25	Rectangular	0.01 to 5	0.029	1.03	0.97	-0.0136	0.040	1.01	0.99	0.0112	0.13	0.91
26	Rectangular	0.01 to 5	0.028	1.17	0.96	-0.0136	0.039	1.14	1.00	0.0103	0.13	0.91
27	Rectangular	0.01 to 5	0.027	0.84	0.97	-0.0136	0.037	0.82	0.99	0.0115	0.11	0.95
28	Rectangular	0.01 to 5	0.018	0.80	0.94	-0.0128	0.028	0.79	1.00	0.0082	0.09	0.91

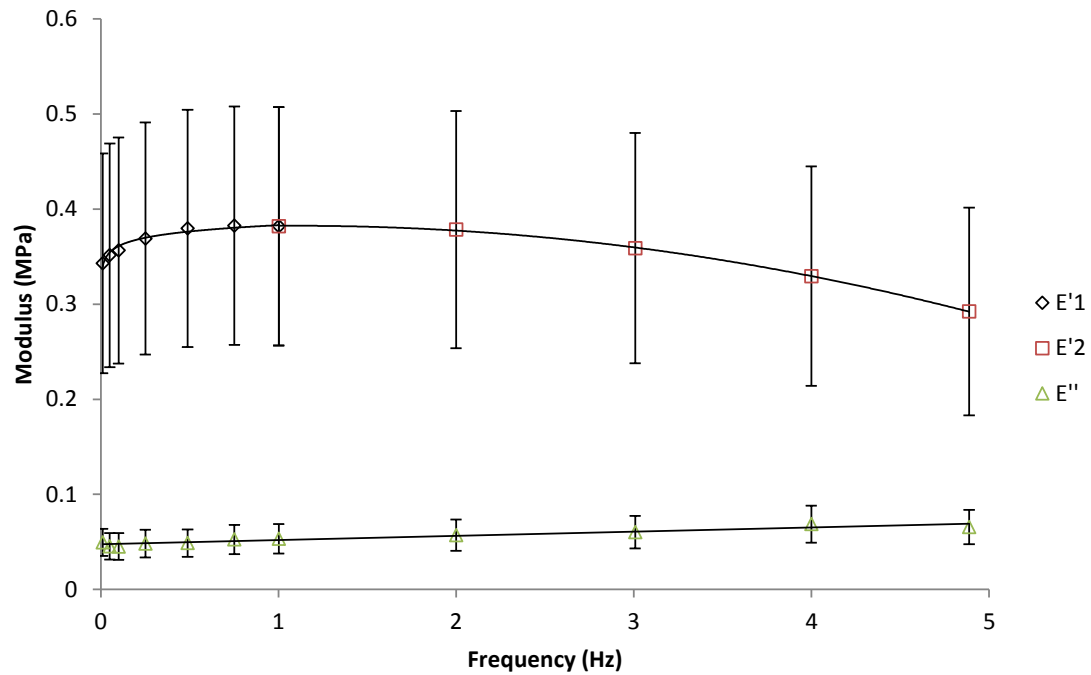


**Figure 3.13 - Storage ( $E'$ ) and loss modulus ( $E''$ ) against frequency ( $f$ ) for rectangular specimens. Data points represent the average values, with one standard deviation error bars.  $E'1$  refers to the data points subjected to the first curve fit of storage stiffness up to 1 Hz (described by equation 3.11) and  $E'2$  refers to the data points subjected to the second curve fit of storage stiffness up to the end testing frequency (described by equation 3.12).**

**The loss stiffness ( $E''$ ) curve fit is described by equation 3.15.**

### 3.4 Discussion

The objective of this chapter was to investigate the viscoelastic properties of bladder tissue. Bladder tissue was found to be viscoelastic throughout the frequency range tested. Both the looped and rectangular bladder specimens showed consistent trends for storage and loss stiffness, where the same curve fits were used for both types of specimen. Similar curve fits have been used in many other studies to describe viscoelastic properties of tissues including articular cartilage (Fulcher *et al.*, 2009) and heart chordae (Wilcox *et al.*, 2014). In this study the loss stiffness ( $k''$ ) exhibited similar results throughout the frequency sweep with a near constant value over the frequency range; a similar trend has been seen in other viscoelastic tissues such as articular cartilage (Fulcher *et al.*, 2009) and chordae tendineae from the heart (Wilcox *et al.*, 2014). Storage stiffness ( $k'$ ) however showed an initially increasing trend at low frequencies and then a decreasing trend at higher frequencies. Furthermore, the storage stiffness of the tissue did not change greatly throughout the test; the average minimum value was 82% of the maximum value. The findings for storage stiffness are in contrast to the same findings for articular cartilage (Fulcher *et al.*, 2009) and heart chordae (Wilcox *et al.*, 2014) where an increasing trend was found.

The range of frequencies tested varied from very low (0.01 Hz) to high (5 or 10 Hz) and this was intended to show the bladder response at physiological and traumatic conditions, respectively. The results indicate that the stiffness values at these frequencies were similar, with average storage stiffness values of 1.78 N/mm (low frequency), 1.74 N/mm (high frequency) and 0.71 N/mm (low frequency), 0.61 N/mm (high frequency) for

looped and rectangular specimens, respectively. It was expected that the results would be quite similar for the two different types of specimen. This was because the looped specimens, which had two load bearing structures, received a preload of 20 N and the rectangular specimens, which had one load bearing structure, received a preload of 10 N. However, this was not the case as the storage stiffness results for the looped specimens are more than two and a half times that of the rectangular specimens.

The majority of previous mechanical testing of bladder studies have used rectangular specimens to test a variety of bladder muscle uniaxially (Finkbeiner and O'Donnell, 1990; van Mastrigt *et al.*, 1978; Griffiths *et al.*, 1979; Alexander, 1971). However, testing of looped specimens has been described in relation to bladder tissue by Alexander (1976) whilst testing series elasticity of rat bladders. Looped uniaxial testing was incorporated into this study to attempt to more closely imitate the function of the bladder but also to serve as a comparison for the rectangular uniaxial testing. It was shown that comparatively higher stiffness values were recorded in the looped specimens and therefore multidirectional tension of bladder tissue stresses the tissue in a manner that makes it become stiffer and able to elastically store more energy during deformation. No other studies have compared the properties of bladder using the two methods described in this study.

Previous studies have found mechanical properties for rectangular transverse lateral sections of the bladder. Zanetti *et al.* (2012) found the secant modulus to be 0.1 - 0.45 MPa; secant modulus is similar to Young's modulus, however, the modulus is taken from the origin to anywhere on the stress strain curve. Korossis *et al.* (2009) found the elastin phase slope to be 0.04 MPa and the collagen phase slope to be 0.6 MPa. The phase slope is similar to

Young's modulus, however, the phase slope can be taken from any two points on the stress strain curve, and it is also sometimes referred to as the tangential modulus. In another study Dahms *et al.* (1998) found the elastic modulus as 0.26 MPa. All of these studies used static stress strain experiments. The average dynamic modulus for the rectangular specimens for this investigation was 0.36 MPa which is comparable to the range found by Zanetti *et al.* (2012). However, there are difficulties when comparing our results with material properties reported in the literature because viscoelastic properties are by definition rate dependant. Therefore, comparisons made for the results obtained at different frequencies and strain rates can be misleading.

A study by Gilbert *et al.* (2008) states that collagen fibres, which are responsible for the mechanical response of the tissue, are predominantly aligned in the longitudinal direction. This may justify the low stiffness as the looped and rectangular specimens were tested in the transverse direction. Furthermore, bladder tissue has little elastin in any region of the bladder (Korossis *et al.*, 2009). Elastin stores the elastic energy of the material (Silver *et al.*, 2001) and the lack of elastin may account for the high deformation of the bladder tissue both after the bladder pressure experiment (section 3.2.2) and during the preloading of the DMA testing (section 3.2.6).

If a similar study is performed on human bladder tissue the results of this study can be used to determine whether porcine bladders are a good comparison model. This has been done previously with corneas and arteries (Zeng *et al.*, 2001; van Andel *et al.*, 2003). If the results from this study are validated by a human study then new urological procedures can be confidently tested on porcine bladders before being trialled in humans.

Any tissue engineered bladder tissue can also be compared to the values found in this study to determine if they have suitable viscoelastic properties. So far there has been clinical experience in the implantation of tissue engineered bladders, albeit limited (Li *et al.*, 2014; Atala, 2011). Some partial cystectomy procedures involve the use of *autologous* material as a replacement material for the bladder (Pokrywczynska *et al.*, 2014). The mechanical appropriateness of the small intestine and other *autologous* replacement tissues can now be tested. It is hoped that a material better suited to the role of replacement bladder for urine storage can be found without the associated adverse effects, such as excess mucus production and electrolyte imbalance (Pokrywczynska *et al.*, 2014).

Understanding the viscoelastic properties of bladder tissue is also important for computer simulations of bladders such as Finite Element Analysis (FEA) or Computational Fluid Dynamics (CFD) studies which include bladder deformation. The correct viscoelastic properties need to be used for meaningful models. Previous CFD studies of the bladder have assumed the bladder wall to be rigid (Jin *et al.*, 2010) or have simulated the contracting detrusor muscle as fluid pressure (Pel and van Mastrigt, 2007). For example, an application of the results from this study into an extended FEA model to include CFD, a Fluid Structure Interaction (FSI) model, could involve the investigation of tumour cell re-implantation during transurethral bladder tumour resection (Bryan *et al.*, 2010). The results from this study would also be able to validate FE (Finite Element) models, FEA could then be used to model the traumatic deformation of the bladder during a road traffic accident or to find the allowable probing force during transurethral resection of bladder tumour surgery (TURBT).

One possible limitation of this study was the freezing of specimens prior to testing. It is generally accepted that freezing does not influence the mechanical properties of biological materials. The majority of previous studies including tests on vocal tissue (Chan and Titze, 2003), ligaments (Woo *et al.*, 1986) and articular cartilage (Szarko *et al.*, 2010), state that there is no effect. However, other studies disagree with such findings, for example Venkatasubramanian *et al.* (2006) concluded that the freezing of *porcine* femoral arteries does affect its mechanical properties. Freezing technique is also important and Pelker *et al.* (1984) describe that freeze drying reduces the torsional strength of long rat bones when compared to freezing alone. As all specimens tested in the current study underwent the same storage procedures, it would not be expected that the trends found would be affected by freezing.

### 3.5 Chapter Summary

The conclusions of this chapter are as follows:

- *Porcine* bladder tissue is viscoelastic through the range of frequencies tested, 0.01 to 5 or 10 Hz.
- The viscoelastic relationship changed with respect to frequency, where the average stiffness values were: 1.89 N/mm (storage) and 0.24 N/mm (loss) for the looped specimens and 0.74 N/mm (storage) and 0.11 N/mm (loss) for the rectangular specimens.
- Potential applications of these study findings include: enabling the use of *porcine* bladder as a comparable model to human bladder; comparisons to any tissue engineered or *autologous* bladder material; Finite Element Analysis and Computational Fluid Dynamic modelling of the bladder.



## 4. Viscoelastic Properties of Human Bladder Tumours

### 4.1 Introduction

The aim of this chapter was to determine the viscoelastic properties of human bladder tumours. These properties have rarely been studied, despite such data being highly relevant to the development of improved surgical devices, diagnostic tools, computational models and surgical trainers. Previous studies on tumours have investigated the Young's modulus of bladder tumour cells (Lekka *et al.*, 1999; Lekka *et al.*, 2001; Lekka *et al.*, 2012), but did not take into account the likelihood of a tumour being viscoelastic, as is the case for the normal bladder tissue tested in chapter 3. Further, these studies only considered the properties at a cellular level and not at the tissue level. Testing at the tissue level is important as replacement is conducted at this scale, and there will be differences in how cells mechanically behave when they form a tissue structure. Viscoelastic material properties are important as they account for the time dependent nature of a biological tissue's mechanical behaviour. For example, the Young's modulus of a tissue will change depending on the loading/strain rate that is applied. This chapter describes the use of Dynamic Mechanical Analysis (DMA) to quantify the frequency-dependent viscoelastic properties of human bladder tumours on the macro scale in terms of storage ( $E'$ ) and loss ( $E''$ ) modulus. Section 4.2 details the preliminary testing and the materials and methods used for the final testing, including obtained ethical permission. Section 4.3 describes the results in terms of storage and loss modulus, section 4.4 discusses the significance of the results and their potential applications and finally section 4.5 summarises the chapter.

## 4.2 Materials and Methods

### 4.2.1 Preliminary Testing Methods

As the author was aware that the availability of human bladder tumours would be low, all preliminary testing was conducted on *porcine* bladder supplied by Fresh Tissue Supplies (East Sussex, UK). Once defrosted, using Ringer's solution (Oxoid Ltd, Basingstoke, UK), from a -40 °C freezer, areas of the central region of three *porcine* bladders (the central region is detailed in section 3.2.4) were dissected into rectangular specimens roughly similar to the geometries of the human tumours described later in this chapter. These geometries were estimated to be 15 mm x 10 mm x 5 mm by the medical researchers and surgeons Dr Richard Bryan, Mr Prashant Patel and Mr Richard Viney of the Institute of Cancer and Genomic Sciences, University of Birmingham and Queen Elizabeth Hospital Birmingham. The bladder specimens were cut using surgical scissors (Fischer Scientific, Loughborough, UK) after which each specimen was measured using Vernier callipers (Fisher Scientific, Loughborough, UK) with a precision of 0.1 mm.

Tensile DMA was attempted initially, for consistency with the previous DMA tests on bladder tissue (chapter 3). However, due to the small size of the specimens, mean width of 13.3 mm (standard deviation 2.0 mm), mean depth 9.7 mm (standard deviation 2.7 mm) and height of 4.6 mm (standard deviation 0.9 mm), great difficulty was experienced in trying to fix the specimens into the grips, as shown in figure 3.4b (Chapter 3). Also, when the author did manage to fix the specimens into the grips, the small preload that was applied pulled the

specimens out of the grips. Therefore, it was clear that compression would have to be used for the testing of these smaller samples.

Under compression, DMA was attempted using load control. For these tests cuboidal specimens from the same three *porcine* bladders were used. However, difficulty was experienced in testing specimens under repeatable conditions. It was not feasible to use the same mean load and load amplitude ( $0.6 \text{ N} \pm 0.5 \text{ N}$  was attempted) for each specimen due to geometric variation. For example, the slightly smaller specimens could not be strained sufficiently to induce the same loads as the larger specimens, due to their lower specimen height. Furthermore, high stress relaxation was observed, which has also been discussed previously in section 3.2.5 and this added to the difficulty of attempting load led DMA. Therefore, displacement led DMA was used, which is also the case in the previous chapter.

The specimens were tested using a Bose Electroforce 3200 testing machine, fitted with a 22 N load cell, using WinTest Dynamic Mechanical Analysis (DMA) software (Bose Corporation, Electroforce Systems Group, Minnesota, USA). A 22 N load cell was used here as the loads were all to be lower than 5 N. An added benefit of using the 22 N load cell was a higher resolution in comparison to the 250 N load cell used in chapter 3 (both load cells have a maximum error of less than 1% of their maximum load). Other biological and synthetic materials have been compressively tested using Bose testing machines (Patel *et al.*, 2008; Fulcher *et al.*, 2009; Gadd and Shepherd, 2011; Omari *et al.*, 2015). The specimens were compressed using a stainless steel cylindrical plate with thickness of 4 mm and a diameter of 20 mm; the test set-up can be seen in figure 4.1.



**Figure 4.1 – Compressive DMA set-up for *porcine* bladder specimens and human bladder tumours.**

Three *porcine* bladder specimens were subjected to a compressive pre-load of 0.5 N and then subjected to a preconditioning cycle in compression at 1 Hz with a mean displacement of 0.75 mm and an amplitude (mean to peak/trough) of 0.15 mm. Preconditioning ensures that the first frequency tested is comparable to the rest of the frequencies tested thereafter. It has been described in the previous chapter and has also been used in other studies by Öhman *et al.*(2009) and Wilcox *et al.*(2014). After this preconditioning cycle the specimens were subjected to 19 test frequencies ranging from 0.01 – 30 Hz using the same mean displacement and amplitude. A dwell time of 10 seconds in between each frequency was used. The mean displacement and amplitude were selected as the author did not want to unnecessarily plastically deform the specimens whilst still inducing sufficient load to be measured by the load cell. The mean displacement was around 15 % of the mean specimen height and the displacement amplitude was approximately 20 % of the mean. The frequency range was selected as it was comparable to the frequencies tested in the preliminary testing described in the previous chapter and also comparable to

the frequencies used by DeWall *et al.*(2012) when testing liver malignancies, including tumours. Storage ( $E'$ ) and loss ( $E''$ ) moduli were calculated from the displacement sine wave input and load sine wave output using the WinTest DMA software. The method that the software uses to calculate the phase angle ( $\delta$ ) and dynamic stiffness ( $k^*$ ) was described in detail in section 2.4.6.  $E'$  and  $E''$  were calculated from (Fulcher *et al.*, 2009):

$$E' = \frac{k^* \cos \delta}{S} \quad (4.1)$$

$$E'' = \frac{k^* \sin \delta}{S} \quad (4.2)$$

where  $S$  is the shape factor, for a cuboid, which was calculated from:

$$S = \frac{wd}{h} \quad (4.3)$$

where  $w$  is the width,  $d$  is the depth and  $h$  is the height of a specimen.

#### 4.2.2 Preliminary Testing Results

The storage and loss modulus against frequency dependent trends for the three *porcine* specimens that were subjected to compression DMA can be observed in figures 4.2 and 4.3.

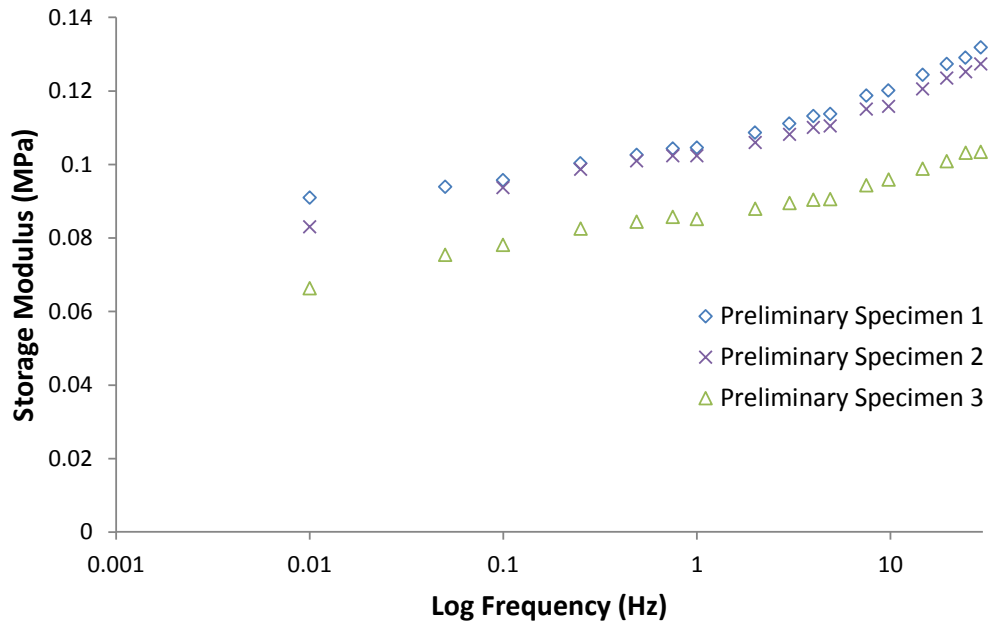


**Figure 4.2 – Storage modulus ( $E'$ ) against log frequency ( $f$ ) for the three preliminary *porcine* specimens.**

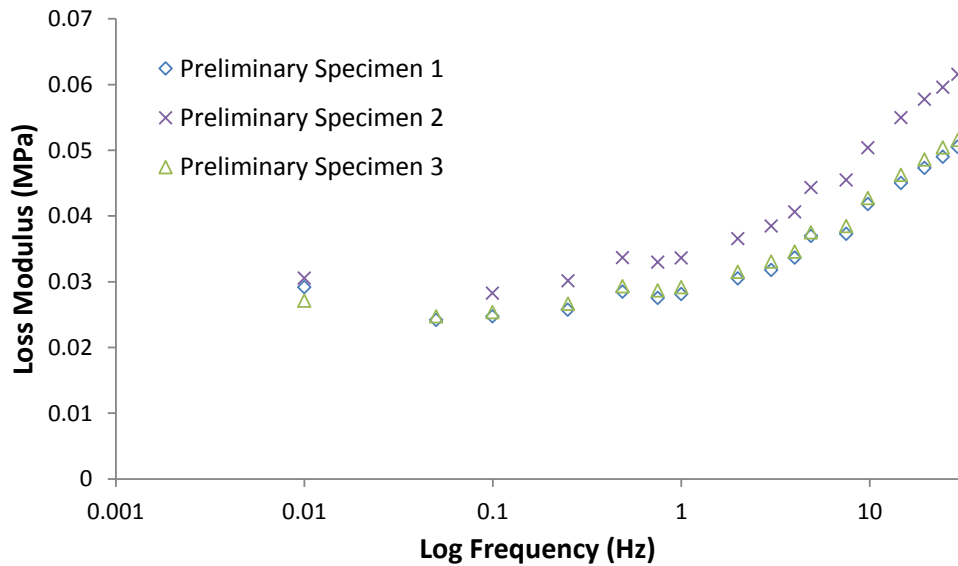


**Figure 4.3 – Loss modulus ( $E''$ ) against log frequency ( $f$ ) for the three preliminary *porcine* specimens.**

The results showed that *porcine* bladder specimens exhibited frequency dependant behaviour and that the storage modulus was higher than the loss modulus for every frequency tested. Furthermore, from preliminary tests it was feasible to characterise empirical frequency-dependent relationships for both storage and loss moduli. The storage modulus presented logarithmic trends against frequency, with  $R^2$  values of over 0.93, whilst the loss modulus presented second order polynomial trends against frequency, with  $R^2$  values over 0.97. As these results showed that trends could be characterised, providing evidence that the method of testing was suitable, it was decided that displacement led compression DMA would be used for testing the human bladder tumour specimens. The mean displacement and amplitude would, however, be altered to reflect the individual height of the specimen rather than the mean of all the specimens. This was necessary so that the variation in specimen geometry was accounted for, therefore, all specimens were subjected to the same strains.

#### **4.2.3 Final Testing Methods**

Ten human bladder tumour specimens were obtained from 8 patients recruited to the West Midlands (UK) Bladder Cancer Prognosis Programme (BCPP, ethics approval 06/MRE04/65) (Zeegers *et al.*, 2010). All human tissue specimens and data used in this study were collected with informed donor consent in compliance with national and institutional ethical requirements. BCPP methodology and patient characteristics have been described in detail elsewhere (Zeegers *et al.*, 2010; Bryan *et al.*, 2013). Tumour specimens were frozen in liquid nitrogen immediately after removal during TURBT and subsequently stored at -80°C. There is consensus that freezing does not affect the mechanical properties of soft tissues

(Chan and Titze, 2003; Szarko *et al.*, 2010; Woo *et al.*, 1986). Before dynamic mechanical testing, the specimens were defrosted in Ringer's solution (Oxoid Ltd, Basingstoke, UK) until thawed. All subsequent testing was carried out in a controlled environment at room temperature, 20°C. The basic patient and tumour characteristics, which are defined in section 2.3, for each specimen used, are provided in table 4.1, with a representative selection of specimens shown in figure 4.4.

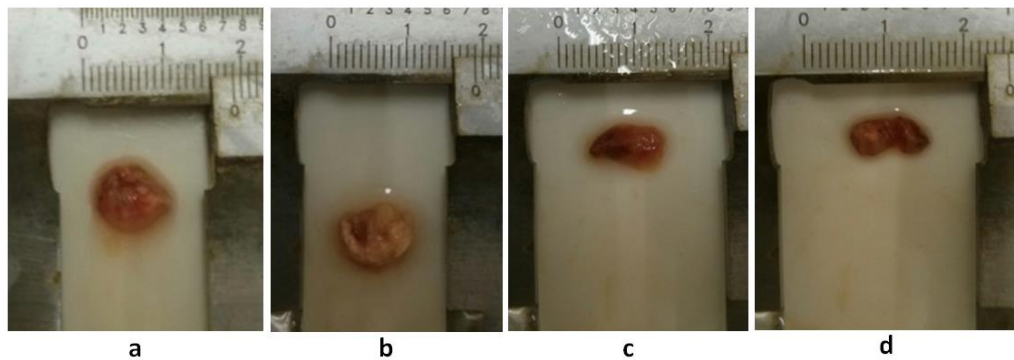


**Figure 4.4 – Human bladder tumour specimens: (a) specimen 2; (b) specimen 3; (c) specimen 6; (d) specimen 7.**

Each specimen was measured using Vernier callipers. The specimens were approximated to a cuboid and three measurements for width, depth and height were taken for each specimen. Mean and standard deviation values for these dimensions can be found in table 4.1.



**Table 4.1 - Individual information for the 10 bladder tumour specimens. Three of the specimens used (2, 6 & 7) were from the same individual. SD refers to standard deviation.**

Specimen Number	Grade/ Stage	Architecture	Age at collection	Gender	Mean Dimensions (SD)		
					Width (mm)	Depth (mm)	Height (mm)
1	Non-UBC	pap	83	Male	5.4 (0.2)	5.5 (0.5)	3.1 (0.2)
2	G3pT2+	pap	72	Male	8.1 (1.5)	7.5 (0.7)	5.0 (0.2)
3	G1pTa	pap	62	Male	3.8 (0.2)	4.9 (0.5)	3.0 (0.5)
4	G3pT2+	mixed	90	Female	12.5 (2.6)	8.1 (1.1)	5.2 (0.4)
5	Non-UBC	mixed	73	Female	4.4 (1.3)	7.6 (0.6)	3.2 (0.2)
6	G3pT2+	pap	72	Male	3.9 (0.4)	6.8 (1.4)	3.0 (0.2)
7	G3pT2+	pap	72	Male	6.2 (0.3)	18.3 (0.2)	4.8 (0.4)
8	G2pT1	pap	73	Male	3.2 (0.1)	6.6 (0.3)	1.0 (0.2)
9	G3pT2+	mixed	68	Female	5.3 (1.0)	10.5 (1.8)	3.9 (0.4)
10	G3pT2+	pap	83	Male	4.7 (1.0)	9.8 (0.9)	2.8 (1.5)

Specimens were tested in a random order chosen using the Excel (2010, Microsoft, Washington, USA) random number function. The specimens were initially given a preload of 0.1 N and were then subjected to a preconditioning cycle of 5 Hz. The preload was lowered from preliminary testing as the specimens were smaller than had been expected; also the preconditioning frequency was increased to fall in line with the rectangular testing described in the previous chapter. After this the specimens were tested from 0.01 to 30 Hz in 14 steps with the same dwell time of 10 seconds between frequencies; this was consistent with the bladder tissue testing procedure in chapter 3 and a study on liver tumours by DeWall *et al.* (2012).

For both the preconditioning cycle and the frequencies from 0.01 to 30 Hz the specimens were subjected to a sinusoidally varying displacement ( $y$ ) in the form:

$$y = x + z \sin(2\pi ft) \quad (4.4)$$

where  $x$  is the mean displacement (20% of a specimen height; table 4.1),  $z$  is the amplitude (0.1 $x$ ),  $t$  is time (in seconds) and  $f$  is the test frequency. The mean displacement was increased from the preliminary testing to ensure a sufficient load was being registered and the amplitude was lowered to 10% of the mean so as to avoid plastic deformation for each specimen during testing. In this instance the amplitude was defined as the peak/trough displacement to the mean displacement. For example, specimen number 5 had an average height of 3.2 mm which equated to testing parameters of a mean displacement ( $x$ ) of 0.64 mm compression and amplitude ( $z$ ) of 0.064 mm. The values for mean displacement and amplitudes for each specimen can be found in table 4.2.

**Table 4.2 – Human bladder tumour testing parameters.**

Specimen Number	Testing Parameters	
	Mean Displacement (mm)	Amplitude (mm)
1	0.613	0.061
2	1.007	0.101
3	0.600	0.060
4	1.033	0.103
5	0.640	0.064
6	0.593	0.059
7	0.953	0.095
8	0.207	0.021
9	0.780	0.078
10	0.567	0.057

Storage modulus and loss modulus were then calculated, plotted against frequency and regression analysis was undertaken using Sigma Plot (version 11.0, Systat Software Inc., London, UK). The curve fit relationship was considered significant if  $p < 0.05$ . The 95% confidence intervals were also generated using Sigma Plot.

### 4.3 Results

Out of the ten specimens studied, the results of three were rejected. Specimen 8 was rejected as the mechanical testing did not induce sufficient load (thus the signal to noise ratio of the measured load was too low for use). The results for specimen 6 were not recorded due to a machine error and for specimen 3 the results were more than 15 standard deviations higher than the mean of the other specimens (figure 4.5) and it was rejected using Peirce's criterion (Peirce, 1852; Ross, 2003; Patel *et al.*, 2010).

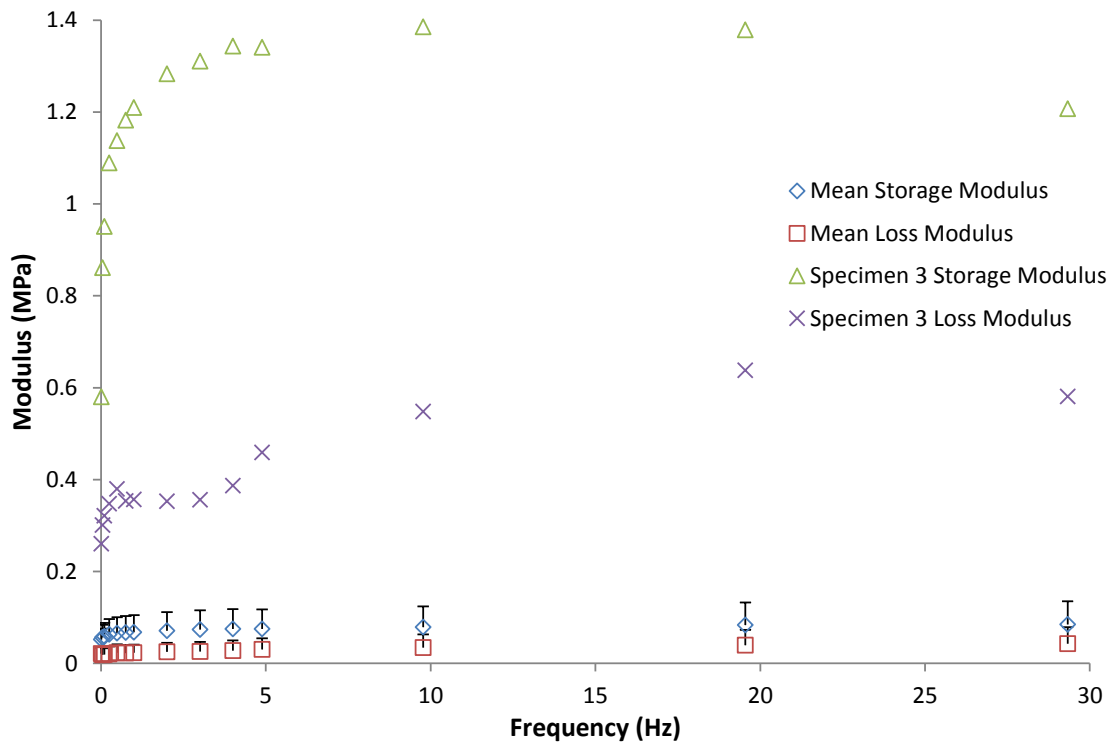


**Figure 4.5 – Mean storage ( $E'$ ) and loss modulus ( $E''$ ) against frequency ( $f$ ) with 1 standard deviation positive error bars and specimen 3 storage ( $E'$ ) and loss modulus ( $E''$ ) against frequency ( $f$ ).**

For the generation of 95% confidence intervals, the specimen number ( $n$ ) was taken as 6 because the 7 specimens came from 6 different patients which equated to 6 independent observations (Ranstam, 2012).

The storage modulus was higher than the loss modulus for every frequency of each specimen tested. Storage modulus was found to increase with increasing frequency following a logarithmic trend (figure 4.6). The trends for the storage modulus ( $E'$ ) against frequency ( $f$ ) were described by the logarithmic curve fit:

$$E' = A_T \ln(f) + B_T \quad \text{for } 0.01 \leq f \leq 30 \quad (4.5)$$

where  $A_T$  and  $B_T$  are constants (see table 4.3 for constants for each specimen). This logarithmic curve fit showed a good correlation to the original data with  $R^2$  values all above 0.7. All relationships were found to be significant ( $p < 0.05$ ).

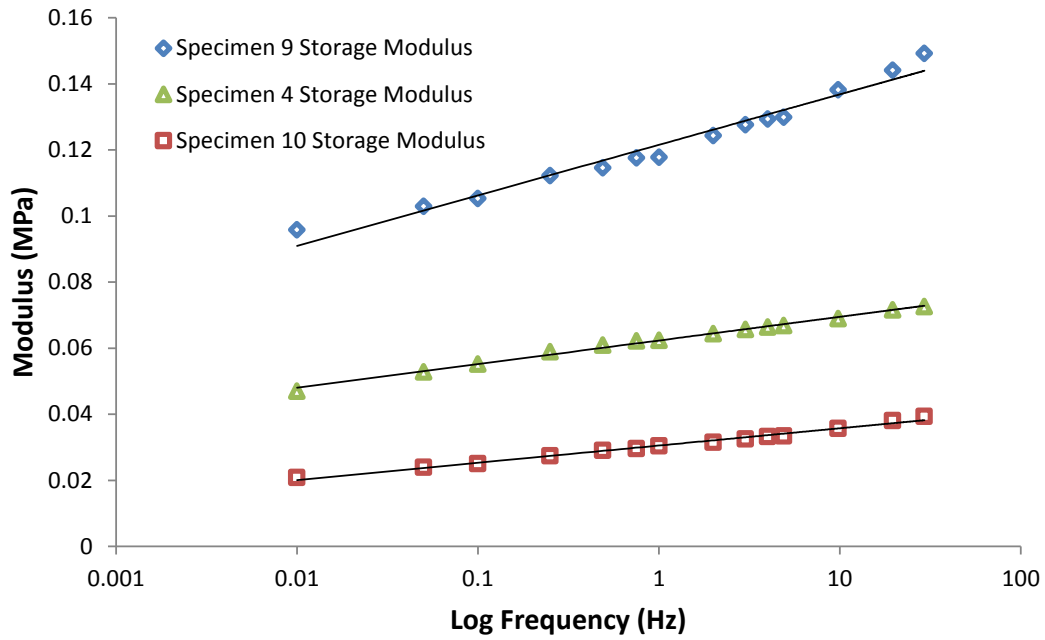


**Figure 4.6 – Storage modulus ( $E'$ ) against log frequency ( $f$ ) for three individual tumour specimens. The curve fit is given by equation 4.5.**

The mean storage modulus for all specimens against frequency (figure 4.7) followed the same trend as the individual specimens. The curve fit for the mean storage modulus can be seen in equation 4.6. From 0.01 Hz to 30 Hz the mean storage modulus increased from 0.05 MPa to 0.085 MPa.

$$E' = 0.0042 \ln(f) + 0.069 \quad \text{for } 0.01 \leq f \leq 30 \quad (4.6)$$

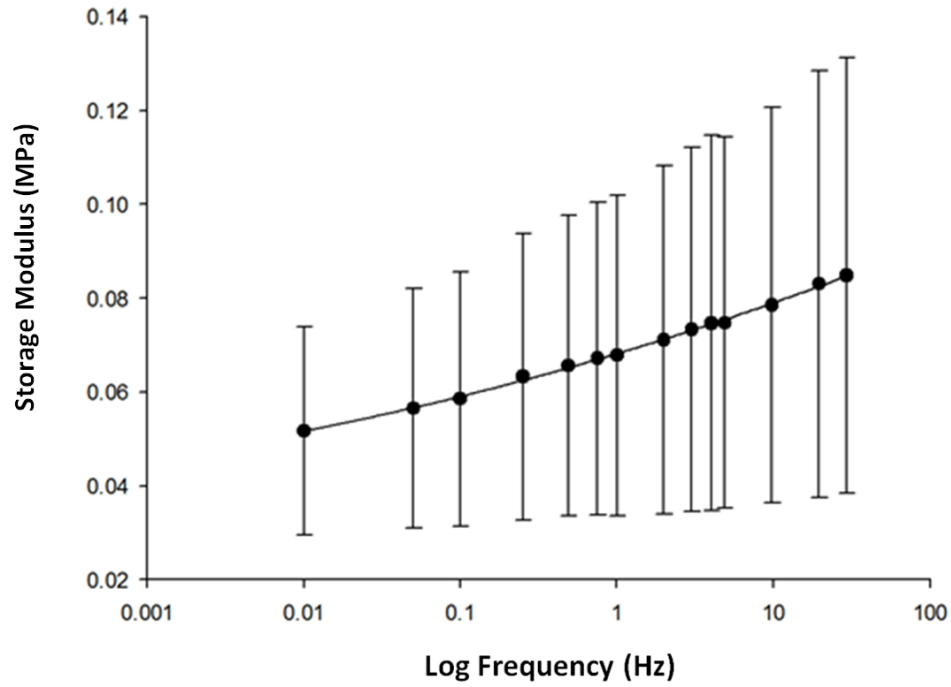


**Figure 4.7 – Mean storage modulus ( $E'$ ) against log frequency ( $f$ ). Error bars represent the 95% confidence intervals for the sample. The mean curve fit for the storage modulus against log frequency is stated in equation 4.6.**

For the individual specimens, the loss modulus was initially at a roughly constant value with increasing frequency until around 1 Hz where the loss modulus started to increase (figure 4.8). The trends for the loss modulus ( $E''$ ) against frequency ( $f$ ) were described by a second order polynomial curve fit:

$$E'' = C_T(f^2) + D_T(f) + E_T \quad \text{for } 0.01 \leq f \leq 30 \quad (4.7)$$

where  $C_T$ ,  $D_T$  and  $E_T$  are constants (see table 4.3 for constants for each specimen). This polynomial curve fit showed a good correlation with  $R^2$  values all above 0.69. All relationships were found to be significant ( $p < 0.05$ ).

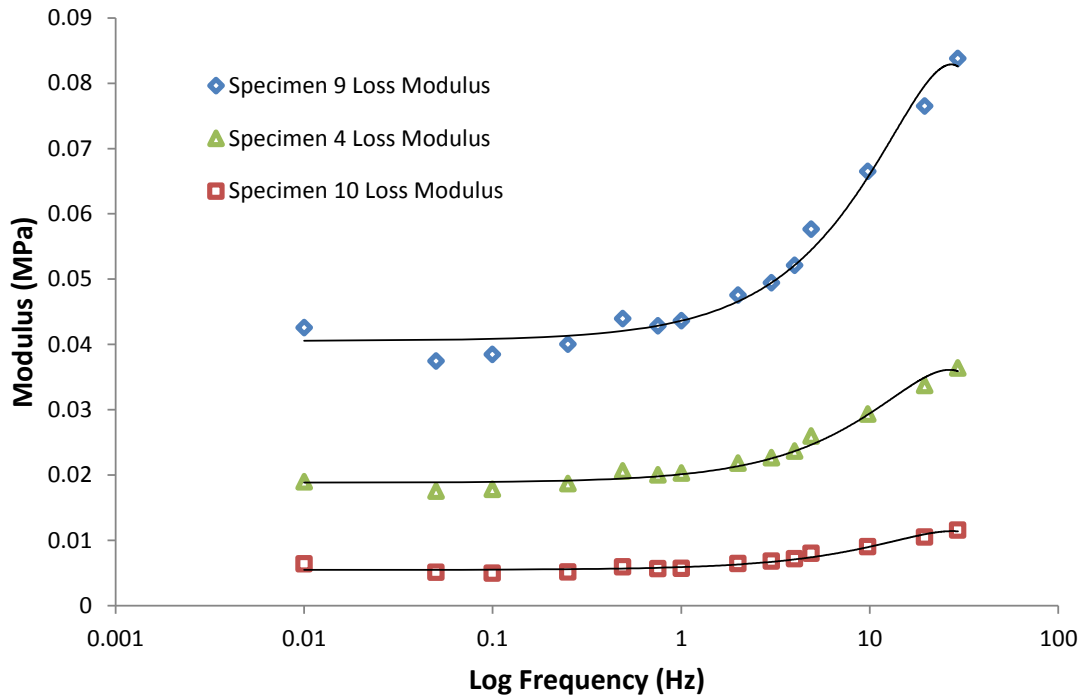


**Figure 4.8 – Loss modulus ( $E''$ ) against log frequency ( $f$ ) for three individual tumour specimens. The curve fit is given by equation 4.7.**

The mean loss modulus for all specimens against frequency (figure 4.9) followed the same trend as the individual specimens. The curve fit for the mean loss modulus can be seen in equation 4.8. The mean loss modulus was initially at around 0.02 MPa at frequencies less than or equal to 1 Hz and then increased to 0.043 MPa by 30 Hz.

$$E'' = -0.00003(f^2) + 0.0017(f) + 0.0150 \quad \text{for } 0.01 \leq f \leq 30 \quad (4.8)$$

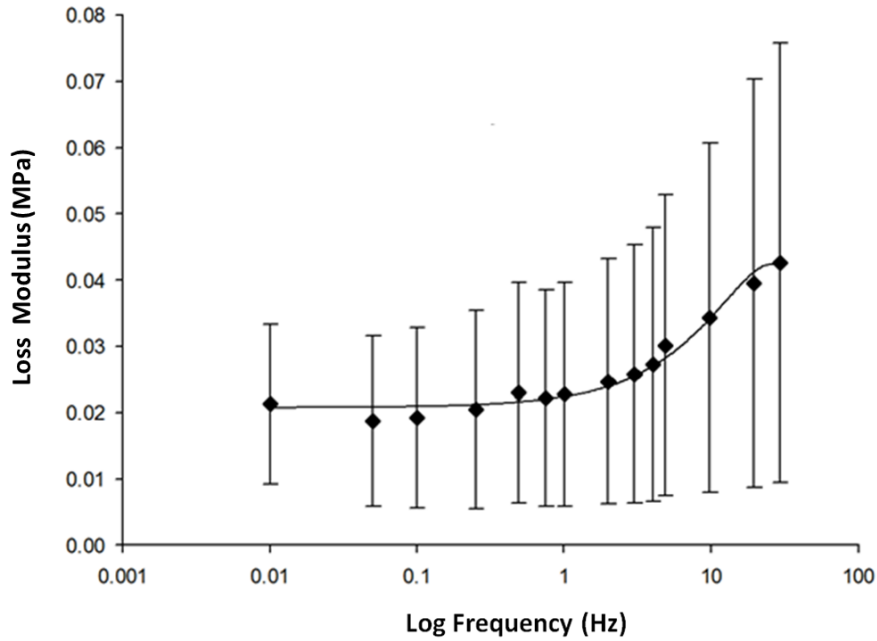


**Figure 4.9 – Mean loss modulus ( $E''$ ) against log frequency ( $f$ ). Error bars represent 95% confidence intervals for the sample. The mean curve fit for the storage modulus against log frequency is stated in equation 4.8.**

**Table 4.3 – Curve fit results for storage and loss modulus. All coefficients were found to be statistically significant ( $p < 0.05$ ).**

Specimen Number	Storage Modulus Curve Fit ( $E' = A_T \ln(f) + B_T$ )			Loss Modulus Curve Fit ( $E'' = C_T f^2 + D_T f + E_T$ )			
	$A_T$	$B_T$	$R^2$	$C_T (x10^{-3})$	$D_T$	$E_T$	$R^2$
1	0.0132	0.1200	0.997	-0.107	0.0050	0.0045	0.953
2	0.0017	0.0365	0.865	-0.016	0.0008	0.0098	0.939
3	0.0031	0.0624	0.995	-0.025	0.0013	0.0188	0.981
4	0.0012	0.0641	0.848	-0.016	0.0008	0.0167	0.904
5	0.0013	0.0481	0.705	-0.007	0.0004	0.0093	0.691
6	0.0066	0.1216	0.966	-0.058	0.0031	0.0406	0.982
7	0.0023	0.0306	0.989	-0.008	0.0004	0.0055	0.960
Mean	0.0042	0.0690	0.909	-0.03	0.0017	0.0150	0.916



## 4.4 Discussion

The results of this chapter show that bladder tumours are viscoelastic throughout the range of frequencies that were tested. Furthermore, the storage modulus was constantly higher than the loss modulus. In comparison to chapter 3 on the tensile viscoelastic properties of *porcine* bladder where the mean values of storage and loss modulus were 0.36 MPa and 0.05 MPa, respectively, human bladder tumour had a mean storage modulus of 0.07 MPa and a mean loss modulus of 0.02 MPa. In spite of differences in the mammal tested and the type of loading, consistencies in the general trends of the storage and loss modulus were found. At low frequencies (below 1 Hz) the storage modulus of the porcine bladder in chapter 3 did show a logarithmic trend similar to the one seen in the results of this chapter, and the porcine bladder loss modulus showed an increasing trend against frequency which can also be seen in the human bladder tumour results presented here.

DeWall *et al.* (2012) used similar testing equipment and protocols to characterize the viscoelastic properties of normal and tumourous liver tissue. They found that the background (normal) tissue storage modulus was higher than the malignant tissue for each of the frequencies tested. Over a comparable frequency range the storage modulus of the liver tumours (0.01 MPa) was less than the storage modulus found for human bladder tumours in this chapter (0.08 MPa).

Lekka *et al.* (2012) also found that cancerous cells of a variety of tissue decreased in stiffness in comparison to normal tissue. They reported a value of 0.001 MPa for the Young's modulus of bladder cancer tumours, whereas this chapter reports a higher value of 0.06 MPa (dynamic modulus) at a comparable loading rate. However, comparison is difficult due

to the differences in testing at the cellular and tissue levels and also because dynamic modulus is a viscoelastic property as opposed to Young's modulus which assumes the material to be purely elastic. Dynamic modulus can be calculated from the orthogonal of the storage and loss moduli,  $E^* = \sqrt{E'^2 + E''^2}$  (Hukins *et al.*, 1999).

The translational utility of the findings in this chapter lie in several areas:

- **Diagnostic:** Ultrasound elastography is effective in the detection of tumours in breast cancer (Gheonea *et al.*, 2011). Elastography makes use of external tissue compression and ultrasound imaging to map the stiffness of different areas of tissue. The differences in the mechanical properties of normal and tumourous tissue point oncologists to potential regions of malignancy. In breast cancer, malignant tissue was found to be stiffer by Itoh *et al.* (2006) than benign tissue when using ultrasound elastography. There have also been many studies which make use of magnetic resonance elastography (MRE) to study the viscoelastic properties of tissue. MRE is a method which images tissue whilst it is subjected to shear waves, from this elastograms are generated, which are 'maps' of tissue stiffness (Mariappan *et al.*, 2010). A few examples include: studies of the brain (Klatt *et al.*, 2007; Streitberger *et al.*, 2012), liver (Klatt *et al.*, 2007; Asbach *et al.*, 2008) and breast tissues (Sinkus *et al.*, 2005). If the modulus values for normal and malignant bladder tissue are known there is the potential for diagnosis with imaging techniques that use mechanical stimulation. Currently such tools are not used in the diagnosis of bladder cancer, but the author believes that in the future

this may become a favourable solution in comparison to cystoscopy, biopsy or cross-sectional imaging.

- **Surgical training:** In applications such as training for surgery, such as TURBT, it may be advantageous for the surgeon to practice or learn to use existing or new (an example of which is detailed in chapter 5) equipment to cut through material with similar viscoelastic properties to tumour tissue. Ahmadzadeh and Hukins (2014) have described a method of manufacturing materials with certain viscoelastic properties that could be used in this instance. The Uro Trainer manufactured by Karl Storz GmbH (Tuttlingen, Germany) is a virtual reality trainer which provides haptic feedback based on the experience of surgeons (Reich *et al.*, 2006). More realistic feedback may be achievable for a range of different tumours with their respective viscoelastic properties.
- **Instrument design:** An indentation system similar to that described by Appleyard *et al.* (2001) for cartilage could be manufactured to measure and assess the viscoelastic properties of tumours *in vivo*. The viscoelastic properties of any suspicious bladder tissue or lesions could then be ascertained *in vivo* and these measurements could be used to distinguish between tumorous and healthy tissue; appropriate action could then be taken during the same procedure. This is in contrast to taking a biopsy, waiting for results and then undergoing another procedure.
- **Computational models:** The values presented in this study would be able to inform better computational models of the bladder. For example, Chai *et al.* (2012) have presented a finite element model of the bladder and surrounding

organs using a linear elastic material model. However, this study only took into account the Poisson's ratio and Young's modulus of the tissues, which do not account for the time dependant nature of soft tissues. Viscoelastic properties could be incorporated into models investigating the differing areas of stress concentration, when comparing the filling behaviour of a healthy bladder (using the viscoelastic properties determined in chapter 3) to a tumour-containing bladder. Also, fluid structure interaction models to investigate the path of tumour cells during TURBT are possible. Methods for combining fluids and structures in computational models have previously been described by Espino *et al.* (2015).

A possible limitation of the testing described in this chapter may be in the shape assumption of a cuboid for the tumour specimens. The majority of the specimens tested had on inspection a rectangular shape, when observing the specimen from above. However, as can be seen in figure 4.4a and 4.4b, this varied and these specimens were more cylindrical in appearance. The errors in the calculated shape factor are expected to have only a limited effect on the results as the mean overestimation (percentage increase) of the shape factor is 17% (with a 9% standard deviation) when comparing the shape factor of a cylinder to a cuboid. For example, specimen number 6 had a shape factor of 8.9 mm when it was approximated to a cuboid, this is in comparison to 7.5 mm when it was approximated to be a cylinder using the equation from Fulcher *et al.*(2009) below:

$$S = \frac{\pi D^2}{4h} \quad (4.9)$$

where  $D$  is the diameter. This comparison results in a shape factor percentage decrease of 18% when going from a cuboid to cylinder for specimen number 6. In reality, the shape of the specimens was probably somewhere in between a cuboid and a cylinder so the actual overestimation would have been less. Furthermore, the individual trends for each specimen would not be changed by a difference in shape factor, only offset, as the shape factor was constant for each specimen.

Due to the low sample size of the human tissue, the variables of grade, stage, type, age and gender were not compared. Future studies investigating these variables could be of great value; for example, Swaminathan *et al.* (2011) demonstrated that as ovarian tumour cells become more invasive, their stiffness decreases. Furthermore, DeWall *et al.* (2012) have hypothesized that tissue properties may also be useful in diagnosing different tumour types. If there is a relationship between the viscoelastic behaviour of bladder tumours and their grade, stage or type this would be of great value in diagnostic procedures.

Human tissues are in high demand but are rarely available and for this reason preliminary testing was conducted entirely using *porcine* bladder tissue instead of human bladder tumour. Tissue testing on similar mammals to humans is often the best model that can be found. However, in the specific case of tumour characterisation, sourcing animal specimens is not necessarily any easier than sourcing human tumour specimens. This is because animals destined for the food chain are generally required to be healthy and often slaughtered when still relatively young. For example, all of the *porcine* bladders used in this study came from pigs less than a year old.

## 4.5 Chapter Summary

The conclusions of this chapter are as follows:

- Bladder tumours exhibit frequency dependent viscoelastic behaviour through the range of frequencies tested (0.01 – 30 Hz).
- The storage modulus exhibited a logarithmically increasing trend against frequency with a mean value of 0.069 MPa and the loss modulus exhibited a quadratic increasing trend against frequency with a mean of 0.027 MPa.
- Applications of these findings include the diagnosis of bladder cancer, computer simulations of the bladder and the manufacture of more realistic tumour models in surgical trainers.

## 5 Design of a Surgical Instrument for the Removal of Bladder Tumours

### 5.1 Introduction

Bladder cancer is the 4<sup>th</sup> most common and 13<sup>th</sup> most common cancer in men and women, respectively in the UK (Cancer Research UK, 2014). The gold standard for treating the non-muscle invasive form, which affects about 75 – 85% of bladder cancer sufferers at presentation (Babjuk *et al.*, 2008), is transurethral resection of bladder tumours (TURBT). There are problems with this procedure, the most significant of which is tumour cell dissemination and re-implantation elsewhere on the bladder wall (Kondas *et al.*, 1999; Bryan *et al.*, 2010). Although much research is under way to investigate some of the other issues, such as whether novel imaging techniques have sufficient resolution to detect smaller tumours (Bach *et al.*, 2015), apart from research into removing tumours *en bloc* little has been done to reduce the scattering effect of the procedure (Wilby *et al.*, 2009; Bach *et al.*, 2015).

The aim of this chapter is to design and prototype a novel surgical instrument to arrest the spread of tumour cells during TURBT. This chapter describes the design requirements (section 5.2), the concept design development (section 5.3) and then the development of Nitinol actuation methods (section 5.4). After this, the finalised design is presented (section 5.5), then the methods of prototype manufacture (section 5.6) and the *in vitro* testing of the prototype (section 5.7). This is followed by a discussion (section 5.8), some thoughts on how the device can be developed further in the future (section 5.9) and the chapter summary (section 5.10).

## 5.2 Design Requirements

The design requirements for the instrument enhancement were formulated in accordance to BS EN ISO 16061:2009 (British Standards Institution, 2009) and BS ISO 8600-1:2013 (British Standards Institution, 2013). The instrument enhancement should:

- Be able to remove an entire tumour from the bladder.
- Limit tumour cells from re-implanting elsewhere on the bladder wall.
- Not increase surgery time which generally takes 51 minutes (Pandit and Carey, 2006).
- Not cause harm to the patient.
- Not cause an immune response from the body and hence be manufactured from biocompatible materials.
- Be able to enter and exit the bladder via the urethra.
- Not impede the surgeon's view of the tumour.
- Be single use. Therefore, sterilisation will only be performed by the manufacturer.
- Be able to work with existing surgical instruments for TURBT, such as various sheaths, cystoscopes, light source and diathermy loop. Hence, current instruments will not be altered.
- Be able to work in an isotonic or hypotonic aqueous environment at 37 °C for times of up to one hour (Pandit and Carey, 2006).
- Be no more than 350 mm long (with all parts connected), more than 8.5 mm bore and no more than 11 mm in outside diameter.



- The main design consideration was that the add-on device should be able to limit the movement of tumour cells after the main tumour has been cut into.

## **5.3 Design Development**

### **5.3.1 Design Solutions**

Brainstorming led to three potential solutions to the problem of tumour cell re-implantation:

1. A polymer spray that would ‘stick’ the cells of the tumour together. This would mean that when the tumour is then cut into, the smaller tumour cells will not move away from the larger pieces of cut tumour, thus reducing the likelihood of tumour cell re-implantation.
2. The development of existing irrigation channels used with surgical instruments for TURBT. Altering the existing design of the irrigation channels to ensure that tumour cells are ‘sucked’ straight back out of the scope after resection rather than moving towards other areas of the bladder wall.
3. A cone add-on device that would be able to open once inside the bladder and physically restrict the movement of tumour cells to other areas of the bladder during resection.

The polymer spray solution was inspired by surgical glues, such as the hydrophobic light-activated adhesive described by Lang *et al.* (2014), for the repair of large blood vessels and cardiac wall defects. However, the idea was rejected due to the difficulty of accurately

spraying another liquid when already within an aqueous environment. Also it might be difficult for the spray to penetrate within the tumour, so when it was cut into, only the cells on the outside would be 'stuck' to the main tumour; the other tumour cells, as before, would be able to break off from the main tumour.

The development of irrigation channels was excluded as it was felt that any improvement would be dependent on the dimensions of the bladder in which it was being used. Also higher rates of irrigation may be difficult to achieve due to the limited diameter of the irrigation channels and could lead to problems for the surgeon, such as decreased visibility.

Therefore, after careful consideration of the design requirements, a concept of an add-on cone to current resectoscope sheaths was selected as the solution for development. The concept was that limiting fluid transfer to within the cone would effectively block tumour cells from reaching other areas of the bladder wall. The closed cone would have to be inserted into the bladder along with the current resectoscope instrument through the urethra and then be able to open once inside the bladder (figure 5.1). The cone once opened would then be positioned against the wall of the bladder covering the tumour, creating a flat surface against which the surgeon could operate. The creation of this flat surface may be aided by a negative pressure within the cone induced by the irrigation system currently used in the resectoscope. The tumour would then be resected as normal and once finished the cone would close and be taken out of the bladder.

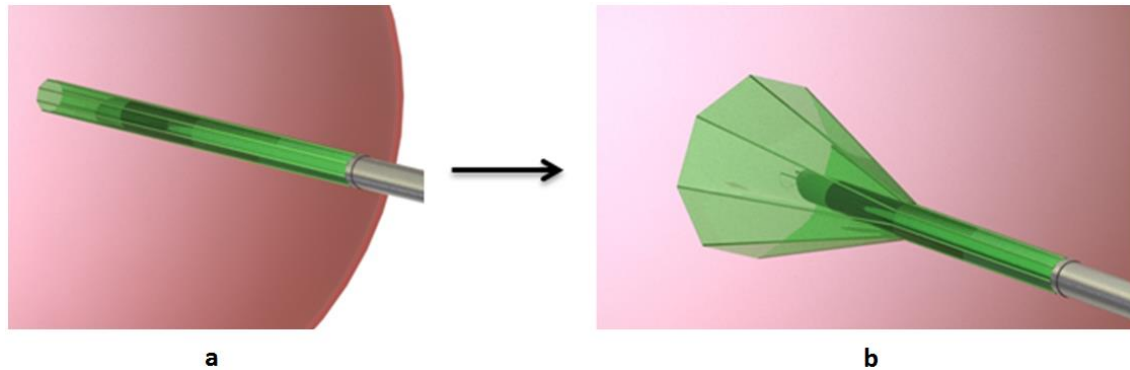


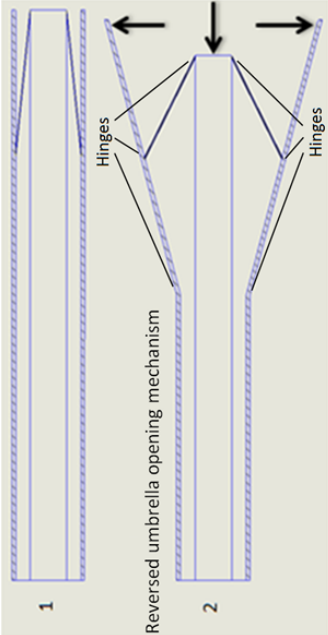
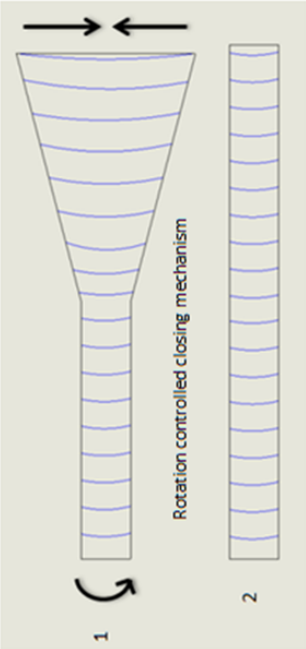
**Figure 5.1 – Closed (a) and open (b) position of the cone concept within the bladder.**

### **5.3.2 Cone Actuation Methods**

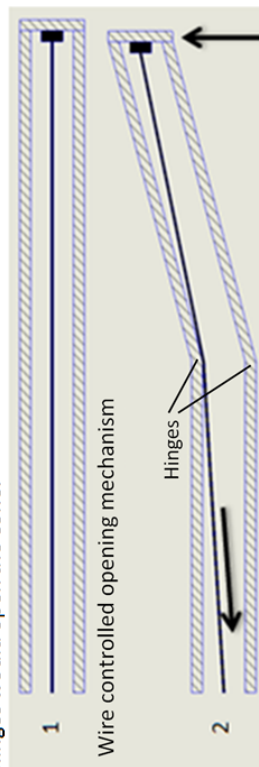
The greatest challenge associated with this design was the method of opening the cone. Due to the limited diameter of the urethra and that of the existing instruments, actuation (opening) of the cone would be difficult. Current resectoscopes have an outer diameter of around 8.5 mm and any add on device would aim not to have a diameter greater than 11 mm. This outer diameter was selected on advice from medical researchers and surgeons Dr Richard Bryan, Mr Prashant Patel and Mr Richard Viney of the Institute of Cancer and Genomic Sciences, University of Birmingham and Queen Elizabeth Hospital Birmingham.

Several different methods of actuating the cone were explored and these can be seen in table 5.1.

Table 5.1 – Potential cone actuating methods, with their potential advantages and disadvantages.

Solution	Description	Advantages	Disadvantages
Reverse Umbrella	<p>Cone opened by centre column being pushed towards the centre of the scope.</p> 	Enough force would be provided by the mechanism to open the cone.	Hinges would need to be fixed to the current outer sheath.
Rotation Wire	<p>Rotation of the wiring at the base of the cone housing would transfer down to the end of the cone and create a closing force.</p> 	The cone would open when the rotation was released. Therefore, the surgeon would not have to control the cone whilst operating.	Torque would have to be applied when the cone was being inserted into the bladder. This would induce stress in the wire at a time when failure could cause harm.

Shape Memory Polymer (SMP)	Use of a shape memory polymer to open the cone. Lendlein and Langer (2002) have previously reported the potential for using shape memory polymers which can exhibit up to 400% deformation between a temporary and permanent shape.	It may be possible to manufacture the entire cone out of one shape memory polymer.	Lack of knowledge/equipment needed to synthesize appropriate polymers. Furthermore, actuation times can be up to several minutes (Liu <i>et al.</i> , 2007) which are too long for this application.
Elastic Alloy	Inspired by the tool that mechanics use to pick up non-magnetic parts from hard to reach areas. The use of an elastic alloy that, when a sheath surrounding the cone was removed, would open to form a cone. This would work on the principle that the alloy would not be stressed past its elastic limit.	Potentially very simple to manufacture.	Difficult to find an alloy that would remain in the elastic range at the angles required. This solution would require two extra sheaths on top of the current resectoscope.
Shape Memory Alloy (SMA)	Use of Nickel Titanium (Nitinol) to open the cone once inside the bladder. Nitinol can be trained to conform to different shapes at different temperatures.	Available at small enough thicknesses to be used in this application.	Potential difficulty in training several shape memory alloys to actuate to the same angle, at the same time.
Wire Tension	A wire controlled opening mechanism, which when used in combination with hinges would open the cone.	Simplistic mechanical approach.	Would have to be controlled at the bottom of the scope where the surgeon will be operating. Complicating this area further is undesirable. Further, the manufacture of a mechanism at this scale would be very difficult. Requires a fairly large amount of tension to be transferred down a small diameter wire. Fixing the wire to the body of the mechanism will also be difficult at this scale.



<b>Bimetallic Strip</b>	Two different materials which expand at different rates when heated may also be able to provide the movement required. This bimetallic strip type of device, if correctly manufactured, may be able to provide the required movement under heating and cooling.	Appropriate size for the application.	Correct manufacturing techniques such as sputtering not available for a strip of appropriate size.
<b>Electroactive Polymer (EAP)</b>	Use of an electroactive polymer or dielectric elastomer. A soft dielectric EAP hinge has been described by Lochmatter and Kovacs (2008) that can achieve rotations of up to 30°.	Potentially the entire cone can be made out of the polymer, of which only certain parts will actuate.	May be difficult to manufacture a hinge at the appropriate size for a surgical instrument.
<b>Piezoelectric</b>	The piezo electric effect has previously been described by Karpelson <i>et al</i> (2012) to drive micro aerial robots such as replica insects, centipedes and cockroaches. Very high driving frequencies have been achieved in these robots such as 300 Hz for the insect.	Good fatigue properties. Billions of cycles can be achieved without adverse effects.	May not provide enough force or displacement for actuation of the cone. More appropriate for high frequency applications.
<b>Magnetic</b>	A magnetic actuator or solenoid to provide open/closed cone configurations.	Simple on and off configurations.	Solenoids were thought to be too large for this application.

### 5.3.3 Actuation Method Selection

After careful consideration the shape memory alloy Nitinol was selected to create the opening of the cone. The primary reasons were that it enables a device to conform to different shapes (i.e. one shape for access to the bladder, and another when inside the bladder) and that it is readily available in the relatively small thicknesses desired for this application. Furthermore, the type of movement that would be required from an actuating cone made from Nitinol has previously been described by Villanueva *et al.* (2010) in the form of a jellyfish device. Nitinol has also already been used within the body in different applications such as stents, heart valve frames, orthodontic implants and bone plates (Duerig *et al.*, 1999; Machado and Savi, 2003). Another Nitinol device, which has similarities with the cone concept shown in figure 5.1, used in the body is the AngioGuard filter device which is essentially a stent in combination with a filter which is used to remove debris from blood vessels (Fasseas *et al.*, 2001). Nitinol has also already been used in the urinary system to aid in the removal of renal calculi (kidney stones) (Kourambas *et al.*, 2000). Considering the extensive use of Nitinol within the body, it was deemed to be a sound biocompatible material on which to base a new device. There is also promising research in the area of shape memory metals, i.e. providing scope for further development in future. Chluba *et al.* (2015), for example, have described a copper nickel titanium alloy which has vastly improved fatigue performance compared with traditional Nitinol. However, these different SMAs were not as readily available and also these materials have not been extensively used in the body so they were not considered suitable for use in this study.

## 5.4 Preliminary Nitinol Testing

### 5.4.1 One-Way Shape Memory Effect

Nitinol wire (50% nickel and 50% titanium), of diameter 0.5 mm, was acquired from Dynalloy Inc (Tustin, California, USA). To test the ability of the Nitinol wire to demonstrate the one-way shape memory effect (OWSME) and move from one position to another, the wire was heated, whilst being constrained in a roughly circular shape in a crucible (Fischer Scientific, Loughborough, UK), to 550 °C for 15 minutes in a Carbolite LMF1 furnace (Carbolite, Derbyshire, UK). These parameters were found through trial and error for the training of a high temperature (HT) austenite crystal structure into Nitinol wire, after considering the methods described by Morgan and Broadley (2004). Then, after the wire was cooled (quenched), by placing it into cold water using tongs, it was deformed to a different shape (a coil in this case) after which boiling water, from a kettle, was poured over the wire. The results can be seen below in figure 5.2.

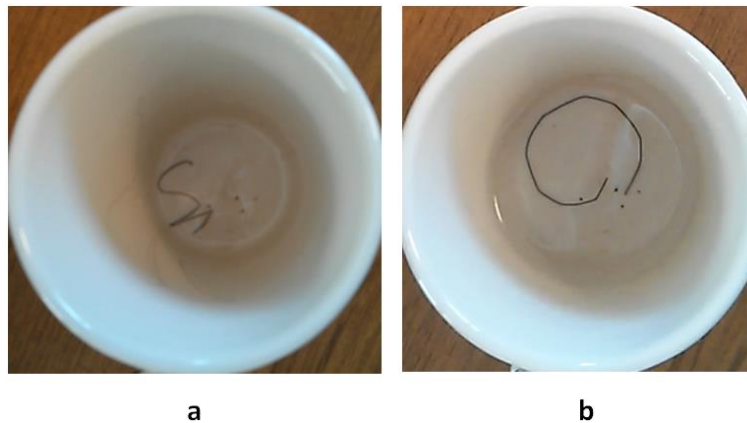


**Figure 5.2 – Transition of a 0.5 mm diameter Nitinol wire from a) deformed martensite to b) austenite (after insertion in boiling water).**



It is clear that the Nitinol changes from a deformed shape to the pre-trained roughly circular shape. This is due to the rise in temperature taking the Nitinol past its transition temperature of approximately 55 °C. This induced a change in the crystal structure, from deformed martensite to austenite, which enables the material to change shape (Otsuka and Wayman, 1999). This test successfully demonstrated the one-way shape memory effect.

### **5.4.2 Wire Actuation with Loading**

To see whether Nitinol wire could actuate, and hence still be able to demonstrate the OWSME whilst being loaded, required a further test. This was important for the SMA's ability to open the cone design previously described in section 5.3.1. Again a Nitinol wire of 0.5 mm diameter was used and a roughly circular shape was trained into the wire using the same HT training parameters described in section 5.4.1. The Nitinol wire was then deformed by hand so that an M8 nut could hang from the wire. A heat gun (Toolstation, Bridgwater, UK) was then used to heat the wire and, therefore, cause it to actuate. The mass of the Nitinol wire was 0.15 g and the mass of the M8 nut was 4.61 g (measured with an Ohaus GA200D electronic balance, Nänikon, Switzerland). The results of this actuation test with load can be seen in figure 5.3.

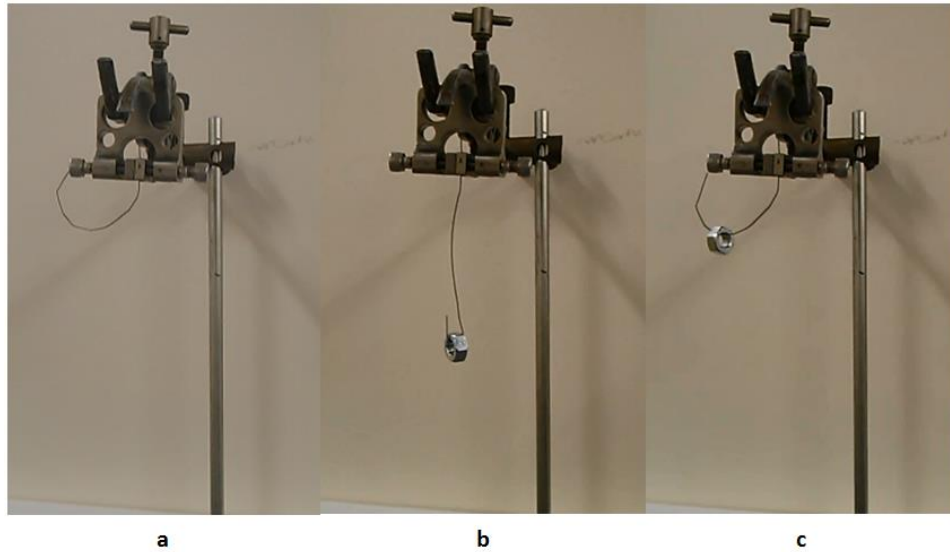


**Figure 5.3 – M8 nut lifting with 0.5 mm diameter Nitinol wire. a) pre-trained Nitinol wire with no M8 nut, b) deformed Nitinol wire with M8 nut, before heating, c) Nitinol wire with M8 nut returned to original position post heating.**

The results showed that the 0.5 mm diameter Nitinol could lift an M8 nut thirty times its own mass. However, it was seen that the wire did not return fully to its original pre-trained austenite shape; this was due to the mass of the nut bending the Nitinol wire. This effect was noted for the future training parameters of the actuating cone.

#### **5.4.3 Two-Way Shape Memory Effect**

The two-way shape memory effect was also explored as it was potentially desirable for the cone instrument. Having two pre-trained shapes to conform to could be beneficial, as this would correspond to the open and closed states of the cone device. Theoretically, Nitinol wire is able to be trained to two different shapes; one shape above its transition temperature and one shape below (Lahoz *et al.*, 2002). The 0.5 mm diameter Nitinol wire

was HT trained to conform to a 50° angle. After this high temperature training and subsequent quenching, the wire was heated past its transition temperature and then manually bent to 90° whilst it cooled. This was repeated 30 times in an attempt to train a martensite crystal structure shape into the wire. These methods were derived from the training techniques described by Luo and Abel (2007) and Fortini *et al.* (2014). After this TWSME training the wire was again heated past its transition temperature, using the same heat gun described in 5.4.2, to see if it would cool down to the 90° cool shape. The results can be seen in figure 5.4.

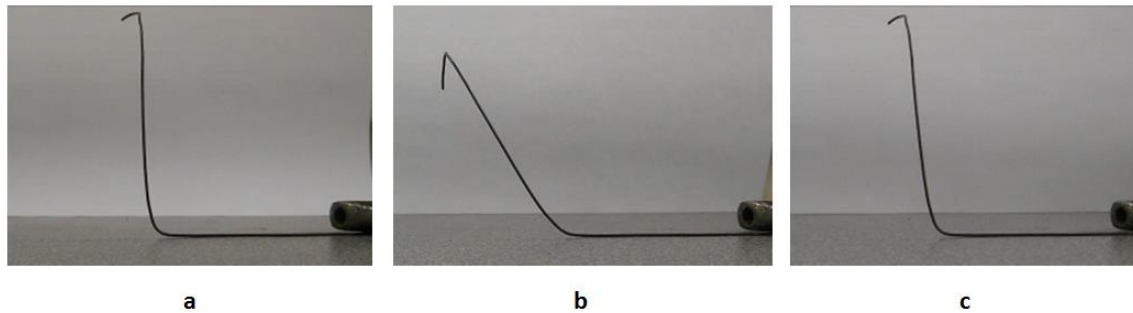


**Figure 5.4 – Two- way shape memory effect trial. a) is the pre-trained Nitinol wire at room temperature, b) is the Nitinol wire immediately after being heated past its transformation temperature with a heat gun and c) is the wire after four minutes of cooling.**

The Nitinol wire was able to exhibit the two-way shape memory effect, however, it took four minutes for the wire to cool to the 90° cold shape. This time could be reduced with enhanced cooling, such as refrigeration. However, as the application was for a surgical instrument operating at body temperature of 37°, it was concluded that the TWSME for this specific Nitinol wiring would not be feasible to use.

#### **5.4.4 Nitinol Actuation with Current**

For its intended use as part of a surgical instrument the author set about finding a reliable and easy actuation method to bring the wire past its transition temperature, therefore, actuation using a current was trialled. A Nitinol wire (90 mm length; 0.5 mm diameter) was heated using electrical current to enable the wire to actuate. A supply of 2.3 A and 30 V, from a model LT 30/2 Farnell Instruments power pack (Wetherby, UK), was used with connective wiring and crocodile clips from RS Components (Corby, UK) to bring the Nitinol to and past its activation temperature. When measured using a steel 1 mm diameter k-type touch thermocouple (RS Components, Corby, UK), connected to a Comark model 6600 digital thermometer (Norwich, UK), the Nitinol wire reached an average temperature of 58.2 °C (with a standard deviation of 1.9 °C) when it had finished actuating. The test set-up for this can be seen in figure 5.5.

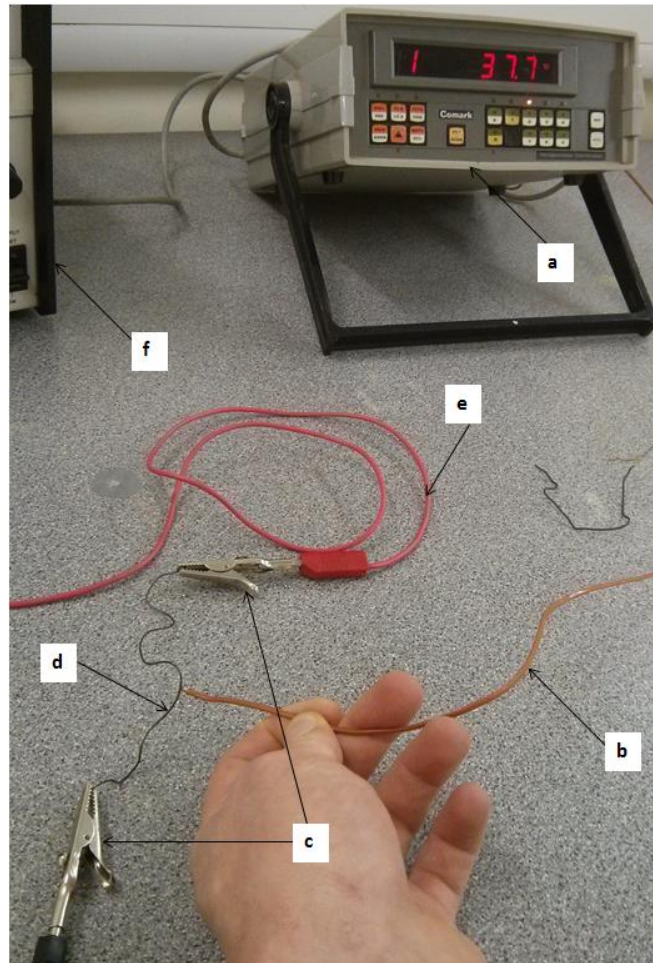


**Figure 5.5 – Nitinol wire transition temperature measure set-up. a) Digital thermometer, b) thermocouple, c) crocodile clips, d) Nitinol wire, e) connective wiring and f) power pack.**

In comparison, other Nitinol wires 0.75 mm and 1 mm in diameter, also obtained from Dynalloy Inc (Tustin, California, USA), reached an average temperature of 39.9 °C and 29.2 °C, respectively. This temperature was not sufficient to bring the wires past their transition temperature; this was clear as the wires did not move to their pre-trained shapes. These lower temperatures can be explained by the greater thickness of the 0.75 mm and 1 mm wires in comparison to the 0.5 mm wire as their electrical resistivity or volume resistivity was the same.

Using the same power pack and thermocouple, the transition temperature of the 0.5 mm diameter Nitinol wire was also determined. The wire was connected to the power pack, again with crocodile clips and connective wiring, and then the current was slowly increased from 0 A to 2.3 A. Whilst the current was being increased, the thermocouple temperature was also monitored. When the transition temperature of the Nitinol was reached, the wire moved to its pre-trained shape. The transition temperature for this alloy was measured to be around 55 °C.

#### **5.4.5 Nitinol Preliminary Testing Findings**

The 0.5 mm diameter wire was found to be the diameter of choice rather than the 0.75 mm and 1 mm wires. The smaller diameter wire required less energy to actuate than the larger wires and would also allow for a reduced outer diameter of the proposed cone add-on device.

Furnace heating was seen as the best way to HT train the Nitinol wire to 550 °C. There was the potential, with a high current producing power pack, to use resistance heating to train the HT shape into the wire. However, this was not used as there were potential safety issues with using such high current. Furthermore, the jig used to train Nitinol with current would need to be ceramic so the wire would not short circuit; this was an issue as ceramics were not readily available. Steel, however, could be used as a jig material for furnace HT training, and it was readily available.

Current was found to be the best method to actuate the Nitinol wire. Other methods of bringing the Nitinol wiring past its activation temperature were explored, these included

using: a heat gun, an oven and a water bath. These methods were trialled, extensively used in preliminary testing of the wire and were shown to be effective. However, for ease of integration in the operating theatre, resistance heating was selected. For example, using a water bath to heat the wiring would equate in surgery to changing the temperature of the irrigating fluid during surgery. This would not be ideal as changing the temperature of the irrigating fluid would increase surgery time and also there may be adverse effects such as increasing core body temperature.

3D printing the Nitinol in a flat configuration that could then be 'curled' around the scope was also explored. However, it was found that the jigs that would be necessary for subsequent training would be too complex and too large for the furnace described in section 5.4.1. Furthermore, quoted prices for 3D printed Nitinol were higher than the price of standard Nitinol wiring, £7/g as opposed to £6.40/g.

## **5.5 Final Design**

### **5.5.1 Detailed Design**

From the preliminary testing that was conducted in section 5.4, it was concluded that the cone instrument would be opened using eight 0.5 mm diameter Nitinol wires. Eight wires were selected as the similar AngioGuard filter device (Fasseas *et al.*, 2001), previously described in section 5.3.3, used this configuration. These would be actuated using resistance heating and would be able to open to around 30° so that at the end of the cone there would be enough room for tumour resection. The wires would need to be fitted into a stable base,

or wire housing, that would form the sheath to go around the existing instrument. For the section of the instrument that was to open, a flexible polymer (termed polymer leaves) would be used in between the Nitinol wires that could tolerate the movement and also confine the irrigation of the resectoscope. The OWSME would be used so that the Nitinol wires would have to be HT trained at an open position and hence inserted into the bladder in a closed position. Below is a render of the design that was proposed with the resectoscope that is currently used in the centre of the cone (figure 5.6).

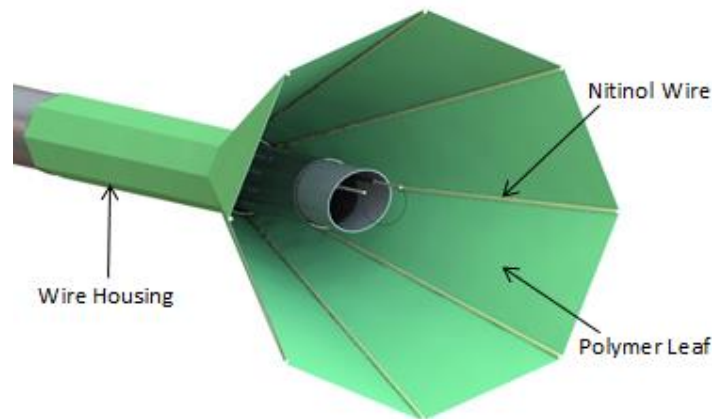


**Figure 5.6 – Final design render.**

### **5.5.2 Wiring Configuration**

An image of the electrical connections for the cone device can be seen in figure 5.7. The polymer leaves were removed from this image to make the path of the electrical connections clearer.



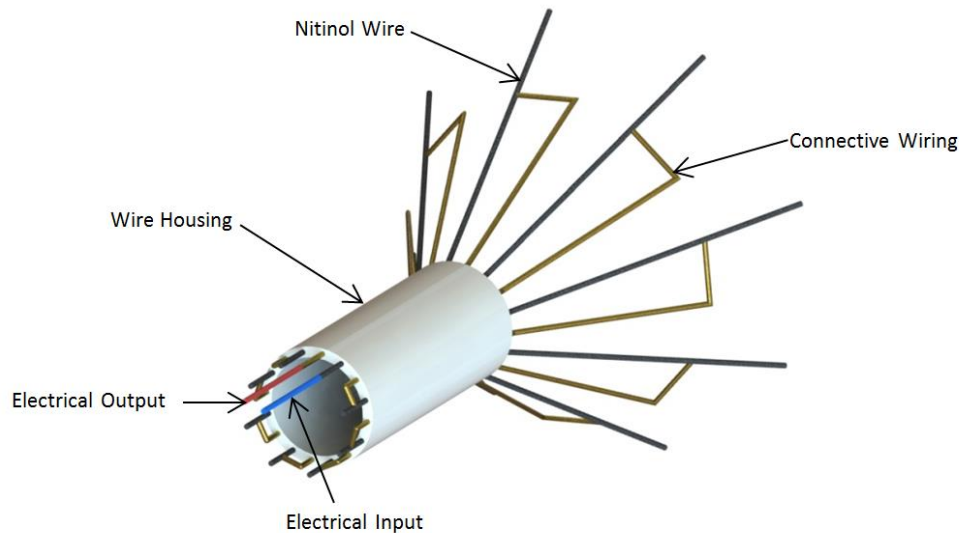


**Figure 5.7 – Render of prototype including Nitinol wires (dark grey), connective wiring (gold) and wire housing (white). The blue and red wires show the input and output of the electrical connection, respectively.**

The connective wiring was made up of 3 strands of 0.2 mm diameter tin coated copper wire (RS Components, Corby, UK). These were connected from the top of one Nitinol wire to the bottom of the next as opposed to the top of two of the Nitinol wires and then the bottom of the next. Testing showed that the connective wire length would have to increase once the device was opened if the connections were at the top of the Nitinol wiring; this was not desirable and can be seen in one of the prototypes manufactured (figure 5.8). The connective wiring protruding away from the Nitinol wires (away from the centre of the cone) is potentially a problem, especially when inserting the device through the urethra.

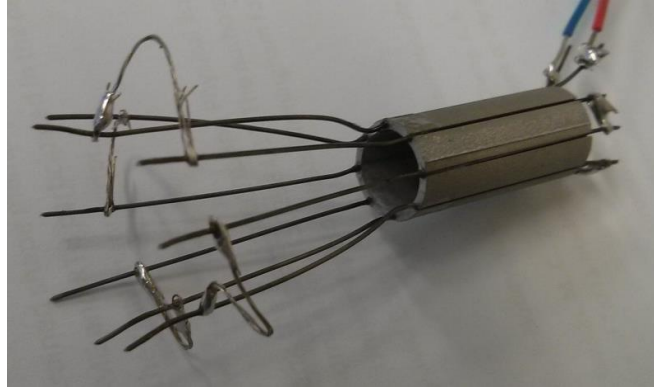


**Figure 5.8 – Aluminium wire housing prototype.**

The Nitinol circuit diagram can be seen in figure 5.9. A series configuration was used, as opposed to a parallel configuration, as a high current was required rather than a split in the current (Patrick and Fardo, 2013). Preliminary testing using two Nitinol wires showed that when parallel configurations were used, only one of the wires actuated. This was due to differences in resistance arising from the strength of connection to the Nitinol, the length of the Nitinol wire and the amount of oxide layer that had built up on the Nitinol wiring. Preliminary testing of the same two pieces of Nitinol wiring showed a series configuration to be preferable as both wires actuated. Furthermore, for the final design, a series configuration was used as 8 times less current was required; this enabled a lower rating power pack to be used.

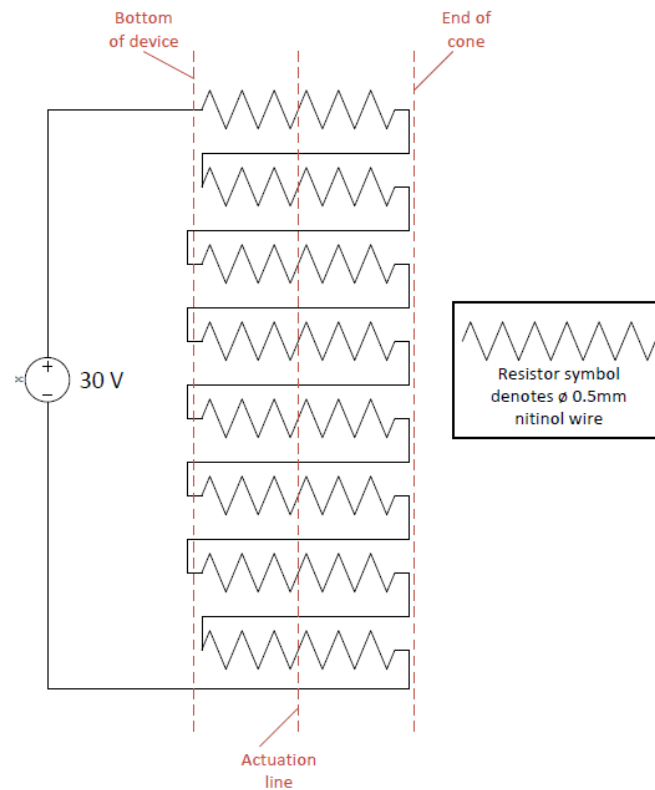


**Figure 5.9 – Prototype circuit diagram.**

### 5.5.3 Risk Assessment

A risk assessment on the design was conducted and the results can be seen in table 5.2. This was to attempt to minimise the risks associated with the design by critically evaluating any perceived failures. Furthermore, it enabled improvements to the design to enhance its safety and solutions to problems should they occur. It should be stressed that the designed instrument is intended as a single use device.

Table 5.2 – Risk assessment for actuating cone device addition to the current resectoscope (Likelihood of Harm; Y – Yes/Very High, Pr – Probable, Po – Possible, R – Remote. Severity of Harm; F – Fatality, Mj – Major, Mn – Minor).

Component	Hazard	Likelihood of Harm					Severity of Harm			Control Measures to Reduce or Eliminate Risk
		Y	Pr	Po	R	Fa	Mj	Mn		
Cone	One of the Nitinol wires breaks	x	x	x	✓	x	x	✓	Nitinol wiring will be extensively tested both mechanically and cyclically to failure to ensure that this is a remote occurrence. If the wire were to break in the operating theatre the whole device would be removed, then replaced and the procedure continued.	
Cone	One of the polymer leaves is torn open by the wire loop or otherwise	x	x	✓	x	x	x	✓	Polymer leaves will be tested to attempt to reduce this risk. If this hazard does occur the surgery would pause, the whole device removed, then replaced and the procedure continued.	
Cone	Bladder wall-end of cone seal fails	x	x	✓	x	x	x	✓	Surgery can take place without a seal, but this would negate the effectiveness of the cone in arresting the spread of tumours cells. The cone device would be replaced.	

Cone	End of Nitinol wires press into bladder wall	x	x	x	✓	x	x	✓
		The polymer leaves will be manufactured longer than the Nitinol wires so that the polymer will press into the wall before the end of the wires. This should also aid the effectiveness of the end of cone-bladder wall seal.						
Electrical Connection	Circuit fails	x	x	✓	x	x	x	✓
		Circuit failure will result in the cone not being able to open. Remove and replace the cone instrument.						

## 5.6 Prototype Manufacture

### 5.6.1 Nitinol Wire

Nitinol wire of 0.5 mm diameter was cut into eight 90 mm section lengths and HT trained using the same furnace and parameters described in section 5.4.1. This heat treatment made the wire ductile and able to form shapes; when the Nitinol had been received it exhibited superelastic behaviour which made it difficult to work with.

The preheated ductile sections of wire were then fixed to a steel jig (figure 5.10). With the use of bolts, nuts and washers the sections of the wire were bent to an angle of 40°. This jig was then inserted into the same furnace as before and heated to 550 °C for 15 minutes. The jig was then quenched in water until cool (less than 20 seconds) and the wires were removed from the jig.



**Figure 5.10 – High temperature training jig.**

The heat treatment described trained the 40° high temperature shape into the Nitinol. The Nitinol could then be deformed into any shape and once heated past its

activation temperature (~55 °C for this specific alloy) it returned to the 40° bent shape. For the designed instrument the desired actuation was from a straight (closed) wire to a 30° bend (open) wire. The loss of 10° accounted for the stiffness of the polymer leaves in between the Nitinol wires.

The Nitinol wires were connected around the wire housing using a tin based solder (Fisher Scientific, UK) and connective wiring made up of 3 strands of 0.2 mm diameter tin coated copper wiring (as described in section 5.5.2). Great difficulty was experienced when soldering to nickel titanium due to the oxide layer that had built up around the wire, therefore, flux (Toolstation, Bridgwater, UK) was used with good results.

### **5.6.2 Wire Housing**

Once the wires had been trained, the 'bases' of the wire were inserted into a 3D printed cylindrical housing (figure 5.11). The housing was manufactured using an Eden 250 additive manufacturing machine (Objet, Billerica, USA) and made out of an acrylic monomer based resin (brand name Fullcure 720). The outside diameter and bore of the wire housing were 11 mm and 9 mm, respectively. There were also 16, 0.75 mm diameter holes through the wall of the housing all at a 10 mm pitch circle diameter (appendix D). This housing provided a stable structure against which the wires could actuate.

The 0.75 mm diameter through holes were used as the 3D printing machine was unable to adequately print smaller diameter holes at the length required. Holes of diameter 0.5 mm were unsuccessfully trialled to provide an interference fit for the 0.5 mm diameter Nitinol wiring that was to be housed. A smaller hole diameter would have enabled a smaller

outer diameter of the housing. As a smaller outer diameter was desirable, another wire housing, manufactured from aluminium (figure 5.8) using wire EDM (electrical discharge machining), was trialled. Wire EDM was undertaken by Dr Richard Hood of the Advanced Manufacturing Centre, School of Mechanical Engineering, University of Birmingham. Using this method the outer diameter of the wire housing was decreased to 10.5 mm, however, the aluminium short circuited the device which meant that it did not actuate. As an adequate method of insulating the Nitinol wiring from the housing was not available, the manufacture of the wire housing reverted to using the 3D printed method mentioned earlier.

### **5.6.3 Polymer Leaves**

Latex was used as the polymer material as it exhibits low stiffness and has a Young's modulus in the range of 1.5 – 2.5 MPa. It also has a comparatively high elastic limit of 20 – 30 MPa (Granta Design Ltd, 2013) compared to other similar elastomers, such as polyurethane and silicone. Three layers of Liquid latex (MB Fibreglass, Newtonabbey, UK) were painted onto a custom made aluminium cone along with the Nitinol wiring and connective wiring (figure 5.11). Each layer was allowed to dry for 10 minutes before the next layer was applied. The aluminium cone was 40 mm long with a minor diameter of 7.9 mm and a major diameter of 30 mm, which equated to an angle of 15°. The aluminium cone mimicked the shape of the device when halfway open. In preliminary tests three layers of latex showed good strength, flexibility and the ability to provide a sealed environment (described in section 5.7). When the third layer of latex was dry, washing up liquid was



rubbed onto the surface to ensure the latex did not stick to itself when being removed from the aluminium cone. The whole prototype was then removed from the cone.



**Figure 5.11 – Finished cone prototype (left) and aluminium cone onto which the latex was painted (right).**

Polyurethane and silicone were considered as alternatives to latex for the cone, however, these materials exhibit higher values for Young's modulus (2 – 30 MPa and 8 - 30 MPa, respectively). Also, latex has an elastic limit comparable to polyurethane (25 – 51 MPa) and higher than silicone (5.4 – 7 MPa) (Granta Design Ltd, 2013). The liquid latex was cheaper and was ready to use when acquired as opposed to the silicone and polyurethane which required the mixing of two components.

## 5.7 Prototype Testing

### 5.7.1 Prototype Actuation

The ability of the prototype to actuate was tested using a 2.3 A, 30 V supply as previously described in section 5.4.4. The opening actuation time for the prototype device was around 12 seconds; the prototype is shown in figure 5.12 going from the closed (top) to open (bottom) state. The opening time could be reduced by increasing the current as this increases the heating of the Nitinol wires. However, a higher current is more likely to melt the latex, the solder and potentially the 3D printed wire housing used here for the prototype.

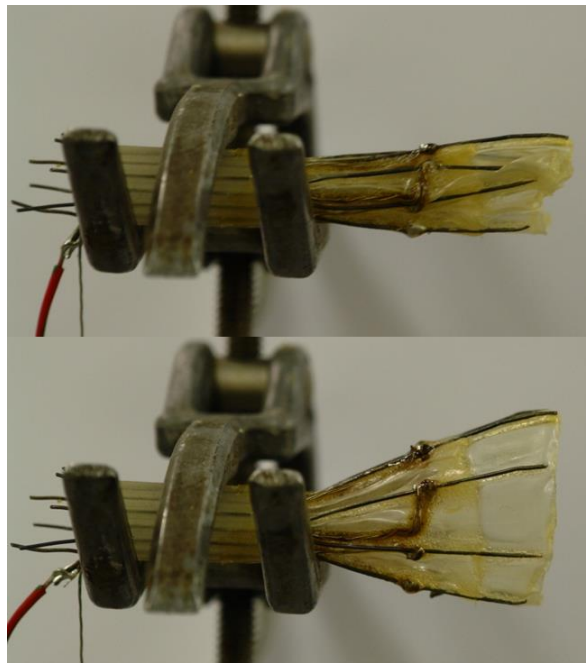


**Figure 5.12 – Closed (top) and open (bottom) prototype.**

### **5.7.2 Fluid Testing Methods**

The ability of the prototype to open and seal in a liquid environment was tested in two experiments. The cone prototype was inserted into a Perspex cylinder (figure 5.13) in hypotonic and isotonic aqueous environments at 37 °C. These parameters corresponded to different operating conditions of TURBT. Crocodile clips were attached to the electrical connections of the device which were then actuated using the same 2.3 A, 30 V supply.

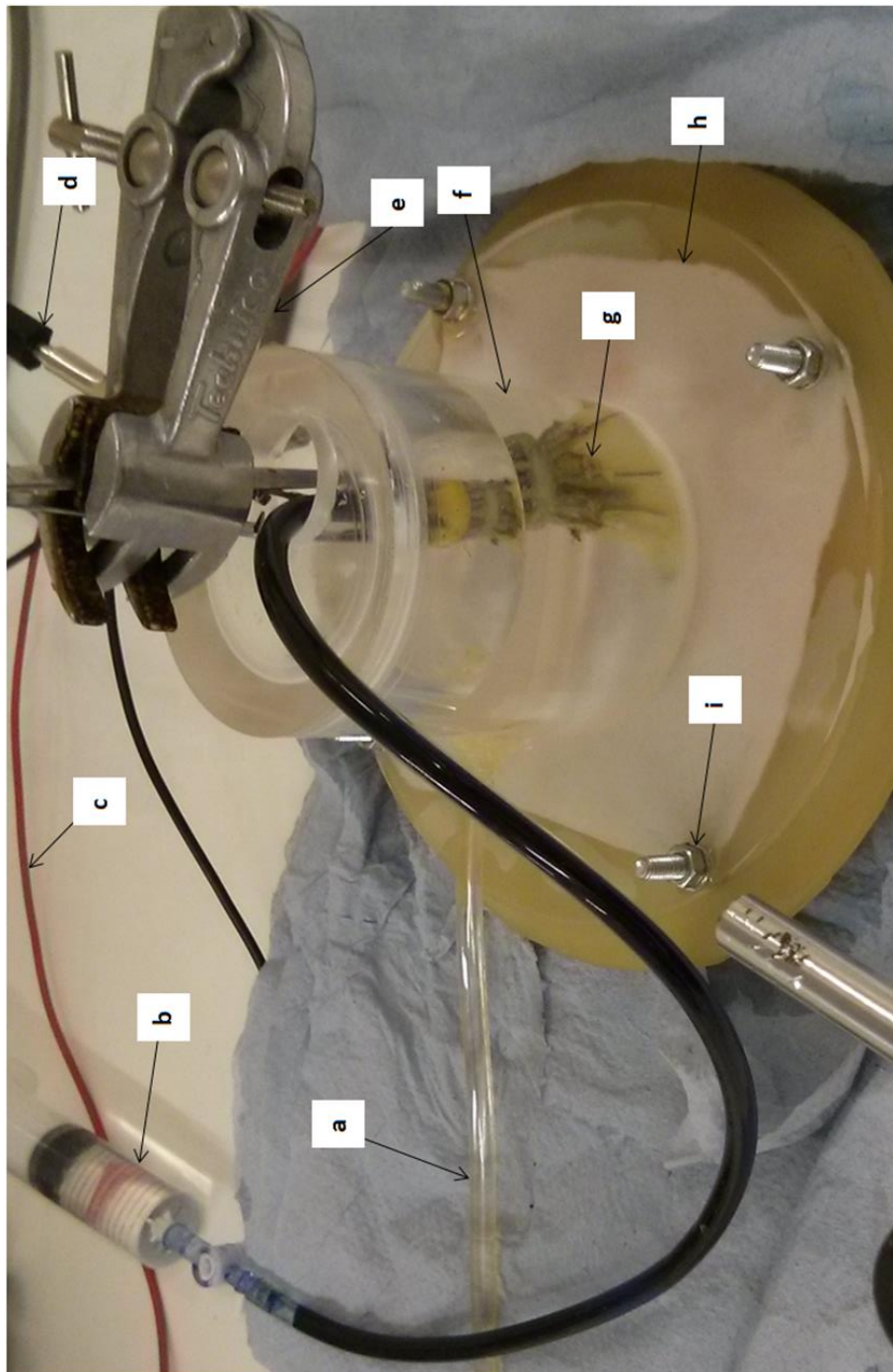
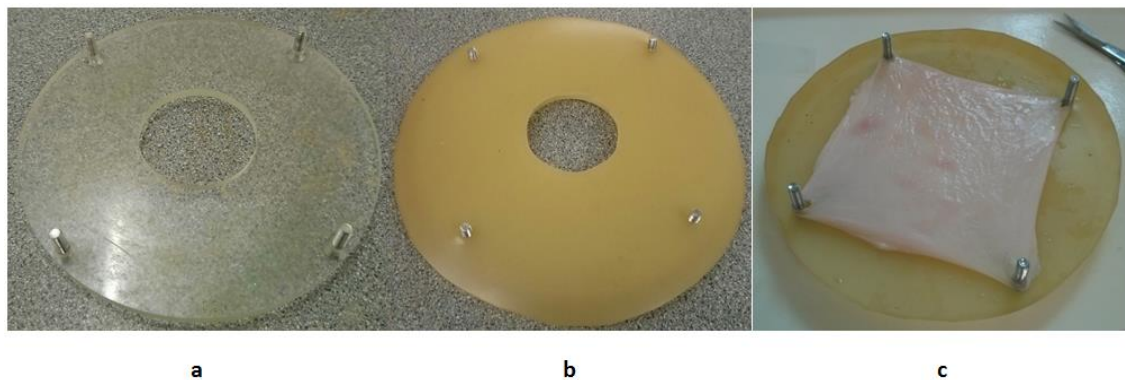


Figure 5.13 – Instrument dye test set-up. a) simulation irrigation fluid input. b) 50ml syringe for input of dye. c) negative electrical connection.

d) positive electrical connection. e) clamp stand and tweezer set-up to insert and remove instrument. f) perspex housing. g) instrument. h)

stretched porcine bladder specimen. i) M5 bolt, washer and nut.

The ability of the prototype to seal and potentially hold tumour cells within the device was tested. This was done by pressing the open device against a stretched *porcine* bladder wall specimen at the bottom of the Perspex testing device and adding blue dye (Coomassie Brilliant Blue 250R, Sigma Aldrich, Gillingham, UK). The device was attached to a set of forceps and then on to a clamp stand (both Fisher Scientific, UK) which enabled the device to be lowered into the bladder simulation environment. The *porcine* bladder sample was obtained from Fresh Tissue Supplies (East Sussex, UK). The dome and trigone regions of the bladder were removed and another cut was made adjacent to the first two incisions to create a roughly rectangular sample of bladder. The bladder sample was then stretched by hand, with the inner bladder wall facing up so as to make contact with the device. Four holes were then made in the rectangular sample so that it could fit over the bolts securing the Perspex testing device (figure 5.14).



**Figure 5.14 – Bottom of Perspex testing device. a) bottom of Perspex device. b) rubber added on top of the Perspex. c) stretched porcine bladder added on top of the rubber.**

All incisions and cuts were made using surgical scissors (Fisher Scientific, UK). Plastic tubing (Fisher Scientific, UK) was then inserted through the middle of the device into the cone so that the blue dye could be injected using a 50 ml syringe (Fisher Scientific, UK). The ability of the latex to keep the dye within the cone was tested with dye that was less dense ( $958 \text{ kg/m}^3$ ) than the surrounding fluid (hypotonic  $1000 \text{ kg/m}^3$  or isotonic  $1005 \text{ kg/m}^3$ ). Conversely the bladder wall cone interface seal was then tested using a dye denser (supplemented with salt,  $1185 \text{ kg/m}^3$ ) than the surrounding fluid. In total this amounted to two dye tests of the device. The device was then observed over 5 minutes to see whether the dyes remained within the cone. The tests were recorded using a Google Nexus 4 video recording device (San Francisco, USA). The entire test set up can be seen in figure 5.13.

### 5.7.3 Fluid Testing Results

Figure 5.15 shows the closed and open states of the prototype device in a hypotonic solution. It should be noted that for this test the bottom of the Perspex testing device was fitted with rubber as only the opening ability of the instrument was being tested, not its ability to seal to the bladder wall.

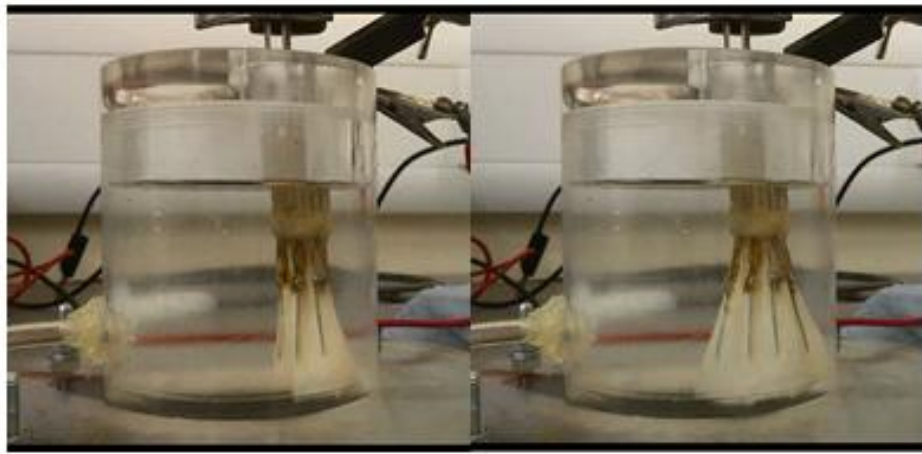


**Figure 5.15 – Closed and open state of the prototype device in fluid. For this test rubber was used at the bottom of the test device.**

The time taken for the device to open was 20 seconds. This was found to be repeatable and very similar results were found when testing in an isotonic solution. The time taken for the device to open was longer than the 12 second actuation in air and was attributed to the increased heat transfer in the fluid. The subsequent dye test results can be seen in figure 5.16.



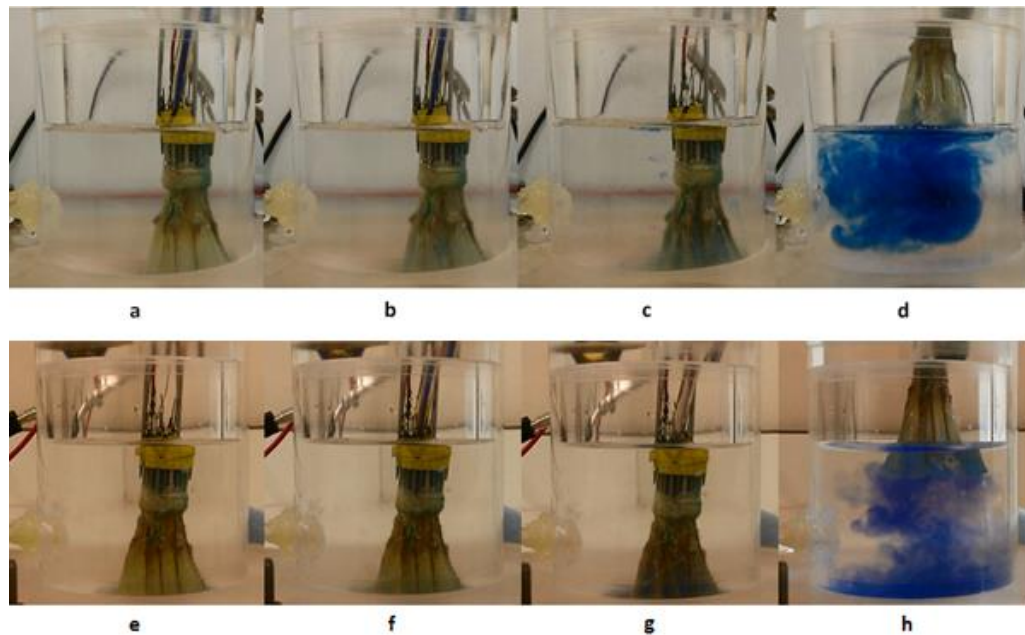


**Figure 5.16 – Instrument dye tests. Less dense blue dye a – d. Denser blue dye e – h.**

**Where: a) & e) are the inserted devices pressed against a sample of *porcine* bladder wall, b) & f) are the dyes being inserted into the device which is where the timing of the test started, c) & g) are the device with blue dyes inside once the tubing has been removed and d) & h) are the blue dyes escaping once the device is taken out after the 5 minute test had been completed.**

The vast majority of the dye remained within the device during the 5 minute tests (figure 5.16b-c & 5.16f-g). A small amount of dye can be seen leaving the cone in the test with the less dense dye (figure 5.16c). This may be due to small holes in the latex or gaps in the connection of the latex to the wire housing. In the test with the denser dye (figure 5.16e-h) only small quantities of dye left the device and this may be due to a fold in the latex which was in contact with the bladder wall. For each test the effect of buoyancy due to the



different densities of the respective dyes can be seen after the device was removed, where the dye rises when less dense (figure 5.16d) and sinks when denser than the surrounding fluid (figure 5.16h).

## 5.8 Discussion

This chapter has described a novel enhancement to current surgical instruments used for transurethral resection of bladder tumours (TURBT). It is hoped that this design will, if implemented, decrease the recurrence of non-muscle invasive bladder cancer (NMIBC) by restricting the area in which tumour cells are allowed to travel (Bryan *et al.*, 2010; Kondas *et al.*, 1999). This chapter has also described the manufacture of a working prototype and *in vitro* testing to determine the ability of the add-on device to contain substitute tumour cells.

Observations following *in vitro* testing demonstrate that the device is able to actuate in both hypotonic and isotonic irrigation fluids, which are commonly utilised during TURBT, and hence can be used with both mono and bi-polar energy sources. The device was also able to restrict the majority of the blue dye, which was used to simulate cells, within the cone part of the device. Different densities of blue dye were used and it allowed for testing of the seal at the bladder wall cone interface (denser dye) and the effectiveness of the latex in keeping the dye within the cone (less dense dye). Some leaking of the dye was seen and this has been attributed to insufficient contact with the bladder wall and/or small unseen tears in the latex cone.

Once the device is deployed, it may also be feasible to induce a pressure differential between the fluid in the cone and the fluid in the rest of the bladder. By controlling the

irrigation a positive pressure in the remainder of the bladder would gently push the device against the bladder wall. Furthermore, the irrigation system, when used within the device, may be more effective in drawing the tumour cells back through the scope as there would be less volume of fluid within the cone, as opposed to irrigating the entire bladder.

As has been described in section 5.4.3, extensive work was carried out on attempting to use the two-way shape memory effect for the device. This was desirable as the device could have been trained for open and closed configurations; however, the low force and slow return speed in the absence of enhanced cooling made this unworkable. Instead the device would be able to open using the one-way shape memory effect and then, when the current to the device is turned off and the Nitinol wiring becomes ductile, the device will close whilst being removed through the urethra.

The device is intended as a single use surgical instrument and as such if there are any defects or failures with the device before or during surgery it would just be discarded and another cone device used. Being a single use device also means that the hospital or healthcare trust would not be responsible for sterilising the equipment, they would simply throw it away after use. Single use instruments are currently being used in orthopaedic procedures such as total knee replacements. For example, cutting guides and trial implants used for knee replacement surgeries are being used and improvements in procedure efficiency, infection rate and cost have been reported (Bhadra *et al.*, 2012; Mont *et al.*, 2013; Siegel *et al.*, 2015).

## **5.9 Chapter Summary**

This chapter has presented the development of a novel instrument in which the concept of actuation with shape memory alloys using current actuation has been proven. It has also been shown that the prototype designed, manufactured and tested is able to limit fluid transfer to within an opening cone environment.

## 6 Overall Discussion and Conclusions

This thesis has described the methods and measurement of *porcine* urinary bladder and then human bladder tumour viscoelastic properties. This thesis has also presented the design, prototyping and testing of a novel instrument to assist the removal of non-muscle invasive bladder cancer (NMIBC).

Chapter 3 used tensile dynamic mechanical analysis to quantify the viscoelastic properties of *porcine* bladder tissue. The testing technique made use of rectangular and looped specimens from which storage and loss stiffnesses were found. The results were expressed in terms of stiffness so that the rectangular and looped specimens could be compared. Whenever rectangular specimens of soft tissue are tested uniaxially, specimen slippage in grips is always a potential issue. To the author's knowledge there has been only one other study on bladder tissue using loops by Alexander (1976). Using looped specimens is advantageous as slippage cannot occur and it also simplifies the procedure for securing specimens to fixtures. For the bladder it may also be more physiologically relevant to test looped specimens if only uniaxial testing machines are available. This is because the looped specimens are 'curled' around the testing apparatus which may better resemble normal bladder filling than just gripping a rectangular section of bladder wall. The looped specimens exhibited the same trends for storage and loss stiffness against frequency as the rectangular specimens. To account for the difference in specimen geometry the looped specimens were stressed to twice the preload of the rectangular specimens, 20 N for looped and 10 N for rectangular specimens. However, the magnitudes of the stiffnesses recorded did not account

for the increased preload where the storage stiffness for the looped specimens was on average 2.6 times that of the rectangular specimens. To a lesser extent, the same was also the case for the loss stiffness of the looped specimens which where, on average, 2.1 times that of the rectangular specimens. These increases can be seen when comparing figures 3.11 and 3.12 and may be due to the effects that the 'curled' ends of the looped bladder specimens (around the testing apparatus) have on the stiffness of the tissue.

Chapter 4 used dynamic mechanical analysis but quantified the compressive viscoelastic properties of human bladder tumours. Average storage and loss moduli are reported for the tumour specimens tested. However, the sample size was not sufficient to compare any of the tumour specimens with respect to other variables, such as: gender, age of patient, type, stage and grade. Characterisation with respect to these variables would be of great significance in diagnosis where, for example, if the mechanical properties of a tumour were to change with respect to grade, tumours could be characterised without a biopsy and subsequent microscopy. This could then be used to quickly inform subsequent treatment. The mechanical properties of human tumours could be used to manufacture more appropriate synthetic tumours for surgical trainers. If relationships are found in the viscoelastic properties in the tumour variables described earlier, different tumours could be manufactured depending on grade, stage etc.

The viscoelastic properties of the rectangular *porcine* bladder from chapter 3 and human bladder tumours from chapter 4 can be compared as they are both expressed in terms of modulus (figures 3.13, 4.7 and 4.9). The storage modulus of the *porcine* bladder initially exhibited a logarithmic increasing trend against frequency (0.01 – 1 Hz) which then

changed into a second order polynomial trend which decreased with frequency from 1 – 5 Hz. This is in contrast to the human bladder tumour storage modulus trend which increased logarithmically throughout the entire frequency sweep (0.01 – 30 Hz). The loss modulus of the *porcine* bladder exhibited a linearly increasing trend. This was, however, very shallow and only increased by 0.016 MPa, which was 29.6% of the mean loss modulus value over the range of frequencies from 0.01 to 5 Hz. The human bladder tumour loss modulus also only exhibited a small increase of 0.009 MPa, which was 39.1% of the mean loss modulus value over 0.01 to 5 Hz. However, this increase was better described by a second order polynomial fit. The magnitudes of the moduli were larger for the *porcine* bladder. Over comparable frequencies (0.01 – 5 Hz) the average storage modulus for the human bladder tumours was 0.066 MPa in comparison to 0.35 MPa for the pig bladder. The average loss modulus was 0.023 MPa and 0.054 MPa for the human bladder tumour and pig bladder specimens, respectively.

Chapter 4 included the description of preliminary compressive mechanical testing of *porcine* bladder specimens. This preliminary testing was necessary to determine the protocol for the human tumour specimens; hence similar sizes of specimen were used. Tensile testing was attempted but the small size of the specimens made this impractical. In comparison to the human bladder tumour specimens, with similar testing methods over the same frequencies, the pig bladder displayed similar trends. This can be seen when comparing figures 4.2 and 4.3 to figures 4.7 and 4.9. The storage moduli for both tumour and bladder samples displayed logarithmic increasing trends against frequency; both the loss modulus results against frequency displayed increasing trends which were characterised by second order polynomials. As before, the *porcine* bladder did exhibit higher average storage and loss

moduli, however, in this case the difference was smaller. The average storage moduli for the human tumours ranged between 0.052 MPa and 0.085 MPa (over 0.01 - 30 Hz) in comparison to 0.08 MPa and 0.12 MPa (also over 0.01 - 30 Hz) for the *porcine* bladder. The average loss moduli for the human tumours were 0.019 MPa and 0.043 MPa (0.01 and 30 Hz) in comparison to 0.024 MPa and 0.055 MPa (0.01 and 30 Hz) for the *porcine* bladder.

This higher stiffness of the normal tissue corresponds to the atomic force microscopy studies conducted by Lekka *et al.* (1999; 2012) where the normal bladder cells exhibited a Young's modulus around one order of magnitude higher than that of the tumour cells, 0.01 MPa in comparison to 0.001 MPa, respectively. The differences between the properties of normal and malignant tissue found in this thesis may have potential uses in diagnosis of bladder cancer, whether it is in novel diagnostic instrument design or for use in diagnostic imaging procedures.

The *porcine* rectangular specimen tensile tests from chapter 3 (figure 3.13) and the *porcine* preliminary compression tests in chapter 4 (figures 4.2 and 4.3) exhibited similar trends. The storage moduli for both were initially described, until 1 Hz, by an increasing logarithmic curve fit which, for the compression tests, continued for the remainder of the frequencies tested (0.01 – 30 Hz). In contrast the tensile specimens showed a decreasing second order polynomial trend for the rest of the frequencies they were subjected to (until 5 Hz). The mean value for the storage modulus of the compression specimens was 0.096 MPa (0.01 – 5 Hz) in comparison to 0.36 MPa (0.01 – 5 Hz) for the tensile specimens. The loss modulus for the compression specimens exhibited a second order polynomial increasing trend against frequency over the entire range of frequencies tested (0.01 – 30 Hz), whereas,

the tensile specimens exhibited a linear small increase against frequency (0.01 – 5 Hz). The mean value for the loss modulus of the compression specimens was 0.031 MPa (0.01 – 5 Hz) in comparison to 0.054 MPa (0.01 – 5 Hz) for the tensile specimens. The higher moduli for the tensile tests may be due to: the difference in preload that was applied for the different types of test, the difference in the specimen geometry and the differences in compression and tensile testing.

There are limitations in comparing the moduli from the human and *porcine* tests for the following reasons:

- Pig urinary bladder is the best available model for human urinary bladder. The study by Dahms *et al.* (1998) found the elastic modulus of *porcine* and human bladder rectangular strips to be similar (0.26 and 0.25 MPa, respectively). Human normal urinary bladder specimens would be ideal but they are difficult to obtain. There may also be other issues with human specimens as they are likely to be older and may be diseased.
- The *porcine* bladder tests in chapter 3 were tensile and the human bladder tumour tests in chapter 4 were compressive. Ideally both would have been tensile tests, however, this was not possible due to the small sizes of the tumour specimens. The *porcine* bladder tests were tensile so that comparisons could be drawn with the literature, which were tensile studies. The comparison drawn between the tensile *porcine* tests in chapter 3 and the compression preliminary *porcine* tests in chapter 4 shows that they exhibit similar trends for both storage and loss modulus until 1 Hz but differ afterwards. They also exhibit different magnitudes for the moduli. This



presents the difficulties in the comparison of the compressive human and *porcine* tensile specimens.

- Preloads are necessary in mechanical characterisation of tissues to ensure repeatability of results. Due to the difference in specimen size and testing in compression and tension the preloads were different for the two tests. Preloads were important to ensure that the testing machine had an already registered load which it could work from. Testing without preloads caused errors from the machine which resulted in the wrong displacement from the testing machine, this often tripped the pre-set limits of the machine causing a shut down. On reflection preloading each specimen, for both the *porcine* and human tumour specimens, according to their respective volumes may have provided 'fairer' results, however, the preloads used were estimates and difficult to set accurately due to the high stress relaxation exhibited by the tissues. As the volumes for each of the tests were similar the author does not expect that the difference in preload would have been high. Although there were some preload limitations, all specimens, for their respective tests, underwent exactly the same testing procedures.
- The human specimens had been stored at -80 °C compared to the pig bladder which was stored at -40 °C. The effect of storage temperature on urinary bladder is not known (Zanetti *et al.*, 2012), however, Zanetti *et al.* (2012) have also reported that their bladder tissue mechanical testing results agree with other studies where urinary bladders were harvested from the animal source, stored at 4 °C and tested within 48 hours.
- The sample size of the human tumour tests was low due to low availability of human

tissues; however, repeatable results were found and point to differences between the tumours and normal tissue.

The viscoelastic properties from both chapters 3 and 4 are of potential value in device design. The properties of both normal and malignant bladder tissue could facilitate the manufacture of a 'probing' type device which could diagnose tumours during cystoscopy or transurethral resection of bladder tumours (TURBT). Depending on the T-stage of the tumour found and its grade the appropriate surgical course of action, which may well be TURBT, could be taken straight away. To inform this, future work on the viscoelastic properties of normal bladder tissue, in addition to tumourous bladder tissue, would be of great value.

Chapter 5 described the design, prototyping and testing of a device aiming to decrease the recurrence of non-muscle invasive bladder cancer. The device attempts to do this by creating a physical barrier which bladder tumour cells cannot penetrate post piecemeal resection (TURBT). This is important as it would prevent one of the prime mechanisms of recurrence in NMIBC. The device needs developing with different materials and manufacturing techniques if it is to progress towards being a useable instrument. However, it clearly demonstrates proof of concept as a functioning prototype as it limits fluid flow to within the cone device when pressed against urinary bladder wall. There is also a similar device already in use which uses Nitinol to open a polyurethane filter for blood vessels (Fasseas *et al.*, 2001). There also may be other applications in which a current actuated opening cone device has utility.

Chapter 5 details the use of electrical current to heat the nitinol wire past its

transition temperature and hence cause movement. Nitinol medical devices such as stents and bone plates are body temperature response; this means when they are inserted into the body, the temperature change to 37 °C brings the devices past their transition temperature. Body temperature response Nitinol was considered for the device described in chapter 5 but was not used as the author wanted to give the surgeon control of when the cone would open.

The overall conclusions from this thesis are as follows:

- *Porcine* urinary bladder looped specimens exhibit higher average storage and loss stiffnesses (1.89 N/mm and 0.24 N/mm, respectively) compared to rectangular specimens (0.74 N/mm and 0.11 N/mm, respectively).
- Human bladder tumours exhibit lower storage and loss moduli (0.07 MPa and 0.02 MPa, respectively) in comparison to tensile *porcine* (0.36 MPa and 0.05 MPa, respectively) or compression *porcine* (0.10 MPa and 0.03 MPa, respectively) normal urinary bladder tissue.
- The storage modulus was higher than the loss modulus for both the *porcine* normal bladder and human bladder tumour specimens for every frequency tested. Both specimen types also exhibited varying viscoelastic behaviour dependent on the frequency.
- An expanding latex cone device, actuated using nickel titanium shape memory alloy (Nitinol), is effective in confining fluid when the device is pressed against urinary bladder wall.

## 7 Future Work

### 7.1 Tissue Testing

In future, if possible, it would be of value to also test normal human tissue using the same methods described in chapters 3 and 4. This would assess the suitability, in terms of viscoelastic properties, of *porcine* bladder tissue as a model for human normal bladder tissue. If the tissues were significantly similar, then surgical or diagnostic equipment could be confidently tested using a *porcine* model instead of using human bladder specimens. Also the difference between human malignant and normal bladder tissue could be confidently ascertained. Any significant differences would be of great value to diagnostic procedures.

Other authors such as: Gloeckner *et al.* (2002), Nagatomi *et al.* (2004), Gilbert *et al.* (2008) and Chen *et al.* (2013) have investigated properties of the bladder using biaxial test methods. Biaxial testing is of value as the test method is more similar to physiological loading and unloading of the urinary bladder i.e. multidirectional loading. A limitation of the work in this thesis was that no biaxial testing machine was available and there was not enough time to manufacture a jig to alter the Bose Electroforce 3200 uniaxial testing machine to a biaxial testing machine. In addition the author believes converting the Bose Electroforce 3200 testing machine would have been very difficult as any 'off axis' forces or moments applied tended to cause errors and machine shutdowns.

## **7.2 Instrument Development**

The next stages in the development of this device, so it can go from a prototype to surgical instrument, would make use of different materials and techniques. The wire housing would be made from a stiffer material such as stainless steel which is commonly used in current resectoscopes. This would allow for a thinner wall thickness and hence a smaller device, although the channels for the Nitinol wire and other connections would have to be insulated so as not to short circuit the device. Furthermore, the wire housing length would be increased to be compatible with, and connect to, current resectoscopes. Different moulding techniques would also be explored to better incorporate the diameter of the Nitinol when the latex cone is being added. A different grade of latex may also be sought to increase the ultimate strength and to decrease the Young's modulus so that the folding, which can be seen when the device is closed (figure 5.12 & figure 5.15), does not occur. Also, potential additives to the latex to prevent it from sticking to itself once being removed from the mould would be beneficial providing it did not adversely affect the mechanical properties of the latex or its biocompatibility. Other polymers would also be investigated and incorporated so that the device could be used for patients with latex allergies.

Improved techniques for the electrical connections of the device would be beneficial. Soldering to Nitinol was difficult and other techniques such as using copper tape and connections by contact, such as 90° crimps, were trialled but were unsuccessful. If soldering is continued, different techniques and potentially different materials could be sought to decrease the amount of solder being used and remove the need for flux. Methods to prevent accumulation of the oxide layer on the Nitinol wiring would also be advantageous,

as this would decrease the likelihood of any electrical connections failing. During prototype manufacture sandpaper was used to try and remove this layer before forming the connections, but did not have much of an effect.

After manufacture of a next stage prototype, testing with a resectoscope in a model bladder environment such as a whole *porcine* bladder or a surgical trainer should also be completed. The instrument would be added to a current resectoscope so that the opening of the device and the ability of the resectoscope to work in the cone part of the instrument could be seen. This would ensure that the diminished volume of the working environment did not adversely affect the optics of the resectoscope and the electrically active wire loop. Testing of insertion and removal of the instrument would also be completed. Incorporating a comparable tumour material into this testing, which could then be resected, would further gauge the effectiveness of the design in limiting the movement of tumour particles.

## References

- Advanced Bladder Cancer (ABC) Meta-analysis Collaboration (2005) Neoadjuvant chemotherapy in invasive bladder cancer: update of a systematic review and meta-analysis of individual patient data advanced bladder cancer (ABC) meta-analysis collaboration. *European Urology*. **48**, 202–205.
- Ahmadzadeh, S.M.H., Hukins, D.W. (2014) Feasibility of using mixtures of silicone elastomers and silicone oils to model the mechanical behaviour of biological tissues. *Proceedings of the Institution of Mechanical Engineers. Part H, Journal of engineering in medicine*. **228**(7), 730–734.
- Alexander, R. (1971) Mechanical properties of urinary bladder. *American Journal of Physiology*. **220**(3), 1413 – 1421.
- Alexander, R. (1976) Series elasticity of urinary bladder smooth muscle. *American Journal of Physiology*. **231**(5), 1337 – 1342.
- van Andel, C.J., Pistecky, P. V, Borst, C. (2003) Mechanical properties of porcine and human arteries: implications for coronary anastomotic connectors. *The Annals of Thoracic Surgery*. **76**(1), 58–64.
- Appleyard, R.C., Swain, M. V, Khanna, S., Murrell, G.A.C. (2001) The accuracy and reliability of a novel handheld dynamic indentation probe for analysing articular cartilage. *Physics in Medicine and Biology*. **46**, 541–550.
- Arridge, R.G.C., Barham, P.J. (1986) Fourier transform mechanical spectroscopy. *Journal of Physics. D: Applied Physics*. **19**, L89 – L96.
- Asbach, P., Klatt, D., Hamhaber, U., Braun, J., Somasundaram, R., Hamm, B., Sack, I. (2008) Assessment of liver viscoelasticity using multifrequency MR elastography. *Magnetic Resonance in Medicine*. **60**(2), 373–379.

Aspden, R.M. (1991) Aliasing effects in Fourier transforms. *Journal of Physics. D: Applied Physics*. **24**, 803–808.

ASTM International (2010) ASTM E111-04(2010) Standard test method for Young's modulus, tangent modulus and chord modulus.

Atala, A. (2011) Tissue engineering of human bladder. *British Medical Bulletin*. **97**, 81–104.

Babjuk, M., Oosterlinck, W., Sylvester, R., Kaasinen, E., Böhle, A., Palou-Redorta, J. (2008) EAU guidelines on non-muscle-carcinoma of the bladder. *European Urology*. **54**, 303–314.

Babjuk, M., Oosterlinck, W., Sylvester, R., Kaasinen, E., Böhle, A., Palou-Redorta, J., Roupřet, M. (2011) EAU guidelines on non-muscle-invasive urothelial carcinoma of the bladder, the 2011 update. *European Urology*. **59**, 997–1008.

Bach, T., Muschter, R., Herrmann, T.R.W., Knoll, T., Scoffone, C.M., Laguna, M.P., Skolarikos, A., Rischmann, P., Janetschek, G., De la Rosette, J.J.M.C.H., Nagele, U., Malavaud, B., Breda, A., Palou, J., Bachmann, A., Frede, T., Geavlete, P., Liatsikos, E., Jichlinski, P., Schwaibold, H.E., Chlost, P., Martov, A.G., Lapini, A., Schmidbauer, J., Djavan, B., Stenzl, A., Brausi, M., Rassweiler, J.J. (2015) Technical solutions to improve the management of non-muscle-invasive transitional cell carcinoma: summary of a european association of urology section for uro-technology (ESUT) and section for uro-oncology (ESOU) expert meeting and current and future pers. *BJU International*. **115**, 14–23.

Badylak, S.F. (2004) Xenogeneic extracellular matrix as a scaffold for tissue reconstruction. *Transplant Immunology*. **12**(367-377).

Bhadra, A., Kwiecien, G., Harwin, S., Johnson, A., Mont, M., Malkani, A. (2012) Procedure simplification: the role of single-use instruments in total knee arthroplasty. *Surgical Technology International*. **22**, 326–330.

Blandy, J., Reynard, J., Notley, R. (2005) *Transurethral resection*. 5th ed. London: Taylor and Francis.



British Standards Institution (2009) BS EN ISO 16061:2009 Instrumentation for use in association with non-active surgical implants — General requirements.

British Standards Institution (2013) BS ISO 8600-1:2013 Endoscopes — Medical endoscopes and endotherapy devices Part 1 : General requirements.

Bryan, R.T., Collins, S.I., Daykin, M.C., Zeegers, M.P., Cheng, K.K., Wallace, D.M.A, Sole, G.M. (2010) Mechanisms of recurrence of Ta/T1 bladder cancer. *Annals of the Royal College of Surgeons of England*. **92**(6), 519–24.

Bryan, R.T., Kirby, R., O'Brien, T., Mostafid, H. (2014) So much cost, such little progress. *European Urology*. **66**(2), 263–264.

Bryan, R.T., Zeegers, M.P., van Roekel, E.H., Bird, D., Grant, M.R., Dunn, J. a, Bathers, S., Iqbal, G., Khan, H.S., Collins, S.I., Howman, A., Deshmukh, N.S., James, N.D., Cheng, K.K., Wallace, D.M.A. (2013) A comparison of patient and tumour characteristics in two UK bladder cancer cohorts separated by 20 years. *BJU International*. **112**(2), 169–75.

Buehler, W.J., Gilfrick, J. V., Wiley, R.C. (1963) Effects of low temperature phase changes on the mechanical properties of alloys near composition TiNi. *Journal of Applied Physics*. **34**(1475), 1475–1477.

Burger, M., Catto, J.W.F., Dalbagni, G., Grossman, H.B., Herr, H., Karakiewicz, P., Kassouf, W., Kiemeny, L. a, La Vecchia, C., Shariat, S., Lotan, Y. (2013) Epidemiology and risk factors of urothelial bladder cancer. *European Urology*. **63**(2), 234–41.

Callister, W., Rethwisch, D. (2012) *Fundamentals of materials science and engineering: an integrated approach*. 4th ed. New York: John Wiley & Sons.

Cancer Research UK (2014) Bladder cancer statistics. [online]. Available from: <http://www.cancerresearchuk.org/cancer-info/cancerstats/keyfacts/bladder-cancer/uk-bladder-cancer-statistics> [Accessed December 16, 2014].

- Cauberg, E.C.C., de la Rosette, J.J.M.C.H., de Reijke, T.M. (2009) How to improve the effectiveness of transurethral resection in nonmuscle invasive bladder cancer? *Current Opinion in Urology*. **19**(5), 504–10.
- Chai, X., van Herk, M., Hulshof, M., Bel, A. (2012) A voxel-based finite element model for the prediction of bladder deformation. *Medical Physics*. **39**(1), 55–65.
- Chan, R.W., Titze, I.R. (2003) Effect of postmortem changes and freezing on the viscoelastic properties of vocal fold tissues. *Annals of Biomedical Engineering*. **31**(4), 482–491.
- Chen, J., Drzewiecki, B.A., Merryman, W.D., Pope, J.C. (2013) Murine bladder wall biomechanics following partial bladder obstruction. *Journal of Biomechanics*. **46**(15), 2752–2755.
- Chluba, C., Ge, W., Miranda, R.L. De, Strobel, J., Kienle, L., Quandt, E., Wuttig, M. (2015) Ultralow-fatigue shape memory alloy films. *Science*. **348**(6238), 1004–1007.
- Dahms, S., Piechota, H., Dahiya, R., Lue, T., Tanagho, E. (1998) Composition and biomechanical properties of the bladder acellular matrix graft: comparative analysis in rat, pig and human. *British Journal of Urology*. **82**(3), 411–419.
- DeWall, R.J., Bharat, S., Varghese, T., Hanson, M.E., Agni, R.M., Kliewer, M.A. (2012) Characterizing the compression-dependent viscoelastic properties of human hepatic pathologies using dynamic compression testing. *Physics in Medicine and Biology*. **57**, 2273–2286.
- Duerig, T., Pelton, A., Stöckel, D. (1999) An overview of nitinol medical applications. *Materials Science and Engineering*. **275**, 149–160.
- Epstein, J., Amin, M., Reuter, V., Mosotofi, F. (1998) The World Health Organization/International Society of Urological Pathology consensus on classification of urothelial (transitional cell) neoplasms of the urinary bladder. *The American Journal of Surgical Pathology*. **22**(12), 1435–1448.

- Espino, D.M., Shepherd, D.E.T., Hukins, D.W.L. (2015) Transient large strain contact modelling: A comparison of contact techniques for simultaneous fluid–structure interaction. *European Journal of Mechanics - B/Fluids*. **51**, 54–60.
- Fasseas, P., Orford, J.L., Denktas, A.E., Berger, P.B. (2001) Distal protection devices during percutaneous coronary and carotid interventions. *Current controlled trials in cardiovascular medicine*. **2**(6), 286–291.
- Field, M., Pollock, C., Harris, D. (2011) *The renal system: systems of the body series*. 2nd ed. Amsterdam: Elsevier Health Sciences.
- Finkbeiner, A.E., O'Donnell, P.D. (1990) Responses of detrusor smooth muscle to stretch and relaxation: In vitro study. *Urology*. **36**(2), 193–198.
- Fortini, A., Merlin, M., Rizzoni, R., Marfia, S. (2014) TWSME of a NiTi strip in free bending conditions: experimental and theoretical approach. *Fracture and Structural Integrity*. **29**, 74–84.
- Fulcher, G.R., Hukins, D.W.L., Shepherd, D.E.T. (2009) Viscoelastic properties of bovine articular cartilage attached to subchondral bone at high frequencies. *BMC Musculoskeletal Disorders*. **10**, 61.
- Gadd, M.J., Shepherd, D.E.T. (2011) Viscoelastic properties of the intervertebral disc and the effect of nucleus pulposus removal. *Proceedings of the Institution of Mechanical Engineers, Part H: Journal of Engineering in Medicine*. **225**(4), 335–341.
- Ganong, W., Barrett, K. (1997) *Review of medical physiology*. Stamford: Appleton and Lange.
- Gheonea, I.A., Stoica, Z., Bondari, S. (2011) Differential diagnosis of breast lesions using ultrasound elastography. *The Indian Journal of Radiology & Imaging*. **21**(4), 301–5.
- Gil, F.J., Planell, J.A. (1998) Shape memory alloys for medical applications. *Proceedings of the Institution of Mechanical Engineers, Part H: Journal of Engineering in Medicine*. **212**(6), 473–488.

- Gilbert, T.W., Wognum, S., Joyce, E.M., Freytes, D.O., Sacks, M.S., Badylak, S.F. (2008) Collagen fiber alignment and biaxial mechanical behavior of porcine urinary bladder derived extracellular matrix. *Biomaterials*. **29**(36), 4775–82.
- Gloeckner, D.C., Sacks, M.S., Fraser, M.O., Somogyi, G.T., de Groat, W.C., Chancellor, M.B. (2002) Passive biaxial mechanical properties of the rat bladder wall after spinal cord injury. *The Journal of urology*. **167**(5), 2247–2252.
- Granta Design Ltd (2013) CES Edupack.
- Griffiths, D.J., van Mastrigt, R., van Duyl, W.A., Coolsaet, B.L.R.A. (1979) Active mechanical properties of the smooth muscle of the urinary bladder. *Medical and Biological Engineering and Computing*. **17**(3), 281–290.
- Guyton, A., Hall, J. (2010) *Textbook of Medical Physiology*. 12th ed. Philadelphia: Elsevier.
- Guyton, A., Hall, J. (2006) *Textbook of Medical Physiology*. 11th ed. Philadelphia: Elsevier.
- Hashitani, H., Brading, A.F. (2003) Electrical properties of detrusor smooth muscles from the pig and human urinary bladder. *British Journal of Pharmacology*. **140**(1), 146–158.
- Hollenbeck, B.K., Dunn, R.L., Ye, Z., Hollingsworth, J.M., Skolarus, T.A., Kim, S.P., Montie, J.E., Lee, C.T., Wood, D.P., Miller, D.C. (2010) Delays in diagnosis and bladder cancer mortality. *Cancer*. **116**(22), 5235–5242.
- Holmes, A., Hukins, D. (1996) Analysis of load-relaxation in compressed segments of lumbar spine. *Medical Engineering and Physics*. **18**(2), 99–104.
- Hukins, D.W.L., Leahy, J.C., Mathias, K.J. (1999) Biomaterials: defining the mechanical properties of natural tissues and selection of replacement materials. *Journal of Materials Chemistry*. **9**(3), 629–636.
- van Humbeeck, J. (1999) Non-medical applications of shape memory alloys. *Materials Science and Engineering: A*. **273-275**, 134–148.

- Itoh, A., Ueno, E., Tohno, E., Kamma, H., Takahashi, H., Shiina, T., Yamakawa, M., Matsumura, T. (2006) Breast disease: clinical application of US elastography for diagnosis. *Radiology*. **239**(2), 341–350.
- James, N., Hussain, S., Hall, E., Tremlett, J., Rawlings, C., Crundwell, M., Sizer, B., Screenivasan, T., Hendron, C., Lewis, R., Waters, R., Huddart, R. (2012) Radiotherapy with or without chemotherapy in muscle-invasive bladder cancer. *The New England Journal of Medicine*. **366**(16), 1477–1488.
- Jin, Q., Zhang, X., Li, X., Wang, J. (2010) Dynamics analysis of bladder-urethra system based on CFD. *Frontiers of Mechanical Engineering in China*. **5**(3), 336–340.
- Kaplan, A., Litwin, M., Chamie, K. (2014) The future of bladder cancer care in the USA. *Nature Reviews Urology*. **11**, 59–62.
- Karpelson, M., Wei, G.Y., Wood, R.J. (2012) Driving high voltage piezoelectric actuators in microrobotic applications. *Sensors and Actuators, A: Physical*. **176**, 78–89.
- Kaufman, D.S., Shipley, W.U., Feldman, A.S. (2009) Bladder cancer. *Lancet*. **374**(9685), 239–49.
- Klatt, D., Hamhaber, U., Asbach, P., Braun, J., Sack, I. (2007) Noninvasive assessment of the rheological behavior of human organs using multifrequency MR elastography: a study of brain and liver viscoelasticity. *Physics in Medicine and Biology*. **52**(24), 7281–7294.
- Kondas, J., Kiss, L., Hatar, A., Kiss, A., Lukacs, T., Szeldeli, P., Torzsok, F., Bodrogi, I. (1999) The effect of intravesical mitomycin C on the recurrence of superficial (Ta-T1) bladder cancer. A hungarian multicenter study. *International Urology and Nephrology*. **31**(4), 451–456.
- Korossis, S., Bolland, F., Southgate, J., Ingham, E., Fisher, J. (2009) Regional biomechanical and histological characterisation of the passive porcine urinary bladder: Implications for augmentation and tissue engineering strategies. *Biomaterials*. **30**(2), 266–75.
- Kourambas, J., Delvecchio, F., Munver, R., Preminger, G.M. (2000) Nitinol stone retrieval-assisted ureteroscopic management of lower pole renal calculi. *Urology*. **56**(6), 935–939.

Kraklau, D.M., Bloom, D.A. (1998) The cystometrogram at 70 years. *The Journal of Urology*. **160**, 316–319.

Lahoz, R., Gracia-Villa, L., Puértolas, J. A. (2002) Training of the two-way shape memory effect by bending in NiTi alloys. *Journal of Engineering Materials and Technology*. **124**(4), 397.

Lang, N., Pereira, M.J., Lee, Y., Friehs, I., Vasilyev, N. V, Feins, E.N., Ablasser, K., O’Cearbhaill, E.D., Xu, C., Fabozzo, A., Padera, R., Wasserman, S., Freudenthal, F., Ferreira, L.S., Langer, R., Karp, J.M., del Nido, P.J. (2014) A blood-resistant surgical glue for minimally invasive repair of vessels and heart defects. *Science Translational Medicine*. **6**(218), 218ra6.

Lekka, M., Laidler, P., Gil, D., Lekki, J., Stachura, Z., Hryniewicz, A.Z. (1999) Elasticity of normal and cancerous human bladder cells studied by scanning force microscopy. *European Biophysics Journal*. **28**(4), 312–316.

Lekka, M., Laidler, P., Ignacak, J.J., Labd, M., Lekki, J., Struszczyk, H., Stachura, Z., Hryniewicz, A.Z. (2001) The effect of chitosan on stiffness and glycolytic activity of human bladder cells. *Biochimica et Biophysica Acta - Molecular Cell Research*. **1540**(2), 127 – 136.

Lekka, M., Pogoda, K., Gostek, J., Klymenko, O., Prauzner-Bechcicki, S., Wiltowska-Zuber, J., Jaczewska, J., Lekki, J., Stachura, Z. (2012) Cancer cell recognition - Mechanical phenotype. *Micron*. **43**(12), 1259–1266.

Lendlein, A., Langer, R. (2002) Biodegradable, elastic shape-memory polymers for potential biomedical applications. *Science*. **296**(5573), 1673–1676.

Li, S., Sengupta, D., Chien, S. (2014) Vascular tissue engineering: from in vitro to in situ. *Wiley Interdisciplinary Reviews. Systems Biology and Medicine*. **6**(1), 61–76.

Liu, C., Qin, H., Mather, P.T. (2007) Review of progress in shape-memory polymers. *Journal of Materials Chemistry*. **17**(16), 1543–1558.

Lochmatter, P., Kovacs, G. (2008) Design and characterization of an active hinge segment based on soft dielectric EAPs. *Sensors and Actuators, A: Physical*. **141**, 577–587.

- Lorusso, V., Silvestris, N. (2005) Systemic chemotherapy for patients with advanced and metastatic bladder cancer: current status and future directions. *Annals of Oncology - English Edition*. **16**(4), 85–89.
- Lotan, Y., Kamat, A.M., Porter, M.P., Robinson, V.L., Shore, N., Jewett, M., Schelhammer, P.F., White, R.D., Quale, D., Lee, C.T. (2009) Key concerns about the current state of bladder cancer: a position paper from the bladder cancer think tank, the bladder cancer advocacy network, and the society of urologic oncology. *Cancer*. **115**(18), 4096–4103.
- Luo, H., Abel, E. (2007) A comparison of methods for the training of NiTi two-way shape memory alloy. *Smart Materials and Structures*. **16**(6), 2543–2549.
- Lynch, T., Waymont, B., Dunn, J., Begum, G., Bathers, S. (1994) Rapid diagnostic service for patients with haematuria. *British Journal of Urology*. **73**(2), 147–151.
- Machado, L.G., Savi, M.A. (2003) Medical applications of shape memory alloys. *Brazilian Journal of Medical and Biological Research*. **36**, 683–691.
- Mariappan, Y.K., Glaser, K.J., Richard L Ehman (2010) Magnetic resonance elastography: a review. *Clinical Anatomy*. **23**(5), 497–511.
- van Mastrigt, R., Coolsaet, B., van Duyl, W. (1978) Passive properties of the urinary bladder in the collection phase. *Medical and Biological Engineering and Computing*. **16**(5), 471–482.
- van Mastrigt, R., Nagtegaal, J.C. (1981) Dependence of the viscoelastic response of the urinary bladder wall on strain rate. *Medical and Biological Engineering and Computing*. **19**(3), 291–296.
- Menard, K. (2008) *Dynamic mechanical analysis*. Boca Raton: CRC Press Taylor & Francis Group.
- Millard, L., Espino, D.M., Shepherd, D.E.T., Hukins, D.W.L., Buchan, K.G. (2011) Mechanical properties of chordae tendineae of the mitral heart valve: young's modulus, structural stiffness, and effects of aging. *Journal of Mechanics in Medicine and Biology*. **11**(1), 221–230.

- Mohd Jani, J., Leary, M., Subic, A., Gibson, M.A. (2014) A review of shape memory alloy research, applications and opportunities. *Materials & Design*. **56**, 1078–1113.
- Mont, M., McElroy, M., Johnson, A., Pivec, R. (2013) Single-use instruments, cutting blocks, and trials increase efficiency in the operating room during total knee arthroplasty: a prospective comparison of navigated and non-navigated cases. *The Journal of Arthroplasty*. **28**(7), 1135–1140.
- Morgan, N., Broadley, M. (2004) Taking the art out of smart! Forming processes and durability issues for the application of NiTi shape memory alloys in medical devices. *Proceedings for the Materials and Processes for Medical Devices Conference*.
- Mostofi, F., Sobin, L., Torloni, H. (1973) Histological typing of urinary bladder tumours. *International Histological Classification of Tumors; No. 10. Geneva, Switzerland: World Health Organization*, 15–17.
- Nagatomi, J., Gloeckner, D.C., Chancellor, M.B., DeGroat, W.C., Sacks, M.S. (2004) Changes in the biaxial viscoelastic response of the urinary bladder following spinal cord injury. *Annals of Biomedical Engineering*. **32**(10), 1409–1419.
- Natali, A.N., Audenino, A.L., Artibani, W., Fontanella, C.G., Carniel, E.L., Zanetti, E.M. (2015) Bladder tissue biomechanical behavior: experimental tests and constitutive formulation. *Journal of Biomechanics*. **48**(12), 3088–3096.
- Öhman, C., Baleani, M., Viceconti, M. (2009) Repeatability of experimental procedures to determine mechanical behaviour of ligaments. *Acta of Bioengineering and Biomechanics*. **11**(1), 19–23.
- Omari, E.A., Varghese, T., Kliewer, M.A., Harter, J., Hartenbach, E.M. (2015) Dynamic and quasi-static mechanical testing for characterization of the viscoelastic properties of human uterine tissue. *Journal of Biomechanics*. **48**(10), 1–7.
- Orabi, H., Bouhout, S., Morissette, A., Rousseau, A., Chabaud, S., Bolduc, S. (2013) Tissue engineering of urinary bladder and urethra: advances from bench to patients. *The Scientific World Journal*. **2013**, 154564.



Otsuka, K., Wayman, C. (1999) *Shape memory materials*. Cambridge: Cambridge University Press.

Pandit, J.J., Carey, A. (2006) Estimating the duration of common elective operations: implications for operating list management. *Anaesthesia*. **61**(8), 768–76.

Parsons, B.A., Drake, M.J., Gammie, A., Fry, C.H., Vahabi, B. (2012) The validation of a functional, isolated pig bladder model for physiological experimentation. *Frontiers in Pharmacology*. **3**, 52.

Patel, P., Bryan, R.T., Wallace, D.M.A. (2011) Emerging Endoscopic and Photodynamic Techniques for Bladder Cancer Detection and Surveillance. *The Scientific World Journal*. **11**, 2550–2558.

Patel, P.S.D., Shepherd, D.E.T., Hukins, D.W.L. (2008) Compressive properties of commercially available polyurethane foams as mechanical models for osteoporotic human cancellous bone. *BMC Musculoskeletal Disorders*. **9**, 137.

Patel, P.S.D., Shepherd, D.E.T., Hukins, D.W.L. (2010) The effect of screw insertion angle and thread type on the pullout strength of bone screws in normal and osteoporotic cancellous bone models. *Medical Engineering and Physics*. **32**(8), 822–828.

Patrick, D.R., Fardo, S.W. (2013) *Electricity and Electronics Fundamentals*. 2nd ed. Lilburn: Fairmont Press Inc.

Peckham, M. (2011) *Histology at a glance*. Singapore: Wiley-Blackwell.

Peirce, B. (1852) Criterion for the rejection of doubtful observations. *The Astronomical Journal*. **2**, 161 – 163.

Pel, J.J.M., van Mastrigt, R. (2007) Development of a CFD urethral model to study flow-generated vortices under different conditions of prostatic obstruction. *Physiological Measurement*. **28**(1), 13–23.

Pelker, R.R., Friedlaender, G.E., Markham, T.C., Panjabi, M.M., Moen, C.J. (1984) Effects of Freezing and Freeze-Drying on the Biomechanical Properties of Rat Bone. *Journal of Orthopaedic Research*. **1**(4), 405–411.

Pokrywczynska, M., Adamowicz, J., Sharma, A.K., Drewa, T. (2014) Human urinary bladder regeneration through tissue engineering - an analysis of 131 clinical cases. *Experimental Biology and Medicine*. **239**(3), 264–71.

Ranstam, J. (2012) Repeated measurements, bilateral observations and pseudoreplicates, why does it matter? *Osteoarthritis and Cartilage*. **20**(6), 473–475.

Ray, E., O'Brien, T. (2007) Should urologists be spending more time on the golf course? *BJU International*. **100**(4), 728–729.

Reich, O., Noll, M., Gratzke, C., Bachmann, A., Waidelich, R., Seitz, M., Schlenker, B., Baumgartner, R., Hofstetter, A., Stief, C.G. (2006) High-level virtual reality simulator for endourologic procedures of lower urinary tract. *Urology*. **67**(6), 1144–1148.

Reilly, J. (2015) *Applied Statistics*. Dublin: Statistical Solutions.

Remzi, M., Haitel, A., Margulis, V., Karakiewicz, P., Montorsi, F., Kikuchi, E., Zigeuner, R., Weizer, A., Bolenz, C., Bensalah, K., Suardi, N., Raman, J.D., Lotan, Y., Waldert, M., Ng, C.K., Fernández, M., Koppie, T.M., Ströbel, P., Kabbani, W., Murai, M., Langner, C., Roscigno, M., Wheat, J., Guo, C.C., Wood, C.G., Shariat, S.F. (2009) Tumour architecture is an independent predictor of outcomes after nephroureterectomy: A multi-institutional analysis of 1363 patients. *BJU International*. **103**(3), 307–311.

van Rhijn, B.W.G., Burger, M., Lotan, Y., Solsona, E., Stief, C.G., Sylvester, R.J., Witjes, J.A., Zlotta, A.R. (2009) Recurrence and progression of disease in non-muscle-invasive bladder cancer: from epidemiology to treatment strategy. *European Urology*. **56**(3), 430–42.

Rosario, D.J., Reilly, G.C., Ali Salah, E., Glover, M., Bullock, A.J., Macneil, S. (2008) Decellularization and sterilization of porcine urinary bladder matrix for tissue engineering in the lower urinary tract. *Regenerative Medicine*. **3**, 145–156.

- Ross, S.M. (2003) Peirce's criterion for the elimination of suspect experimental data. *Journal of Engineering Technology*. **20**(2), 38–41.
- Sangar, V.K., Ragavan, N., Matanhelia, S.S., Watson, M.W., Blades, R.A. (2005) The economic consequences of prostate and bladder cancer in the UK. *BJU International*. **95**(1), 59–63.
- Shirai, T., Fukushima, S., Tagawa, Y., Sturai, T., Okumura, M., Ito, N. (1989) Cell proliferation induced by uracil-calculi and subsequent development of reversible papillomatosis in the rat urinary bladder. *Cancer Research*. **49**(2), 378–383.
- Siegel, G.W., Patel, N.N., Milshteyn, M.A., Buzas, D., Lombardo, D.J., Morawa, L.G. (2015) Cost analysis and surgical site infection rates in total knee arthroplasty comparing traditional vs. single-use instrumentation. *The Journal of Arthroplasty*. **In Press**.
- Silver, F.H., Freeman, J.W., DeVore, D. (2001) Viscoelastic properties of human skin and processed dermis. *Skin Research and Technology*. **7**(1), 18–23.
- Sinkus, R., Tanter, M., Xydeas, T., Catheline, S., Bercoff, J., Fink, M. (2005) Viscoelastic shear properties of in vivo breast lesions measured by MR elastography. *Magnetic Resonance Imaging*. **23**(2), 159–165.
- Smith, A.B., Deal, A.M., Woods, M.E., Wallen, E.M., Pruthi, R.S., Chen, R.C., Milowsky, M.I., Nielsen, M.E. (2014) Muscle-invasive bladder cancer: evaluating treatment and survival in the national cancer data base. *BJU International*. **114**, 719–726.
- Sobin, L.H., Gospodarowicz, M.K., Wittekind, C. (2009) *TNM classification of malignant tumours*. 7th ed. Oxford: Wiley-Blackwell.
- Stenzl, A., Cowan, N.C., De Santis, M., Kuczyk, M. a., Merseburger, A.S., Ribal, M.J., Sherif, A., Witjes, J.A. (2011) Treatment of muscle-invasive and metastatic bladder cancer: update of the EAU guidelines. *European Urology*. **59**(6), 1009–1018.
- Streitberger, K.-J., Sack, I., Krefting, D., Pfüller, C., Braun, J., Paul, F., Wuerfel, J. (2012) Brain viscoelasticity alteration in chronic-progressive multiple sclerosis. *PLoS ONE*. **7**(1), e29888.

Svatek, R.S., Hollenbeck, B.K., Holmäng, S., Lee, R., Kim, S.P., Stenzl, A., Lotan, Y. (2014) The economics of bladder cancer: costs and considerations of caring for this disease. *European Urology*. **66**, 253–262.

Swaminathan, V., Mythreye, K., Tim O'Brien, E., Berchuck, A., Blobe, G.C., Superfine, R. (2011) Mechanical Stiffness grades metastatic potential in patient tumor cells and in cancer cell lines. *Cancer Research*. **71**(15), 5075–5080.

Sylvester, R.J., van der Meijden, A.P.M., Oosterlinck, W., Witjes, J.A., Bouffieux, C., Denis, L., Newling, D.W.W., Kurth, K. (2006) Predicting recurrence and progression in individual patients with stage Ta T1 bladder cancer using EORTC risk tables: a combined analysis of 2596 patients from seven EORTC trials. *European Urology*. **49**(3), 466–477.

Szarko, M., Muldrew, K., Bertram, J.E. (2010) Freeze-thaw treatment effects on the dynamic mechanical properties of articular cartilage. *BMC Musculoskeletal Disorders*. **11**, 231.

Tortora, G.J., Derrickson, B.H. (2005) *Principles of anatomy and physiology*. New York: John Wiley & Sons.

Trimble, E.L., Ungerleider, R.S., Abrams, J.A., Kaplan, R.S., Feigal, E.G., Smith, M.A., Carter, C.L., Friedman, M.A. (1993) Neoadjuvant therapy in cancer treatment. *Cancer*. **72**(11), 3515–3524.

Uehara, T., Asai, C., Ohno, N. (2009) Molecular dynamics simulation of shape memory behaviour using a multi-grain model. *Modelling and Simulation in Materials Science and Engineering*. **17**(3), 035011.

Venkatasubramanian, R.T., Grassl, E.D., Barocas, V.H., Lafontaine, D., Bischof, J.C. (2006) Effects of freezing and cryopreservation on the mechanical properties of arteries. *Annals of Biomedical Engineering*. **34**(5), 823–32.

Villanueva, A.A., Joshi, K.B., Blottman, J.B., Priya, S. (2010) A bio-inspired shape memory alloy composite (BISMAC) actuator. *Smart Materials and Structures*. **19**(2), 025013.

Wallace, D., Bryan, R., Dunn, J., Begum, G., Bathers, S. (2002) Delay and survival in bladder cancer. *BJU International*. **89**(9), 868–878.

Ward, I., Sweeney, J. (2004) *An introduction to the mechanical properties of solid polymers*. 2nd ed. Chichester: John Wiley & Sons.

Wiesner, C., Jäger, W., Thüroff, J.W. (2010) Surgery illustrated - surgical atlas. Transurethral resection of bladder tumours. *BJU International*. **105**, 1610–1621.

Wilby, D., Thomas, K., Ray, E., Chappell, B., O'Brien, T. (2009) Bladder cancer: new TUR techniques. *World Journal of Urology*. **27**(3), 309–12.

Wilcox, A.G., Buchan, K.G., Espino, D.M. (2014) Frequency and diameter dependent viscoelastic properties of mitral valve chordae tendineae. *Journal of the Mechanical Behavior of Biomedical Materials*. **30**, 186–95.

Woo, S.L., Orlando, C.A., Camp, J.F., Akeson, W.H. (1986) Effects of postmortem storage by freezing on ligament tensile behavior. *Journal of Biomechanics*. **19**(5), 399–404.

Yang, B., Zhang, Y., Zhou, L., Sun, Z., Zheng, J., Chen, Y., Dai, Y. (2010) Development of a porcine bladder acellular matrix with well-preserved extracellular bioactive factors for tissue engineering. *Tissue engineering. Part C, Methods*. **16**(5), 1201–1211.

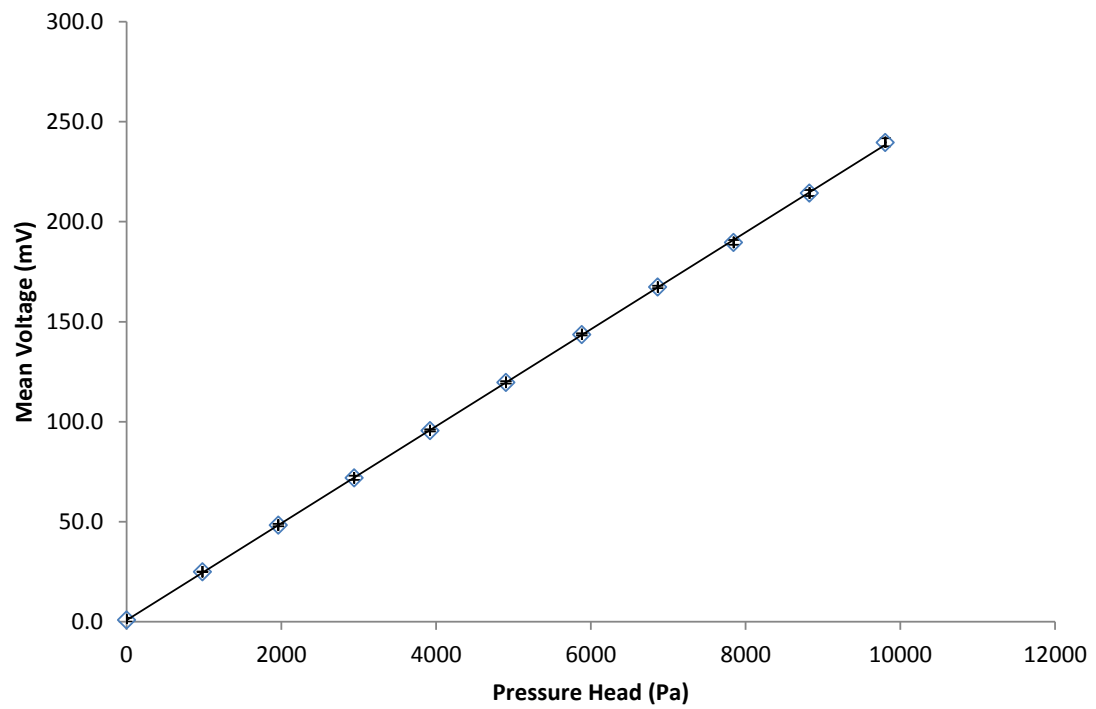
Zanetti, E.M., Perrini, M., Bignardi, C., Audenino, A.L. (2012) Bladder tissue passive response to monotonic and cyclic loading. *Biorheology*. **49**(1), 49–63.

Zeegers, M.P., Bryan, R.T., Langford, C., Billingham, L., Murray, P., Deshmukh, N.S., Hussain, S., James, N., Wallace, D.M.A., Cheng, K.K. (2010) The West Midlands bladder cancer prognosis programme: rationale and design. *BJU International*. **105**(6), 784–788.

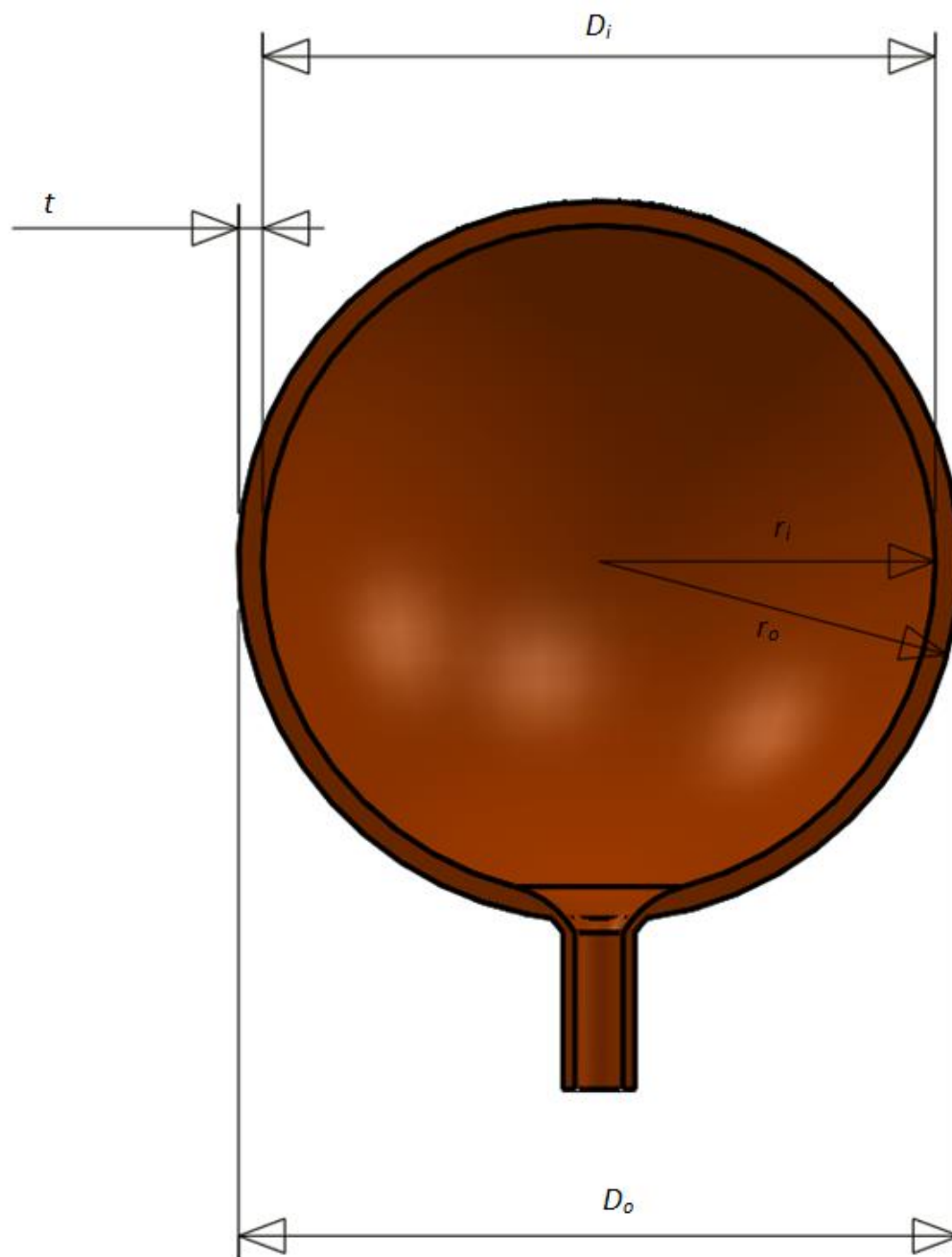
Zeng, Y., Yang, J., Huang, K., Lee, Z., Lee, X. (2001) A comparison of biomechanical properties between human and porcine cornea. *Journal of Biomechanics*. **34**(4), 533–537.

## Appendix A – Pressure Transducer Calibration

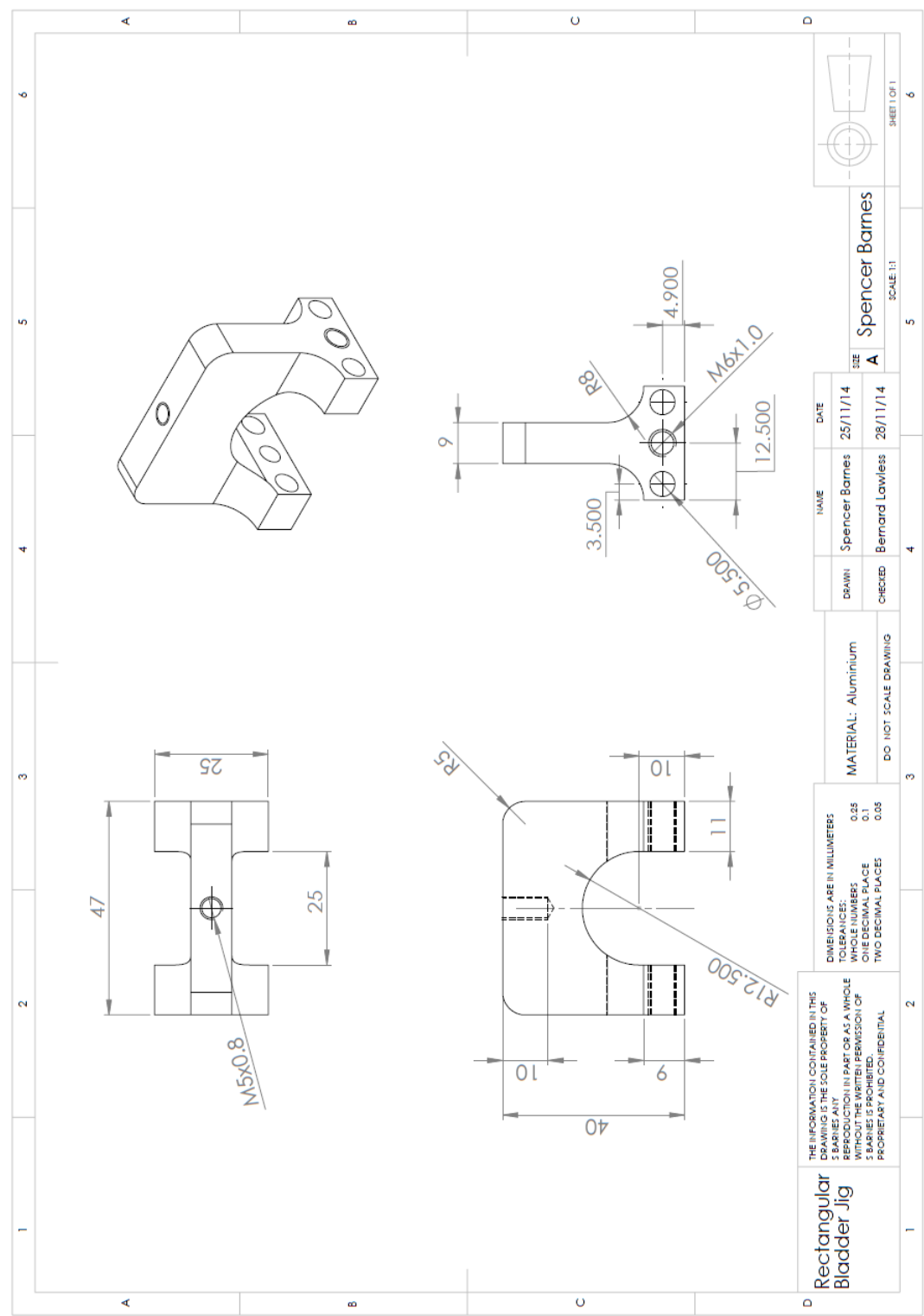
Height (m)	Pressure Head (Pa)	Mean Voltage (mV)
0	0	1.0
0.1	980.7	25.0
0.2	1961.4	48.3
0.3	2942.1	72.0
0.4	3922.8	95.7
0.5	4903.5	119.7
0.6	5884.2	143.7
0.7	6864.9	167.3
0.8	7845.6	189.7
0.9	8826.3	214.3
1	9807	239.7



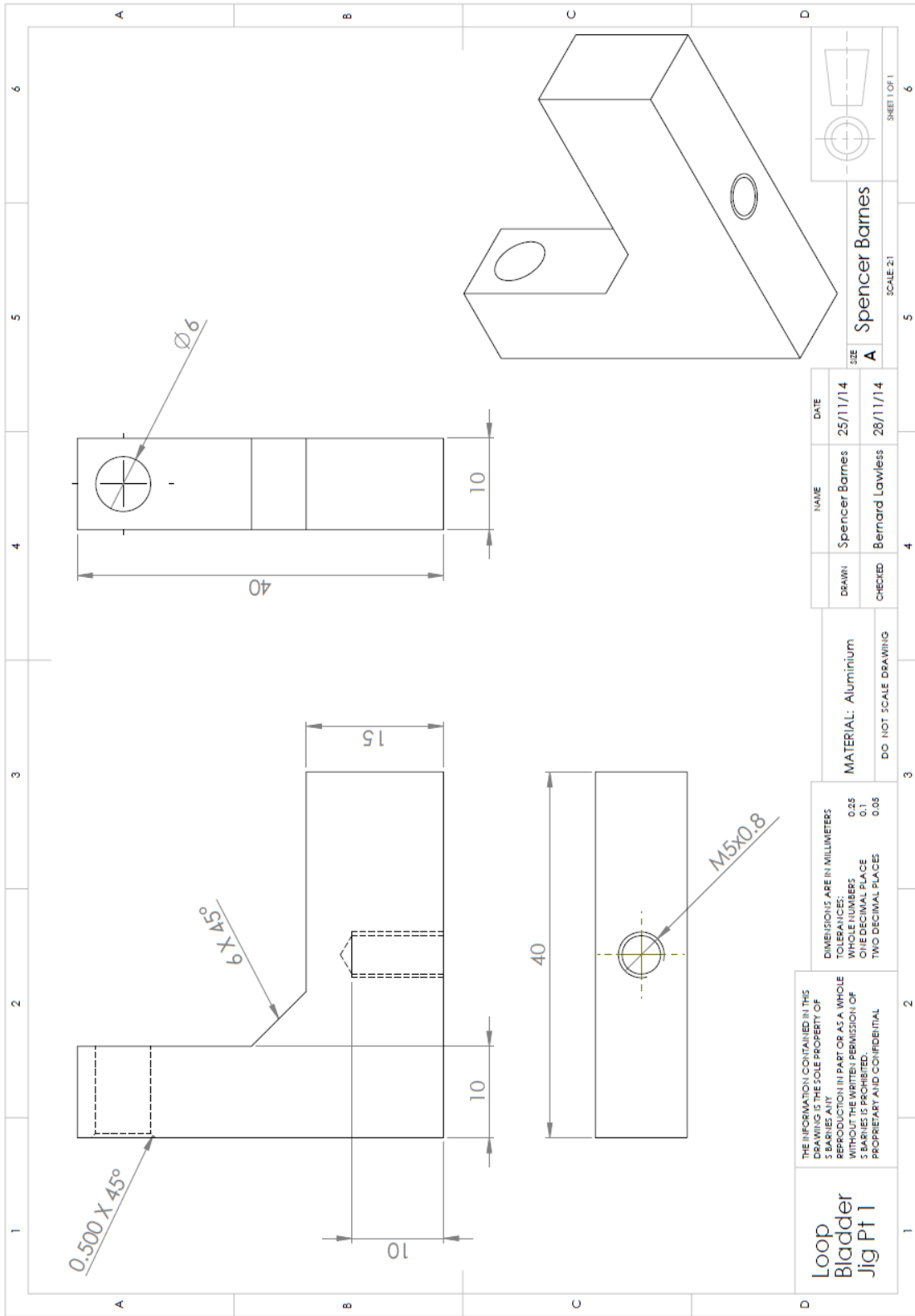
## Appendix B – Bladder Dimension Schematic



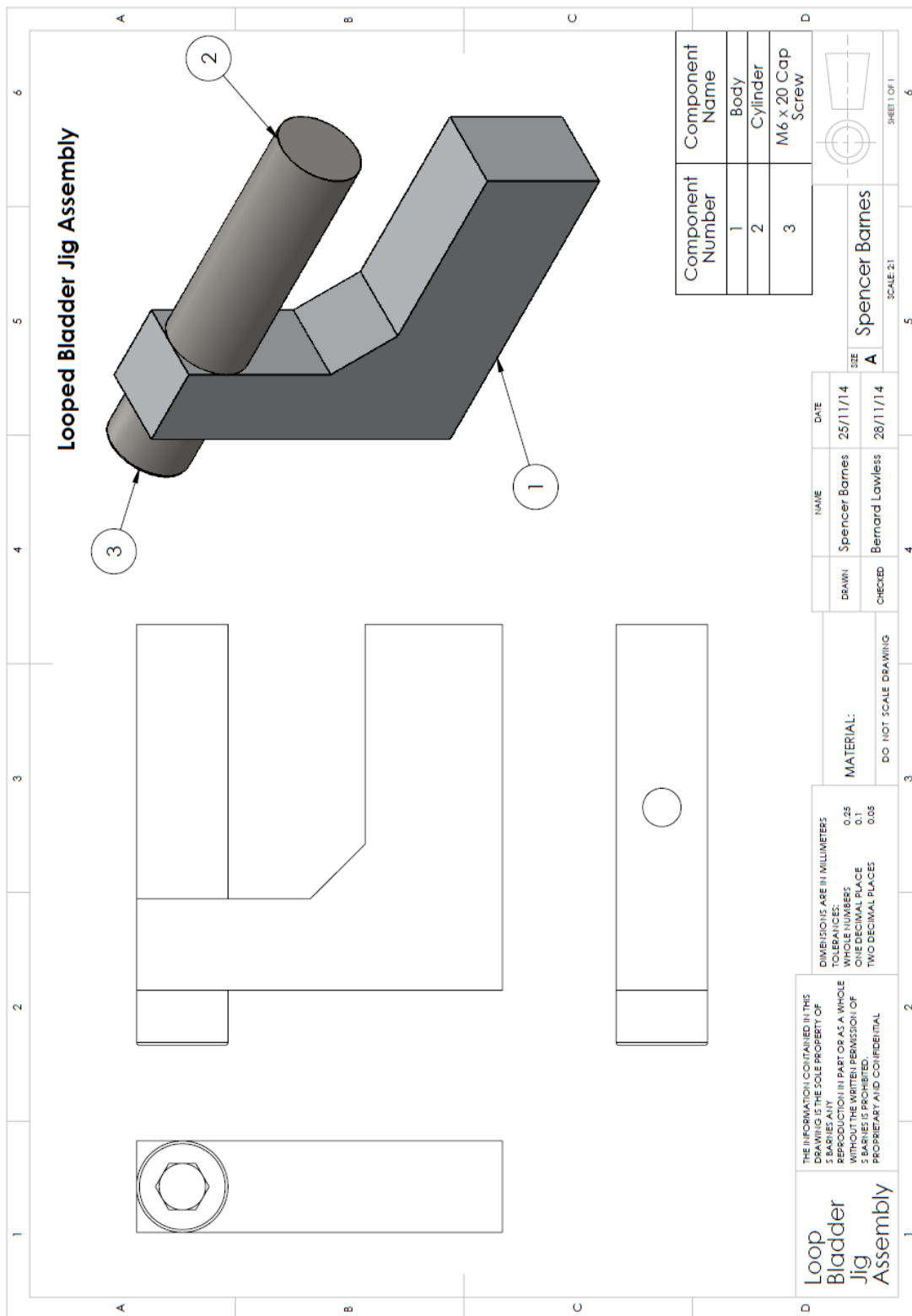
Appendix C – Engineering Drawings for Bladder Testing Jigs











Appendix D – Wire Housing Engineering Drawing

